Arch Comput Methods Eng (2010) 17: 25–76
DOI 10.1007/s11831-010-9040-7

Smoothed Particle Hydrodynamics (SPH): an Overview and Recent Developments

M.B. Liu · G.R. Liu

Received: 1 August 2009 / Accepted: 1 August 2009 / Published online: 13 February 2010

Abstract Smoothed particle hydrodynamics (SPH) is a meshfree particle method based on Lagrangian formulation, and has been widely applied to different areas in engineering and science. This paper presents an overview on the SPH method and its recent developments, including (1) the need for meshfree particle methods, and advantages of SPH, (2) approximation schemes of the conventional SPH method and numerical techniques for deriving SPH formulations for partial differential equations such as the Navier-Stokes (N-S) equations, (3) the role of the smoothing kernel functions and a general approach to construct smoothing kernel functions, (4) kernel and particle consistency for the SPH method, and approaches for restoring particle consistency, (5) several important numerical aspects, and (6) some recent applications of SPH. The paper ends with some concluding remarks.

1 Introduction

1.1 Traditional Grid Based Numerical Methods

Computer simulation has increasingly become a more and more important tool for solving practical and complicated problems in engineering and science. It plays a valuable role in providing tests and examinations for theories, offering insights to complex physics, and assisting in the interpretation and even the discovery of new phenomena. Grid or mesh based numerical methods such as the finite difference methods (FDM), finite volume methods (FVM) and the finite element methods (FEM) have been widely applied to various areas of computational fluid dynamics (CFD) and computational solid mechanics (CSM). These methods are very useful to solve differential or partial differential equations (PDEs) that govern the concerned physical phenomena. For centuries, the FDM has been used as a major tool for solving partial differential equations defined in problem domains with simple geometries. For decades, the FVM dominates in solving fluid flow problems and FEM plays an essential role for solid mechanics problems with complex geometry [1–3]. One notable feature of the grid based numerical models is to divide a continuum domain into discrete small subdomains, via a process termed as discretization or meshing. The individual grid points (or nodes) are connected together in a pre-defined manner by a topological map, which is termed as a mesh (or grid). The meshing results in elements in FEM, cells in FVM, and grids in FDM. A mesh or grid system consisting of nodes, and cells or elements must be defined to provide the relationship between the nodes before the approximation process for the differential or partial differential equations. Based on a properly pre-defined mesh, the governing equations can be converted to a set of algebraic equations with nodal unknowns for the field variables. So far the grid based numerical models have achieved remarkably, and they are currently the dominant methods in numerical simulations for solving practical problems in engineering and science [1–5].

Despite the great success, grid based numerical methods suffer from difficulties in some aspects, which limit their

G.R. Liu is SMA Fellow, Singapore-MIT Alliance.

M.B. Liu (✉)
Key Laboratory for Hydrodynamics and Ocean Engineering, Institute of Mechanics, Chinese Academy of Sciences, #15, Bei Si Huan Xi Road, Beijing 100190, China
e-mail: liumoubin@imech.ac.cn

G.R. Liu
Centre for Advanced Computations in Engineering Science (ACES), Department of Mechanical Engineering, National University of Singapore, 10 Kent Ridge Crescent, Singapore 119260, Singapore

applications in many types of complicated problems. The major difficulties are resulted from the use of mesh, which should always ensure that the numerical compatibility condition is the same as the physical compatibility condition for a continuum. Hence, the use of grid/mesh can lead to various difficulties in dealing with problems with free surface, deformable boundary, moving interface, and extremely large deformation and crack propagation. Moreover, for problems with complicated geometry, the generation of a quality mesh has become a difficult, time-consuming and costly process.

In grid based numerical methods, mesh generation for the problem domain is a prerequisite for the numerical simulations. For Eulerian grid methods such as FDM constructing a regular grid for irregular or complex geometry has never been an easy task, and usually requires additional complicated mathematical transformation that can be even more expensive than solving the problem itself. Determining the precise locations of the inhomogeneities, free surfaces, deformable boundaries and moving interfaces within the frame of the fixed Eulerian grid is also a formidable task. The Eulerian methods are also not well suited to problems that need monitoring the material properties in fixed volumes, e.g. particulate flows [1, 2, 6]. For the Lagrangian grid methods like FEM, mesh generation is necessary for the solids and structures, and usually occupies a significant portion of the computational effort. Treatment of extremely large deformation is an important issue in a Lagrangian grid based method. It usually requires special techniques like rezoning. Mesh rezoning, however, is tedious and time-consuming, and may introduce additional inaccuracy into the solution [3, 7].

The difficulties and limitations of the grid based methods are especially evident when simulating hydrodynamic phenomena such as explosion and high velocity impact (HVI). In the whole process of an explosion, there exist special features such as large deformations, large inhomogeneities, moving material interfaces, deformable boundaries, and free surfaces [8]. These special features pose great challenges to numerical simulations using the grid based methods. High velocity impact problems involve shock waves propagating through the colliding or impacting bodies that can behave like fluids. Analytically, the equations of motion and a high-pressure equation of state are the key descriptors of material behavior. In HVI phenomena, there also exist large deformations, moving material interfaces, deformable boundaries, and free surfaces, which are, again, very difficult for grid based numerical methods to cope with [9].

The grid based numerical methods are also not suitable for situations where the main concern of the object is a set of discrete physical particles rather than a continuum. Typical examples include the interaction of stars in astrophysics, movement of millions of atoms in an equilibrium or non-equilibrium state, dynamic behavior of protein molecules, and etc. Simulation of such discrete systems using the continuum grid based methods is often not a good choice [10, 11].

1.2 Meshfree Methods

Over the past years, meshfree methods have been a major research focus, towards the next generation of more effective computational methods for more complicated problems [4, 6]. The key idea of the meshfree methods is to provide accurate and stable numerical solutions for integral equations or PDEs with all kinds of possible boundary conditions using a set of arbitrarily distributed nodes or particles [4, 6]. The history, development, theory and applications of the major existing meshfree methods have been addressed in some monographs and review articles [4, 6, 7, 12–15]. The readers may refer to these literatures for more details of the meshfree methods. To avoid too much detour from our central topic, this article will not further discuss these meshfree methods and techniques, except for mentioning briefly some of the latest advancements.

For solid mechanics problems, instead of weak formulations used in FEM, we now have a much more powerful weakened weak (W2) formulation for general settings of FEM and meshfree methods [16–19]. The W2 formulation can create various models with special properties, such upper bound property [20–23], ultra-accurate and supper convergent solutions [22, 24–29], and even nearly exact solutions [30, 31]. These W2 formulations have a theoretical foundation on the novel G space theory [16–19]. All most all these W2 models work very well with triangular mesh, and applied for adaptive analyses for complicated geometry.

For fluid dynamics problems, the gradient smoothing method (GSM) has been recently formulated using carefully designed gradient smoothing domains [32–35]. The GSM works very well with unstructured triangular mesh, and can be used effective for adaptive analysis [34]. The GSM is an excellent alternative to the FVM for CFD problems.

One distinct meshfree method is smoothed particle hydrodynamics or SPH. The SPH is a very powerful method for CFD problems governed by the Navier-Stokes equations.

1.3 Smoothed Particle Hydrodynamics

Smoothed particle hydrodynamics is a “truly” meshfree, particle method originally used for continuum scale applications, and may be regarded as the oldest modern meshfree particle method. It was first invented to solve astrophysical problems in three-dimensional open space [36, 37], since the collective movement of those particles is similar to the movement of a liquid or gas flow, and it can be modeled by

the governing equations of the classical Newtonian hydrodynamics.

In SPH, the state of a system is represented by a set of particles, which possess material properties and interact with each other within the range controlled by a weight function or smoothing function [6, 38, 39]. The discretization of the governing equations is based on these discrete particles, and a variety of particle-based formulations have been used to calculate the local density, velocity and acceleration of the fluid. The fluid pressure is calculated from the density using an equation of state, the particle acceleration is then calculated from the pressure gradient and the density. For viscous flows, the effects of physical viscosity on the particle accelerations can also be included. As a Lagrangian particle method, SPH conserves mass exactly. In SPH, there is no explicit interface tracking for multiphase flows—the motion of the fluid is represented by the motion of the particles, and fluid surfaces or fluid-fluid interfaces move with particles representing their phase defined at the initial stage.

SPH has some special advantages over the traditional grid based numerical methods.

1. SPH is a particle method of Lagrangian nature, and the algorithm is Galilean invariant. It can obtain the time history of the material particles. The advection and transport of the system can thus be calculated.
2. By properly deploying particles at specific positions at the initial stage before the analysis, the free surfaces, material interfaces, and moving boundaries can all be traced naturally in the process of simulation regardless the complicity of the movement of the particles, which have been very challenging to many Eulerian methods. Therefore, SPH is an ideal choice for modeling free surface and interfacial flow problems.
3. SPH is a particle method without using a grid/mesh. This distinct meshfree feature of the SPH method allows a straightforward handling of very large deformations, since the connectivity between particles are generated as part of the computation and can change with time. Typical examples include the SPH applications in high energy phenomena such as explosion, underwater explosion, high velocity impact, and penetrations.
4. In SPH method, a particle represents a finite volume in continuum scale. This is quite similar to the classic molecular dynamics (MD) method [11, 40] that uses a particle to represent an atom or a molecule in nano-scale, and the dissipative particle dynamics (DPD) method [41, 42] that uses a particle to represent a small cluster of molecules in meso-cale. Thus, it is natural to generalize or extend SPH to smaller scales, or to couple SPH with molecular dynamics and dissipative particle dynamics for multiple scale applications, especially in biophysics, and biochemistry.
5. SPH is suitable for problems where the object under consideration is not a continuum. This is especially true in bio- and nano- engineering at micro and nano scale, and astrophysics at astronomic scale. For such problems, SPH can be a natural choice for numerical simulations.
6. SPH is comparatively easier in numerical implementation, and it is more natural to develop three-dimensional numerical models than grid based methods.

The early SPH algorithms were derived from the probability theory, and statistical mechanics are extensively used for numerical estimation. These algorithms did not conserve linear and angular momentum. However, they can give reasonably good results for many astrophysical phenomena. For the simulations of fluid and solid mechanics problems, there are challenges to reproduce faithfully the partial differential equations governing the corresponding fluid and solid dynamics. These challenges involve accuracy and stability of the numerical schemes in implementing the SPH methods.

With the development of the SPH method, and the extensive applications to a wide range of problems, more attractive features have been showcased while some inherent drawbacks have also been identified. Different variants or modifications have been proposed to improve the original SPH method. For example, Gingold and Monaghan found the non-conservation of linear and angular momentum of the original SPH algorithm, and then introduced an SPH algorithm that conserves both linear and angular momentum [43]. Hu and Adams also invented an angular-momentum conservative SPH algorithm for incompressible viscous flows [44].

Many researchers have conducted investigations on the SPH method on the numerical aspects in accuracy, stability, convergence and efficiency. Swegle et al. identified the tensile instability problem that can be important for materials with strength [45]. Morris noted the particle inconsistency problem that can lead to poor accuracy in the SPH solution [46]. Over the past years, different modifications or corrections have been tried to restore the consistency and to improve the accuracy of the SPH method. Monaghan proposed symmetrization formulations that were reported to have better effects [47–49]. Johnson and his co-workers gave an axis-symmetry normalization formulation so that, for velocity fields that yield constant values of normal velocity strains, the normal velocity strains can be exactly reproduced [50, 51]. Randles and Libersky derived a normalization formulation for the density approximation and a normalization for the divergence of the stress tensor [52]. Chen et al. proposed a corrective smoothed particle method (CSPM) which improves the simulation accuracy both inside the problem domain and around the boundary area [53, 54]. The CSPM has been improved by Liu et al. in resolving problems with discontinuity such as shock waves in a

discontinuous SPH (DSPH) [55]. Liu et al. also proposed a finite particle method (FPM), which uses a set of basis function to approximate field variables at a set of arbitrarily distributed particles [56, 57]. FPM can be regarded as an improved version of SPH and CSPM with better performance in particle consistency. Batra et al. concurrently developed a similar idea to FPM, and it is named modified SPH (MSPH) [58] with applications mainly in solid mechanics. Fang et al. further improved this idea for simulating free surface flows [59], and they later developed a regularized Lagrangian finite point method for the simulation of incompressible viscous flows [60, 61]. A stress point method was invented to improve the tensile instability and zero energy mode problems [62–65]. Other notable modifications or corrections of the SPH method include the moving least square particle hydrodynamics (MLSPH) [66, 67], the integration kernel correction [68], the reproducing kernel particle method (RKPM) [69, 70], the correction for stable particle method [71, 72], and several other particle consistency restoring approaches [6, 56, 73]. Belytschko and his co-workers have conducted a series of stability and convergence analyses on meshfree particle methods, and some of the numerical techniques and analyses can also be applicable to SPH [13, 72, 74].

This article is organized as follows. In Sect. 1, the background of meshfree particle methods is first addressed with highlights on overcoming the limitations of the grid based numerical models. The invention, features and developments of the SPH method are then briefly introduced. In Sect. 2, the approximation schemes of the SPH method are discussed, while some numerical techniques for developing SPH formulations are presented. The SPH formulations for the N-S equation, which governs the general fluid flow problems, are also given. Section 3 presents a review on the smoothing kernel function. Conditions for constructing smoothing functions are developed with examples of smoothing functions constructed. Section 4 introduces consistency concept of SPH including kernel consistency and particle consistency, and also provides an in-depth review on the existing approaches for restoring particle consistency. Several new approaches are also presented, which include a discontinuous SPH for simulating problems with discontinuity, a general approach to restore particle inconsistency, and a finite particle method. In Sect. 5, some important numerical topics in SPH are discussed. These special topics include (1) solid boundary treatment, (2) representation of solid obstacles, (3) material interface treatment, and (4) tensile instability. Different applications of the SPH method have been reviewed in Sect. 6. Some concluding remarks are given in Sect. 7.

2 SPH Approximation Techniques

The conventional SPH method was originally developed for hydrodynamics problems in which the governing equations are in strong form of partial differential equations of field variables such as density, velocity, energy, and etc. There are basically two steps in obtaining an SPH formulation. The first step is to represent a function and/or its derivatives in continuous form as integral representation, and this step is usually termed as *kernel approximation*. In this kernel approximation step, the approximation of a function and its derivatives are based on the evaluation of the smoothing kernel function and its derivatives. The second step is usually referred to as *particle approximation*. In this step, the computational domain is first discretized by representing the domain with a set of initial distribution of particles representing the initial settings of the problem. After discretization, field variables on a particle are approximated by a summation of the values over the nearest neighbor particles.

2.1 Kernel Approximation of a Function

The kernel approximation in the SPH method involves representation of a function and its derivatives using a *smoothing function*. The smoothing function should satisfy some basic requirements, and it has been called *kernel*, *smoothing kernel*, *smoothing kernel function*, or sometimes even *weight function* in some SPH literature [38, 46, 49, 75]. A detailed discussion on smoothing function, basic requirements and constructing conditions will be given in Sect. 3.

The kernel approximation of a function $f(\boldsymbol{x})$ used in the SPH method starts from the following identity

$$f(\boldsymbol{x}) = \int_{\Omega} f(\boldsymbol{x}')\delta(\boldsymbol{x}-\boldsymbol{x}')d\boldsymbol{x}', \tag{1}$$

where f is a function of the position vector $\boldsymbol{x}$, and $\delta(\boldsymbol{x}-\boldsymbol{x}')$ is the Dirac delta function given by

$$\delta(\boldsymbol{x}-\boldsymbol{x}') = \begin{cases} 1, & \boldsymbol{x}=\boldsymbol{x}', \\ 0, & \boldsymbol{x}\neq\boldsymbol{x}'. \end{cases} \tag{2}$$

In (1), Ω is the volume of the integral that contains $\boldsymbol{x}$. Equation (1) implies that a function can be represented in an integral form. Since the Dirac delta function is used, the integral representation in (2) is exact and rigorous, as long as $f(\boldsymbol{x})$ is defined and continuous in Ω.

The Delta function $\delta(\boldsymbol{x}-\boldsymbol{x}')$ with only a "point" support, and hence (1) cannot be used for establishing discrete numerical models. If replacing the Delta function $\delta(\boldsymbol{x}-\boldsymbol{x}')$ by a smoothing function $W(\boldsymbol{x}-\boldsymbol{x}', h)$ with a finite spatial dimension h, the kernel approximation of $f(\boldsymbol{x})$, $\langle f(\boldsymbol{x})\rangle$, becomes

$$\langle f(\boldsymbol{x})\rangle \doteq \int_{\Omega} f(\boldsymbol{x}')W(\boldsymbol{x}-\boldsymbol{x}', h)d\boldsymbol{x}', \tag{3}$$

where h is the smoothing length defining the influence or support area of the smoothing function W. Note that as long as W is not the Dirac delta function, the integral representation shown in (3) can only be an approximation, except for special cases. Therefore (3) can be written as

$$\langle f(\boldsymbol{x})\rangle = \int_\Omega f(\boldsymbol{x}')W(\boldsymbol{x}-\boldsymbol{x}',h)d\boldsymbol{x}'. \tag{4}$$

A smoothing function W is *usually* chosen to be an *even* function for reasons given later in Sect. 3. It should also satisfy a number of conditions. The first one is the *normalization condition* that states

$$\int_\Omega W(\boldsymbol{x}-\boldsymbol{x}',h)d\boldsymbol{x}' = 1. \tag{5}$$

This condition is also termed as *unity condition* since the integration of the smoothing function produces the unity.

The second condition is the *Delta function property* that is observed when the smoothing length approaches zero

$$\lim_{h\to 0} W(\boldsymbol{x}-\boldsymbol{x}',h) = \delta(\boldsymbol{x}-\boldsymbol{x}'). \tag{6}$$

The third condition is the *compact condition*

$$W(\boldsymbol{x}-\boldsymbol{x}',h) = 0 \quad \text{when } |\boldsymbol{x}-\boldsymbol{x}'| > \kappa h, \tag{7}$$

where κ is a constant related to the smoothing function for a particle at $\boldsymbol{x}$, and κh defines the effective (non-zero) area of the smoothing function. This effective area is usually called as the *support domain* of the smoothing function for a point at $\boldsymbol{x}$ (or the support domain of that point). Using this compact condition, integration over the entire problem domain is localized as integration over the support domain of the smoothing function. Therefore, the integration domain Ω can be the same as the support domain.

In the SPH literatures, the kernel approximation is often said to have h^2 accuracy or second order accuracy [46, 47, 49, 75–77]. The observation can be obtained easily using Taylor series expansion on (4). Note from (7) that the support domain of the smoothing function is $|\boldsymbol{x}'-\boldsymbol{x}| \le \kappa h$, the errors in the SPH integral representation can be roughly estimated by using the Taylor series expansion of $f(\boldsymbol{x}')$ around $\boldsymbol{x}$ in (4). If $f(\boldsymbol{x})$ is differentiable, we can get

$$\begin{aligned}\langle f(\boldsymbol{x})\rangle &= \int_\Omega [f(\boldsymbol{x}) + f'(\boldsymbol{x})(\boldsymbol{x}'-\boldsymbol{x}) + r((\boldsymbol{x}'-\boldsymbol{x})^2)] \\ &\quad \times W(\boldsymbol{x}-\boldsymbol{x}',h)d\boldsymbol{x}' \\ &= f(\boldsymbol{x})\int_\Omega W(\boldsymbol{x}-\boldsymbol{x}',h)d\boldsymbol{x}' + f'(\boldsymbol{x})\int_\Omega (\boldsymbol{x}'-\boldsymbol{x}) \\ &\quad \times W(\boldsymbol{x}-\boldsymbol{x}',h)d\boldsymbol{x}' + r(h^2),\end{aligned} \tag{8}$$

where r stands for the residual. Note that W is an even function with respect to $\boldsymbol{x}$, and $(\boldsymbol{x}'-\boldsymbol{x})W(\boldsymbol{x}-\boldsymbol{x}',h)$ should be an odd function. Hence we should have

$$\int_\Omega (\boldsymbol{x}'-\boldsymbol{x})W(\boldsymbol{x}-\boldsymbol{x}',h)d\boldsymbol{x}' = 0. \tag{9}$$

Using (5) and (9), (8) becomes

$$\langle f(\boldsymbol{x})\rangle = f(\boldsymbol{x}) + r(h^2). \tag{10}$$

It is clear that SPH kernel approximation of an arbitrary field function is of second order accuracy.

2.2 Kernel Approximation of Derivatives

The approximation for the spatial derivative $\nabla\cdot f(\boldsymbol{x})$ is obtained simply by substituting $f(\boldsymbol{x})$ with $\nabla\cdot f(\boldsymbol{x})$ in (4), which gives

$$\langle \nabla\cdot f(\boldsymbol{x})\rangle = \int_\Omega [\nabla\cdot f(\boldsymbol{x}')]W(\boldsymbol{x}-\boldsymbol{x}',h)d\boldsymbol{x}', \tag{11}$$

where the divergence in the integral is operated with respect to the primed coordinate. Considering

$$\begin{aligned}&[\nabla\cdot f(\boldsymbol{x}')]W(\boldsymbol{x}-\boldsymbol{x}',h) \\ &\quad = \nabla\cdot[f(\boldsymbol{x}')W(\boldsymbol{x}-\boldsymbol{x}',h)] \\ &\qquad - f(\boldsymbol{x}')\cdot\nabla[W(\boldsymbol{x}-\boldsymbol{x}',h)],\end{aligned} \tag{12}$$

the following equation is obtained

$$\begin{aligned}\nabla\cdot f(\boldsymbol{x}) &= \int_\Omega \nabla\cdot[f(\boldsymbol{x}')W(\boldsymbol{x}-\boldsymbol{x}',h)]d\boldsymbol{x}' \\ &\quad - \int_\Omega f(\boldsymbol{x}')\cdot\nabla[W(\boldsymbol{x}-\boldsymbol{x}',h)]d\boldsymbol{x}'.\end{aligned} \tag{13}$$

The first integral on the right hand side (RHS) of (13) can be converted using the *divergence theorem* into an integral over the surface S of the domain of the integration, Ω, as

$$\begin{aligned}\langle \nabla\cdot f(\boldsymbol{x})\rangle &= \int_S f(\boldsymbol{x}')W(\boldsymbol{x}-\boldsymbol{x}',h)\cdot\vec{\boldsymbol{n}}dS \\ &\quad - \int_\Omega f(\boldsymbol{x}')\cdot\nabla W(\boldsymbol{x}-\boldsymbol{x}',h)d\boldsymbol{x}',\end{aligned} \tag{14}$$

where $\vec{\boldsymbol{n}}$ is the unit vector normal to the surface S. Since the smoothing function W is usually defined to have compact support (see (7)), the value of W on the surface of the integral in (14) is zero in SPH. Therefore, the surface integral on the right hand side of (14) is also zero. Hence, the kernel approximation of the derivatives can be written from (14) as

$$\langle \nabla\cdot f(\boldsymbol{x})\rangle = -\int_\Omega f(\boldsymbol{x}')\cdot\nabla W(\boldsymbol{x}-\boldsymbol{x}',h)d\boldsymbol{x}'. \tag{15}$$

It is clear that the differential operation on a function is transformed into a differential operation on the smoothing function. In other words, the SPH kernel approximation of the derivative of a field function allows the spatial gradient to be determined from the values of the function and the derivatives of the smoothing function W, rather than from the derivatives of the function itself.

Kernel approximation of higher order derivatives can be obtained in a similar way by substituting $f(\boldsymbol{x})$ with the corresponding derivatives in (4), using integration by parts, divergence theorem and some trivial transformations. Another approach is to repeatedly use (15) to obtain the kernel approximation of the higher order derivatives, since any higher order derivative can always be regarded as the first order derivative of its next lower order derivative.

Following similar analyses based on Taylor series expansion, it is easy to show that the kernel approximation of the derivative is also of second order accuracy. Since the SPH kernel approximations for a field function and its derivatives are of second order accuracy, that is why the SPH method has usually been referred as a method of second order accuracy. However, (10) is not always true because (5) and (9) are sometimes not satisfied. For example, in a 1D problem space, if the support domain is within the problem domain under consideration, the integration of the smoothing function is unity (see (5)), and the integration of the first moment of the smoothing function (see (9)) is zero. Also the surface integral in (14) is zero. Hence the SPH kernel approximations are of second order accuracy, and this is shown in Fig. 1.

However, there are scenarios in which the support domain intersects with the problem domain boundary, as shown in Fig. 2. Therefore, the smoothing function W is truncated by the boundary, and the integration of the smoothing function is no longer unity. The integration of the first moment term of the smoothing function and the surface integral in (14) are also no longer zero. At such scenarios, the SPH kernel approximations are not of second order accuracy.

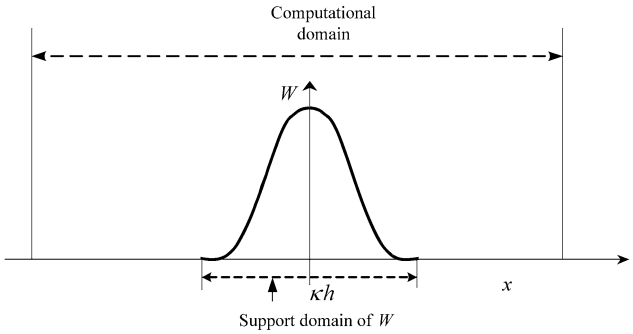

Fig. 1 Schematic illustration of the scenarios in which the support domain is located within the problem domain. For such scenarios, the SPH kernel approximations are of second order accuracy

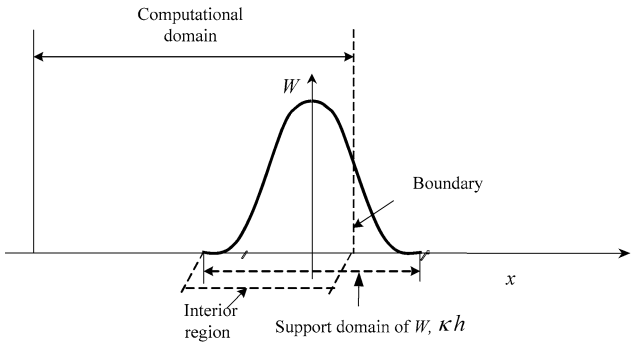

Fig. 2 Schematic illustration of the scenarios in which the support domain intersects with the problem domain. For such scenarios, the SPH kernel approximations are not exactly of second order accuracy

2.3 Particle Approximation

The second step of SPH method is the particle approximation, which involves representing the problem domain using a set of particles, and then estimating field variables on this set of particles. Considering a problem domain Ω filled with a set of particles (usually arbitrarily distributed, see Fig. 3 for illustration in a two-dimensional domain). These particles can either be centered particles initially generated using existing mesh generation tools or concentrated particles initially generated using some kind of space discretization model such as the particle-fill model in AUTODYN [78]. The state of the system is represented by these particles,

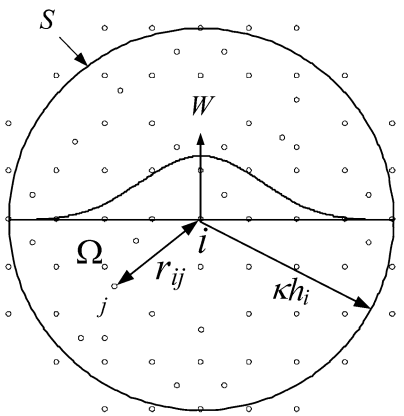

Fig. 3 SPH particle approximations in a two-dimensional problem domain Ω with a surface S. W is the smoothing function that is used to approximate the field variables at particle i using averaged summations over particles j within the support domain with a cut-off distance of κh_i

each associated with field properties. These particles can be used not only for integration, interpolation or differencing, but also for representing the material. The volume of a subsection is lumped on the corresponding particle. Therefore

one particle i is associated with a fixed lumped volume ΔV_i without fixed shape. If the particle mass and density are concerned, the lumped volume can also be replaced with the corresponding mass to density ratio m_i/ρ_i. These particles can be fixed in an Eulerian frame or move in a Lagrangian frame.

After representing the computational domain with a finite number of particles, the continuous form of kernel approximation expressed in (4) can be written in discretized form of a summation of the neighboring particles as follows

$$\langle f(\boldsymbol{x})\rangle = \sum_{j=1}^{N} \frac{m_j}{\rho_j} f(\boldsymbol{x}_j) W(\boldsymbol{x}-\boldsymbol{x}_j, h), \tag{16}$$

where N is the total number of particles within the influence area of the particle at $\boldsymbol{x}$. It is the total number of particles that are within the support domain which has a cut-off distance, characterized by the smoothing length, h, multiplied by a scalar constant κ. This procedure of summation over the neighboring particles is referred to as particle approximation, which states that the value of a function at a particle can be approximated by using the average of the values of the function at all the particles in the support domain weighted by the smoothing function. Following the same procedure, the particle approximation of a derivative can be obtained as

$$\langle \nabla \cdot f(\boldsymbol{x})\rangle = -\sum_{j=1}^{N} \frac{m_j}{\rho_j} f(\boldsymbol{x}_j) \cdot \nabla W(\boldsymbol{x}-\boldsymbol{x}_j, h), \tag{17}$$

where the gradient ∇W in the above equation is evaluated at particle j. Equation (17) states that the value of the gradient of a function at a particle located at $\boldsymbol{x}$ can be approximated by using the summation of those values of the function at all the particles in the support domain weighted by the gradient of the smoothing function. The particle approximation in (16) and (17) converts the continuous form of kernel approximation of a field function and its derivatives to the discrete summations over a set of particles. The use of particle summations to approximate the integral is, in fact, a key approximation that makes the SPH method simple without using a background mesh for numerical integration, and it is also the key factor influencing the solution accuracy of the SPH method.

One important aspect is that the particle approximation in the SPH method introduces the *mass* and *density* of the particle into the equations. This can be conveniently applied to hydrodynamic problems in which the density is a key field variable. This is probably one of the major reasons for the SPH method being particularly popular for dynamic fluid flow problems. If the SPH particle approximation is applied to solid mechanics problems, special treatments are required. One of the ways is to use the SPH approximation to create shape functions, and to establish the discrete system equations [4].

The particle approximation is, however, related to some numerical problems inherent in the SPH method, such as the particle inconsistency and the tensile instability, as will be addressed in the following sections. One basic reason is that the discrete summation is only taken over the particles themselves (collocation). In general, in meshfree methods, to achieve stability and accuracy, the number of sampling points for integration should be more than the field nodes (particles). This is especially true for meshfree methods based on weak forms for solid mechanics problems [4]. Otherwise, it may (not always) lead to some kind of instability problems.

2.4 Techniques for Deriving SPH Formulations

By using the above-described procedure of kernel approximation and particle approximation, SPH formulations for partial differential equations can always be derived. There are in fact a number of ways to derive SPH formulation of PDEs. Benz used one approach to derive the SPH equations for PDEs that is to multiply each term in the PDEs with the smoothing function, and integrate over the volume with the use of integration by parts and Taylor expansions [79]. Monaghan employed a straightforward approach of directly using (16) and (17) [49]. In that approach, the following two identities are employed to place the density inside the gradient operator,

$$\nabla \cdot f(\boldsymbol{x}) = \frac{1}{\rho}[\nabla \cdot (\rho f(\boldsymbol{x})) - f(\boldsymbol{x}) \cdot \nabla \rho], \tag{18}$$

$$\nabla \cdot f(\boldsymbol{x}) = \rho\left[\nabla \cdot \left(\frac{f(\boldsymbol{x})}{\rho}\right) + \frac{f(\boldsymbol{x})}{\rho^2} \cdot \nabla \rho\right]. \tag{19}$$

The above two identities may be substituted into the integral in (11). The same procedure of the particle approximation to obtain (17) is applied to each gradient term on the right hand side of (18) and (19). Note that each expression at the outside of every gradient term is evaluated at the particle itself, the results from (18) and (19) for the divergence of $f(\boldsymbol{x})$ at particle i are obtained as

$$\langle \nabla \cdot f(\boldsymbol{x}_i)\rangle = \frac{1}{\rho_i}\left[\sum_{j=1}^{N} m_j [f(\boldsymbol{x}_j) - f(\boldsymbol{x}_i)] \cdot \nabla_i W_{ij}\right], \tag{20}$$

and

$$\langle \nabla \cdot f(\boldsymbol{x}_i)\rangle = \rho_i\left[\sum_{j=1}^{N} m_j \left[\left(\frac{f(\boldsymbol{x}_j)}{\rho_j^2}\right) + \left(\frac{f(\boldsymbol{x}_i)}{\rho_i^2}\right)\right] \cdot \nabla_i W_{ij}\right]. \tag{21}$$

One of the good features for the above two equations is that the field function $f(\boldsymbol{x})$ appears pairwisely and involves

asymmetric and symmetric SPH formulations. These asymmetric and symmetric formulations can help to improve the numerical accuracy in SPH simulations [6, 49, 56].

Besides the above-mentioned two identities, some other rules of operation can be convenient in deriving the SPH formulations for complex system equations [6]. For example, for two arbitrary functions of field variables f_1 and f_2, the following rules exist.

$$\langle f_1 \pm f_2 \rangle = \langle f_1 \rangle \pm \langle f_2 \rangle, \tag{22}$$

$$\langle f_1 f_2 \rangle = \langle f_1 \rangle \langle f_2 \rangle. \tag{23}$$

Hence, an SPH approximation of the sum of functions equals to the sum of the SPH approximations of the individual function, and an SPH approximation of a product of functions equals to the product of the SPH approximations of the individual functions.

If f_1 is a constant denoted by c, we should have

$$\langle c f_2 \rangle = c \langle f_2 \rangle. \tag{24}$$

It is clear that the SPH approximation operator is a linear operator. It is also easy to show that the SPH approximation operator is commutative, i.e.,

$$\langle f_1 + f_2 \rangle = \langle f_2 + f_1 \rangle, \tag{25}$$

and

$$\langle f_1 f_2 \rangle = \langle f_2 f_1 \rangle. \tag{26}$$

For convenience, the SPH approximation operator "$\langle\,\rangle$" is omitted in later sections.

2.5 SPH Formulations for Navier-Stokes (N-S) Equations

Using the afore-mentioned kernel and particle approximation techniques with necessary numerical tricks, it is possible to derive SPH formulations for partial differential equations governing the physics of fluid flows. For example, for Navier-Stokes equations controlling the general fluid dynamic problems, we have

$$\begin{cases} \frac{D\rho}{Dt} = -\rho \frac{\partial \boldsymbol{v}^\beta}{\partial \boldsymbol{x}^\beta}, \\ \frac{D\boldsymbol{v}^\alpha}{Dt} = \frac{1}{\rho} \frac{\partial \sigma^{\alpha\beta}}{\partial \boldsymbol{x}^\beta} + F, \\ \frac{De}{Dt} = \frac{\sigma^{\alpha\beta}}{\rho} \frac{\partial \boldsymbol{v}^\alpha}{\partial \boldsymbol{x}^\beta}, \end{cases} \tag{27}$$

where the Greek superscripts α and β are used to denote the coordinate directions, the summation in the equations is taken over repeated indices, and the total time derivatives are taken in the moving Lagrangian frame. The scalar density ρ, and internal energy e, the velocity component $\boldsymbol{v}^\alpha$, and the total stress tensor $\sigma^{\alpha\beta}$ are the dependent variables. F is the external forces such as gravity. The spatial coordinates $\boldsymbol{x}^\alpha$ and time t are the independent variables. The total stress tensor $\sigma^{\alpha\beta}$ is made up of two parts, one part of isotropic pressure p and the other part of viscous stress τ, i.e., $\sigma^{\alpha\beta} = -p\delta^{\alpha\beta} + \tau^{\alpha\beta}$. For Newtonian fluids, the viscous shear stress should be proportional to the shear strain rate denoted by ε through the dynamic viscosity μ, i.e., $\tau^{\alpha\beta} = \mu\varepsilon^{\alpha\beta}$, where

$$\varepsilon^{\alpha\beta} = \frac{\partial \boldsymbol{v}^\beta}{\partial \boldsymbol{x}^\alpha} + \frac{\partial \boldsymbol{v}^\alpha}{\partial \boldsymbol{x}^\beta} - \frac{2}{3}(\nabla \cdot \boldsymbol{v})\delta^{\alpha\beta}.$$

Substituting the SPH approximations for a function and its derivative (as shown in (16) and (17)) to the N-S equations, the SPH equations of motion for the N-S equations can be written as

$$\begin{cases} \frac{D\rho_i}{Dt} = \sum_{j=1}^N m_j \boldsymbol{v}_{ij}^\beta \frac{\partial W_{ij}}{\partial \boldsymbol{x}_i^\beta}, \\ \frac{D\boldsymbol{v}_i^\alpha}{Dt} = -\sum_{j=1}^N m_j \left(\frac{\sigma_i^{\alpha\beta}}{\rho_i^2} + \frac{\sigma_j^{\alpha\beta}}{\rho_j^2} \right) \frac{\partial W_{ij}}{\partial \boldsymbol{x}_i^\beta} + F_i, \\ \frac{De_i}{Dt} = \frac{1}{2} \sum_{j=1}^N m_j \left(\frac{p_i}{\rho_i^2} + \frac{p_j}{\rho_j^2} \right) \boldsymbol{v}_{ij}^\beta \frac{\partial W_{ij}}{\partial \boldsymbol{x}_i^\beta} + \frac{\mu_i}{2\rho_i} \varepsilon_i^{\alpha\beta} \varepsilon_i^{\alpha\beta}, \end{cases} \tag{28}$$

where $\boldsymbol{v}_{ij} = \boldsymbol{v}_i - \boldsymbol{v}_j$. Equation (28) is a set of commonly used SPH equations for the N-S equations. It should be noted that by using different numerical tricks, it is possible to get other different forms of SPH equations for the same partial differential equations. The obtained SPH formulations may have special features and advantages suitable for different applications [6]. One typical example is the approximation of density. If the field function is the density, (16) can be re-written as

$$\rho_i = \sum_{j=1}^N m_j W_{ij}. \tag{29}$$

This is another approach to obtain density directly from the SPH summation of the mass of all particles in the support domain of a given particle, rather than from the continuum equation. Compared to the SPH formulations on density change in (28), this summation density approach conserves mass exactly, but suffers from serious boundaries deficiency due to the particle inconsistency. A frequently used way to remediate the boundaries deficiency is the following normalization form by the summation of the smoothing function itself [52, 53]

$$\rho_i = \frac{\sum_{j=1}^N m_j W_{ij}}{\sum_{j=1}^N (\frac{m_j}{\rho_j}) W_{ij}}. \tag{30}$$

3 SPH Smoothing Function

3.1 Review on Commonly Used Smoothing Functions

One of the central issues for meshfree methods is how to effectively perform function approximation based on a set of

nodes scattered in an arbitrary manner without using a predefined mesh or grid that provides the connectivity of the nodes. In the SPH method, the smoothing function is used for kernel and particle approximations. It is of utmost importance in the SPH method as it determines the pattern to interpolate, and defines the cut-off distance of the influencing area of a particle.

Many researchers have investigated the smoothing kernel, hoping to improve the performance of the SPH method, and/or to generalize the requirements for constructing the smoothing kernel function. Fulk numerically investigated a number of smoothing kernel functions in one-dimensional space, and the obtained results are basically valid for regularly distributed particles [39, 75]. Swegle et al. revealed the tensile instability, which is closely related to the smoothing kernel function [45]. Morris studied the performances of several different smoothing functions, and found that by properly selecting the smoothing function, the accuracy and stability property of the SPH simulation can be improved [46, 80]. Omang provided investigations on alternative kernel functions for SPH in cylindrical symmetry [81]. Jin and Ding investigated the criterions for smoothed particle hydrodynamics kernels in stable field [82]. Capuzzo-Dolcetta gave a criterion for the choice of the interpolation kernel in SPH [83]. Cabezon and his co-workers proposed a one-parameter family of interpolating kernels for SPH studies [84].

Different smoothing functions have been used in the SPH method as shown in published literatures. Various requirements or properties for the smoothing functions have been discussed. Major properties or requirements are now summarized and described in the following discussion.

1. The smoothing function must be normalized over its support domain (*Unity*)

$$\int_{\Omega} W(\boldsymbol{x}-\boldsymbol{x}', h)d\boldsymbol{x}' = 1. \tag{31}$$

This normalization property ensures that the integral of the smoothing function over the support domain to be unity. It can be shown in the next section that it also ensures the zero-th order consistency (C^0) of the integral representation of a continuum function.

2. The smoothing function should be compactly supported (*Compact support*), i.e.,

$$W(\boldsymbol{x}-\boldsymbol{x}') = 0, \quad \text{for } |\boldsymbol{x}-\boldsymbol{x}'| > \kappa h. \tag{32}$$

The dimension of the compact support is defined by the smoothing length h and a scaling factor κ, where h is the smoothing length, and κ determines the spread of the specified smoothing function. $|\boldsymbol{x}-\boldsymbol{x}'| \leq \kappa h$ defines the support domain of the particle at point $\boldsymbol{x}$. This compact supportness property transforms an SPH approximation from a global operation to a local operation. This will later lead to a set of sparse discretized system matrices, and therefore is very important as far as the computational efforts are concerned.

3. $W(\boldsymbol{x}-\boldsymbol{x}') \geq 0$ for any point at $\boldsymbol{x}'$ within the support domain of the particle at point $\boldsymbol{x}$ (*Positivity*). This property states that the smoothing function should be non-negative in the support domain. It is not mathematically necessary as a convergent condition, but it is important to ensure a meaningful (or stable) representation of some physical phenomena. A few smoothing functions used in some literatures are negative in parts of the support domain. However in hydrodynamic simulations, negative value of the smoothing function can have serious consequences that may result in some unphysical parameters such as negative density and energy.
4. The smoothing function value for a particle should be monotonically decreasing with the increase of the distance away from the particle (*Decay*). This property is based on the physical consideration in that a nearer particle should have a bigger influence on the particle under consideration. In other words, with the increase of the distance of two interacting particles, the interaction force decreases.
5. The smoothing function should satisfy the Dirac delta function condition as the smoothing length approaches zero (*Delta function property*)

$$\lim_{h\to 0} W(\boldsymbol{x}-\boldsymbol{x}', h) = \delta(\boldsymbol{x}-\boldsymbol{x}'). \tag{33}$$

This property makes sure that as the smoothing length tends to be zero, the approximation value approaches the function value, i.e. $\langle f(\boldsymbol{x})\rangle = f(\boldsymbol{x})$.

6. The smoothing function should be an even function (*Symmetric property*). This means that particles from same distance but different positions should have equal effect on a given particle. This is not a very rigid condition, and it is sometimes violated in some meshfree particle methods that provide higher consistency.
7. The smoothing function should be sufficiently smooth (*Smoothness*). This property aims to obtain better approximation accuracy. For the approximations of a function and its derivatives, a smoothing function needs to be sufficiently continuous to obtain good results. A smoothing function with smoother value of the function and derivatives would usually yield better results and better performance in numerical stability. This is because the smoothing function will not be sensitive to particle disorder, and the errors in approximating the integral interpolants are small, provided that the particle disorder is not extreme [6, 49, 75].

Any function having the above properties may be employed as SPH smoothing functions, and many kinds of

smoothing functions have been used. Lucy in the original SPH paper [36] used a bell-shaped function

$$W(\boldsymbol{x}-\boldsymbol{x}',h) = W(R,h) = \alpha_d \begin{cases} (1+3R)(1-R)^3, & R \le 1, \\ 0, & R > 1, \end{cases} \tag{34}$$

where α_d is $5/4h$, $5/\pi h^2$ and $105/16\pi h^3$ in one-, two- and three-dimensional space, respectively, so that the condition of unity can be satisfied for all the three dimensions. R is the relative distance between two points (particles) at points $\boldsymbol{x}$ and $\boldsymbol{x}'$, $R = \frac{r}{h} = \frac{|\boldsymbol{x}-\boldsymbol{x}'|}{h}$, where r is the distance between the two points.

Gingold and Monaghan in their original paper [37] selected the following Gaussian kernel to simulate the non-spherical stars

$$W(R,h) = \alpha_d e^{-R^2}, \tag{35}$$

where α_d is $1/\pi^{1/2}h$, $1/\pi h^2$ and $1/\pi^{3/2}h^3$, respectively, in one-, two- and three-dimensional space, for the unity requirement. The Gaussian kernel is sufficiently smooth even for high orders of derivatives, and is regarded as a "golden" selection since it is very stable and accurate especially for disordered particles. It is, however, not really compact, as it never goes to zero theoretically, unless R approaches infinity. Because it approaches zero numerically very fast, it is practically compact. Note that it is computationally more expensive since it can take a longer distance for the kernel to approach zero. This can result in a large support domain with more particles for particle approximations.

The most frequently used smoothing function may be the cubic B-spline function, which was originally used by Monaghan and Lattanzio [85]

$$W(R,h) = \alpha_d \times \begin{cases} \frac{2}{3} - R^2 + \frac{1}{2}R^3, & 0 \le R < 1, \\ \frac{1}{6}(2-R)^3, & 1 \le R < 2, \\ 0, & R \ge 2. \end{cases} \tag{36}$$

In one-, two- and three-dimensional space, $\alpha_d = 1/h$, $15/7\pi h^2$ and $3/2\pi h^3$, respectively. The cubic spline function has been the most widely used smoothing function in the emerged SPH literatures since it closely resembles a Gaussian function while having a narrower compact support. However, the second derivative of the cubic spline is a piecewise linear function, and accordingly, the stability properties can be inferior to those of smoother kernels.

Morris has introduced higher order (quartic and quintic) splines that are more closely approximating the Gaussian and more stable [46, 80]. The quartic spline is

$$W(R,h) = \alpha_d \times \begin{cases} (R+2.5)^4 - 5(R+1.5)^4 + 10(R+0.5)^4, & 0 \le R < 0.5, \\ (2.5-R)^4 - 5(1.5-R)^4, & 0.5 \le R < 1.5, \\ (2.5-R)^4, & 1.5 \le R < 2.5, \\ 0, & R > 2.5, \end{cases} \tag{37}$$

where α_d is $1/24h$ in one-dimensional space. The quintic spline is

$$W(R,h) = \alpha_d \times \begin{cases} (3-R)^5 - 6(2-R)^5 + 15(1-R)^5, & 0 \le R < 1, \\ (3-R)^5 - 6(2-R)^5, & 1 \le R < 2, \\ (3-R)^5, & 2 \le R < 3, \\ 0, & R > 3, \end{cases} \tag{38}$$

where α_d is $120/h$, $7/478\pi h^2$ and $3/359\pi h^3$ in one-, two- and three-dimensional space, respectively.

Johnson et al. used the following quadratic smoothing function to simulate high velocity impact problems [86]

$$W(R,h) = \alpha_d \left(\frac{3}{16}R^2 - \frac{3}{4}R + \frac{3}{4} \right), \quad 0 \le R \le 2, \tag{39}$$

where in one-, two- and three-dimensional space, $\alpha_d = 1/h$, $2/\pi h^2$ and $5/4\pi h^3$, respectively. Unlike other smoothing functions, the derivative of this quadratic smoothing function always increases as the particles move closer, and always decreases as they move apart. This was regarded by the authors as an important improvement over the cubic spline function, and it was reported to relieve the problem of compressive instability.

Some higher order smoothing functions that are devised from lower order forms have been constructed, such as the super-Gaussian kernel [85]

$$W(R,h) = \alpha_d \left(\frac{3}{2} - R^2 \right) e^{-R^2}, \quad 0 \le R \le 2, \tag{40}$$

where α_d is $1/\sqrt{\pi}$ in one-dimensional space. One disadvantage of the high order smoothing function is that the kernel is negative in some region of its support domain. This may lead to unphysical results for hydrodynamic problems [75].

The smoothing function has been studied mathematically in detail by Liu and his co-workers. They proposed a systematical way to construct a smoothing function that may meet different needs [38]. A new quartic smoothing function has been constructed to demonstrate the effectiveness of the approach for constructing a smoothing function as follows.

$$W(R,h) = \alpha_d \begin{cases} (\frac{2}{3} - \frac{9}{8}R^2 + \frac{19}{24}R^3 - \frac{5}{32}R^4), & 0 \le R \le 2, \\ 0, & R > 2, \end{cases} \tag{41}$$

where α_d is $1/h$, $15/7\pi h^2$ and $315/208\pi h^3$ in one-, two- and three-dimensional space, respectively. Note that the centre peak value of this quartic smoothing function is defined as 2/3. The quartic smoothing function behaves very much like the widely used cubic B-spline function given in (36), but has only one piece, and hence is much more convenient and efficient to use. More discussions on this quartic smoothing function will give in the next section.

3.2 Generalizing Constructing Conditions

Major requirements of an SPH smoothing function have been addressed in Sect. 3.1. Some of these requirements can be derived by conducting Taylor series analysis. This analysis is carried out at the stage of the SPH kernel approximation for a function and its derivatives. It shows that, to exactly approximate a function and its derivatives, certain conditions need to be satisfied. These conditions can then be used to construct the smoothing functions.

Considering the SPH kernel approximation for a field function $f(\boldsymbol{x})$ as show in (4), if $f(\boldsymbol{x})$ is sufficiently smooth, applying Taylor series expansion of $f(\boldsymbol{x}')$ in the vicinity of $\boldsymbol{x}$ yields

$$\begin{aligned} f(\boldsymbol{x}') &= f(\boldsymbol{x}) + f'(\boldsymbol{x})(\boldsymbol{x}'-\boldsymbol{x}) + \frac{1}{2}f''(\boldsymbol{x})(\boldsymbol{x}'-\boldsymbol{x})^2 + \cdots \\ &= \sum_{k=0}^{n} \frac{(-1)^k h^k f^{(k)}(\boldsymbol{x})}{k!}\left(\frac{\boldsymbol{x}-\boldsymbol{x}'}{h}\right)^k \\ &\quad + r_n\left(\frac{\boldsymbol{x}-\boldsymbol{x}'}{h}\right), \end{aligned} \tag{42}$$

where r_n is the remainder of the Taylor series expansion. Substituting (42) into (4) leads to

$$f(\boldsymbol{x}) = \sum_{k=0}^{n} A_k f^{(k)}(\boldsymbol{x}) + r_n\left(\frac{\boldsymbol{x}-\boldsymbol{x}'}{h}\right), \tag{43}$$

where

$$A_k = \frac{(-1)^k h^k}{k!}\int_\Omega \left(\frac{\boldsymbol{x}-\boldsymbol{x}'}{h}\right)^k W(\boldsymbol{x}-\boldsymbol{x}', h)d\boldsymbol{x}'. \tag{44}$$

Comparing the LHS with the RHS of (43), in order for $f(\boldsymbol{x})$ to be approximated to n-th order, the coefficients A_k must equal to the counterparts for $f^{(k)}(\boldsymbol{x})$ at the LHS of (43). Therefore, after trivil transformation, the following conditions for the smoothing function W can be obtained as follows

$$\left.\begin{aligned} M_0 &= \textstyle\int_\Omega W(\boldsymbol{x}-\boldsymbol{x}', h)d\boldsymbol{x}' = 1 \\ M_1 &= \textstyle\int_\Omega (\boldsymbol{x}-\boldsymbol{x}')W(\boldsymbol{x}-\boldsymbol{x}', h)d\boldsymbol{x}' = 0 \\ M_2 &= \textstyle\int_\Omega (\boldsymbol{x}-\boldsymbol{x}')^2 W(\boldsymbol{x}-\boldsymbol{x}', h)d\boldsymbol{x}' = 0 \\ &\vdots \\ M_n &= \textstyle\int_\Omega (\boldsymbol{x}-\boldsymbol{x}')^n W(\boldsymbol{x}-\boldsymbol{x}', h)d\boldsymbol{x}' = 0 \end{aligned}\right\}, \tag{45}$$

where M_k is the k-th moments of the smoothing function. Note that the first equation in (45) is, in fact, the unity condition expressed in (31), and the second equation in (45) stands for the symmetric property. Satisfaction of these two conditions ensures the first order consistency for the SPH kernel approximation for a function.

Also performing Taylor series analysis for the SPH kernel approximation of the derivatives of a field function $f(\boldsymbol{x})$, using the concept of integration by parts, and divergence theorem with some trivial transformation, the following equations

$$W(\boldsymbol{x}-\boldsymbol{x}', h)|_S = 0 \tag{46}$$

and

$$\left.\begin{aligned} M'_0 &= \textstyle\int_\Omega W'(\boldsymbol{x}-\boldsymbol{x}', h)d\boldsymbol{x}' = 0 \\ M'_1 &= \textstyle\int_\Omega (\boldsymbol{x}-\boldsymbol{x}')W'(\boldsymbol{x}-\boldsymbol{x}', h)d\boldsymbol{x}' = 1 \\ M'_2 &= \textstyle\int_\Omega (\boldsymbol{x}-\boldsymbol{x}')^2 W'(\boldsymbol{x}-\boldsymbol{x}', h)d\boldsymbol{x}' = 0 \\ &\vdots \\ M'_n &= \textstyle\int_\Omega (\boldsymbol{x}-\boldsymbol{x}')^n W'(\boldsymbol{x}-\boldsymbol{x}', h)d\boldsymbol{x}' = 0 \end{aligned}\right\} \tag{47}$$

can be obtained. Equation (46) actually specifies that the smoothing function vanishes on the surface of the support domain. This is compatible to the compactness condition of the smoothing function. Equation (47) defines the conditions with which the derivatives of the smoothing function should be satisfied. Note that (45) and (47) are actually compatible considering integration by parts, divergence theorem and the boundary value vanishing effects (see (46)) of the smoothing function.

Performing Taylor series analysis on the SPH kernel approximation for the second derivatives, similar equations can be obtained. Except for the requirements on the second derivatives of the momentums, the first derivative of the smoothing function also needs to vanish on the surface, which is

$$W'(\boldsymbol{x}-\boldsymbol{x}', h)|_S = 0. \tag{48}$$

Equations (45)–(48) can be used to construct smoothing functions. It can be seen that the conditions of smoothing functions can be classified into two groups. The first group shows the ability of a smoothing function to reproduce polynomials. Satisfying the first group, the function can be approximated to n-th order accuracy. The second group defines the surface values of a smoothing function as well as its first derivatives, and is the requirements of the property of compact support for the smoothing function and its first derivative. Satisfying these conditions, the first two derivatives of the function can be exactly approximated to the n-th order.

3.3 Constructing SPH Smoothing Functions

By using above-mentioned conditions, it is possible to have a systematic way to construct the SPH smoothing functions. If the smoothing function is assumed to be a polynomial dependent only on the relative distance of the concerned points, it can be assumed to have the following form in the support domain with an influence width of κh.

$$W(\boldsymbol{x}-\boldsymbol{x}',h)=W(R)=a_0+a_1R+a_2R^2+\cdots+a_nR^n. \tag{49}$$

It is clear that a smoothing function in the above-mentioned form is a distance function since it depends on the relative distance. It is easy to show that for the second derivative of the smoothing function to exist, a_1 should vanish. Substituting this polynomial form smoothing function into the conditions (see (45)–(48)), the parameters $a_0, a_2, \ldots, a_n$ can be calculated from the resultant linear equations, and then the smoothing function can be determined.

There are several issues that need further consideration. Firstly, a smoothing function derived from this set of conditions (see (45)) will not necessarily be positive in the entire support domain, especially when high order reproducibility is required. Such a negative smoothing function may result in unphysical solutions, for example, negative density (mass) and negative energy. For this reason, smoothing functions used in SPH literatures are generally non-negative for CFD problems. On the other hand, for the even moments ($k=2,4,6,\ldots$) to be zero, a smoothing function has to be negative in some parts of the region. This implies that one cannot have both non-negativity and high-order reproducibility at the same time.

Secondly, in constructing a smoothing function, the center peak value is a factor that needs to be considered. The center peak value of a smoothing function is very important since it determines how much the particle itself will contribute to the approximation. Revisiting (45), if a positive smoothing function is used, the highest order of accuracy for the function approximation is second order. Therefore, the second momentum ($M_2=\int_\Omega(\boldsymbol{x}-\boldsymbol{x}')^2W(\boldsymbol{x}-\boldsymbol{x}',h)d\boldsymbol{x}'$) can be used as a rough indicator to measure the accuracy of the kernel approximation. The smaller the second moment M_2 is, the more accurate the kernel approximation is. The center peak value of a smoothing function is closely related to M_2. A positive smoothing function with a large center peak value will have a smaller second moment M_2. This implies that a smoothing function is closer to the Delta function, and therefore is more accurate in terms of kernel approximations.

Thirdly, in some circumstances, a piecewise smoothing function is preferable since the shape of the piecewise smoothing function is easier to be controlled by changing the number of the pieces and the locations of the connection points. For example, consider the general form of a smoothing function with two pieces,

$$W(R)=\begin{cases}W_1(R), & 0\le R<R_1,\\ W_2(R), & R_1\le R<R_2,\\ 0 & R_2\le R.\end{cases} \tag{50}$$

The function itself and the first two derivatives at the connection points should be continuous, i.e., $W_1(R_1)=W_2(R_1)$, $W_1'(R_1)=W_2'(R_1)$ and $W_1''(R_1)=W_2''(R_1)$. Considering the requirements at these points as well as the compact support property, one possible form of the smoothing function is

$$W(R)=\alpha_d\begin{cases}b_1(R_1-R)^n+b_2(R_2-R)^n, & 0\le R<R_1,\\ b_2(R_2-R)^n, & R_1\le R<R_2,\\ 0, & R_2\le R.\end{cases} \tag{51}$$

It is also feasible to construct smoothing function with more pieces using similar expressions.

To show the effectiveness of this approach to constructing general SPH smoothing functions Liu et al. [38] derived a new quartic smoothing function using the following conditions

- the unity condition,
- compact support of the smoothing function,
- compact support of the first derivative of the smoothing function,
- centre peak value.

The constructed smoothing function is given as $W(R,h)=\alpha_d(\frac{2}{3}-\frac{9}{8}R^2+\frac{19}{24}R^3-\frac{5}{32}R^4)$, for $0\le R\le 2$, where α_d is $1/h$, $15/7\pi h^2$ and $315/208\pi h^3$ in one-, two- and three-dimensional space, respectively. Note that the centre peak value of this quartic smoothing function is defined as $2/3$.

As defined, this quartic function satisfies the normalization condition, while the function itself and its first derivative have compact support. It is very close to the most commonly used cubic spline (see (36)) with a same center peak value of $2/3$, and monotonically decreases with the increase of the distance as show in Fig. 4. However, this quartic function produces a smaller second momentum than the cubic spline function, and therefore can produce better accuracy for kernel approximation. Also this quartic smoothing function has a smoother second derivative than the cubic spline smoothing function, thus the stability properties should be superior to those of the cubic spline function, as reported by many researchers that a smoother second derivative can lead to less instability in SPH simulation [80, 87].

4 Consistency

In early studies, the SPH method has usually been reported to have second order accuracy. This is reasonable, as the ker-

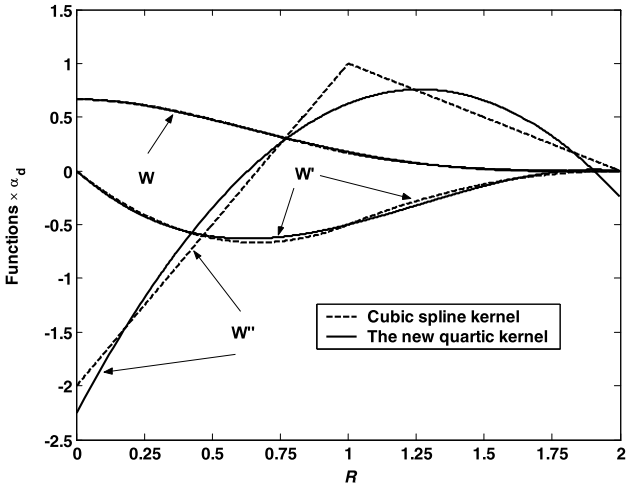

Fig. 4 The quartic smoothing function constructed by Liu et al. by using the smoothing function constructing conditions [38]. The shapes of the quartic function and its first derivative are very close to the shapes of the cubic spline function and its first derivative. However, this one piece smoothing function is expected to produce better accuracy as it has smaller second momentum. It is also expected to be more stable since it has a continuous second derivative

nel approximation of a field function has a remainder of second order (see (8)). However, the kernel approximation of a function and/or its derivatives may not necessarily be of second order accuracy as the smoothing function may not be an even function since it is truncated when approaching the boundary region. Moreover, high order accuracy of the kernel approximation does not necessarily mean high order accuracy of the SPH simulations, as it is the particle approximation rather than the kernel approximation that eventually determines the accuracy of the SPH simulations.

Following the Lax-Richtmyer equivalence theorem, we know that if a numerical model is stable, the convergence of the solution to a well-posed problem will then be determined by the consistency of the function approximation. Therefore the consistency of SPH approximation is crucial. In finite element method, to ensure the accuracy and convergence of an FEM approximation, the FEM shape function must satisfy a certain degree of consistency. The degree of consistency can be characterized by the order of the polynomial that can be exactly reproduced by the approximation using the shape function. In general, if an approximation can reproduce a polynomial up to k-th order exactly, the approximation is said to have k-th order consistency or C^k consistency. The concept of consistency from traditional finite element methods can also be used for meshfree particle methods such as smoothed particle hydrodynamics [3, 6, 13, 72, 74, 88]. Therefore it is similarly feasible to investigate the consistency of SPH kernel and particle approximations in reproducing a polynomial by using the smoothing function.

4.1 Consistency in Kernel Approximation (Kernel Consistency)

For a constant (0th order polynomial) function $f(\boldsymbol{x}) = c$ (where c is a constant) to be exactly reproduced by the SPH kernel approximation, following (1), we require

$$f(\boldsymbol{x}) = \int cW(\boldsymbol{x} - \boldsymbol{x}', h)d\boldsymbol{x}' = c, \tag{52}$$

or

$$\int W(\boldsymbol{x} - \boldsymbol{x}', h)d\boldsymbol{x}' = 1. \tag{53}$$

Equation (53) is exactly the normalization condition described previously.

Further, for a linear function $f(\boldsymbol{x}) = c_0 + c_1\boldsymbol{x}$ (where c_0 and c_1 are constants) to be exactly reproduced, we must have

$$f(\boldsymbol{x}) = \int (c_0 + c_1\boldsymbol{x}')W(\boldsymbol{x} - \boldsymbol{x}', h)d\boldsymbol{x}' = c_0 + c_1\boldsymbol{x}. \tag{54}$$

Using (52), (54) can be simplified as

$$\int \boldsymbol{x}'W(\boldsymbol{x} - \boldsymbol{x}', h)d\boldsymbol{x}' = \boldsymbol{x}. \tag{55}$$

Multiplying $\boldsymbol{x}$ to both side of (53), we have the following identity

$$\int \boldsymbol{x}W(\boldsymbol{x} - \boldsymbol{x}', h)d\boldsymbol{x}' = \boldsymbol{x}. \tag{56}$$

Subtracting (55) from the above identity yields

$$\int (\boldsymbol{x} - \boldsymbol{x}')W(\boldsymbol{x} - \boldsymbol{x}', h)d\boldsymbol{x}' = 0. \tag{57}$$

Equation (57) is the symmetric condition described in Sect. 3.1.

More generally, by performing Taylor series analyses on the kernel approximation of a function $f(\boldsymbol{x})$ $(= \int f(\boldsymbol{x}')W(\boldsymbol{x} - \boldsymbol{x}', h)d\boldsymbol{x}')$ in a one-dimensional space, we have already obtained a set of requirements of the smoothing function in Sect. 3.2, as expressed in (45). Equations (53) (normalization condition) and (57) (symmetric condition) are actually components in (45), which describes the 0th and 1st moments.

For the integrations expressed in (45), the integration domain is assumed to be a fully continuous support domain that is not truncated by the boundaries. Equation (45) states the requirements on the moments of a smoothing function to reproduce certain order of polynomials.

Equation (45) can thus be used as an approximation accuracy indicator. If a smoothing function satisfies (45), a function can be approximated to n-th order accuracy. Furthermore the 0th moment in (45) states the normalization

condition, and the 1st moment states the symmetry property of the smoothing function.

Similar to the consistency concept in the traditional FEM, if an SPH approximation can reproduce a polynomial of up to nth order exactly, the SPH approximation is said to have nth order or C^n consistency. If the consistency of an SPH kernel approximation in continuous form is termed as *kernel consistency*, the kernel consistency of an SPH kernel approximation is of nth order when the smoothing function satisfies (45). Therefore the expressions in (45) are also the kernel consistency conditions of the smoothing function for an SPH kernel approximation.

Note that if the SPH kernel approximations are carried out for regions truncated by boundaries, constant and linear functions can not be reproduced exactly since (53) and (57) are not satisfied for these regions. Therefore we can conclude that, since a conventional smoothing function satisfies the normalization and symmetric conditions, the conventional SPH method has up to C^1 consistency for the interior regions. However, for the boundary regions, it even does not have C^0 kernel consistency.

4.2 Consistency in Particle Approximation (Particle Consistency)

Satisfying the consistency conditions at the kernel approximation stage does not necessarily mean that the discretized SPH model will have such a consistency. This is because such a consistency can be distorted by the particle approximation process in discrete SPH model. Therefore, the consistency analysis should be conducted for the discrete SPH model in the particle approximation process, and this consistency can be termed as *particle consistency*.

The discrete counterparts of the constant and linear consistency conditions as expressed in (53) and (57) are

$$\sum_{j=1}^{N} W(\boldsymbol{x}-\boldsymbol{x}_j,h)\Delta v_j = 1, \tag{58}$$

and

$$\sum_{j=1}^{N} (\boldsymbol{x}-\boldsymbol{x}_j) W(\boldsymbol{x}-\boldsymbol{x}_j,h)\Delta v_j = 0. \tag{59}$$

These discretized consistency conditions are not satisfied in general. One obvious and simple example is the particle approximations at the boundary particles (Fig. 5a). Even for uniform particle distribution, due to the unbalanced particles contributing to the discretized summation, the LHS of (58) is smaller than 1 and the LHS of (59) will not vanish, due to the truncation of the smoothing function by the boundary. For cases with irregularly distributed particles (Fig. 5b), it is also easy to verify that even for the interior particles

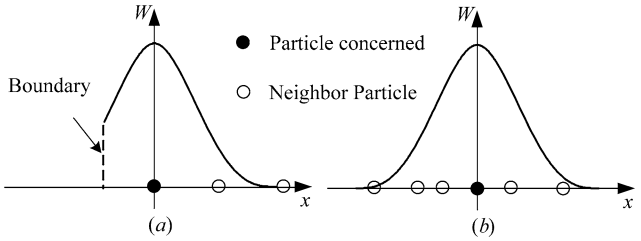

Fig. 5 SPH particle approximations in one-dimensional cases. (**a**) Particle approximation for a particle whose support domain is truncated by the boundary. (**b**) Particle approximation for a particle with irregular particle distribution in its support domain

whose support domains are not truncated, the constant and linear consistency conditions in discretized forms may not be exactly satisfied. Therefore the original SPH method does not even have C^0 consistency in the particle approximation. It is clear that the inconsistency caused by the particle approximation is closely related to the corresponding kernel approximation and particles involved in the approximation. Such an inconsistency problem results in directly the solution inaccuracy in the original SPH method.

Besides the particle approximation features associated with boundary particles or irregular distributed particles, the choice of the smoothing length is also important in the particle approximation process. In a one-dimensional domain with the cubic spline smoothing function, it is easy to verify that for uniformly distributed interior particles, the original SPH method has C^0 particle consistency if the smoothing length is taken exactly as the particle spacing ($h = \Delta x$) since (58) is satisfied. However, varying the smoothing length can results in a dissatisfaction of (58), leading to poor accuracy in the original SPH method. This is a reason why we often need to examine the influence of the smoothing length on the SPH approximation results.

In summary, the original SPH models, in general, do not have even C^0 consistency. Such an inconsistency originates from the discrepancy between the SPH kernel and particle approximations. Boundary particles, irregular distributed particles, and variable smoothing length can usually produce inconsistency in the particle approximation process. In the next section, we discuss ways to restore the consistency in SPH models.

4.3 Review on Approaches for Restoring Consistency

It has been shown that the original SPH method even does not have 0th particle consistency. Different approaches have been proposed to improve the particle inconsistency and hence the SPH approximation accuracy. Some of them involve reconstruction of a new smoothing function so as to satisfy the discretized consistency conditions. However, these approaches are usually not preferred for hydrodynamic simulations because the reconstructed smoothing function

can be partially negative, non-symmetric, and not monotonically decreasing. Approaches which improve the particle consistency without changing the conventional smoothing function are usually more preferable in simulating hydrodynamics.

One early approach [49, 52] is based on the anti-symmetric assumption of the derivative of a smoothing function

$$\sum_{j=1}^{N} W_{i,\alpha}\Delta v_j = 0, \tag{60}$$

where $W_{i,\alpha} = \partial W_i(\boldsymbol{x})/\partial \boldsymbol{x}^{\alpha}$, in which α is the dimension index repeated from 1 to d (d is the number of dimensions). Therefore when approximating the derivative of a function f, the particle approximation can be rewritten as

$$f_{i,\alpha} = \sum_{j=1}^{N}(f_j - f_i)W_{i,\alpha}\Delta v_j, \tag{61}$$

or

$$f_{i,\alpha} = \sum_{j=1}^{N}(f_j + f_i)W_{i,\alpha}\Delta v_j. \tag{62}$$

It should also be noted that (60) is not necessarily valid, even if its corresponding continuous counterpart $\int W_{i,\alpha} d\boldsymbol{x} = 0$ is valid (for interior regions). This is also a manifestation of the particle inconsistency. Therefore (61) and (62) actually use the particle inconsistency in approximating the derivative of the smoothing function to offset or balance the particle inconsistency in approximating the derivatives of a field function, with a hope to improve the accuracy of the approximations.

Randles and Libersky [52] derived a normalization formulation for the density approximation

$$\rho_i = \frac{\sum_{j=1}^{N}\rho_j W_{ij}\Delta v_j}{\sum_{j=1}^{N} W_{ij}\Delta v_j}, \tag{63}$$

and a normalization for the divergence of the stress tensor σ

$$(\nabla\cdot\sigma)_i = \frac{\sum_{j=1}^{N}(\sigma_j - \sigma_i)\otimes\nabla_i W_{ij}\Delta v_j}{\sum_{j=1}^{N}(\boldsymbol{x}_j - \boldsymbol{x}_i)\otimes\nabla_i W_{ij}\Delta v_j}, \tag{64}$$

where $\otimes$ is the tensor product. Again, (63) and (64) also use the inconsistency in approximating the smoothing function and its derivatives to offset the inconsistency in approximating a field function and its derivatives, also with an aim to improve the accuracy of the approximations.

Based on Taylor series expansion on the SPH approximation of a function, Chen et al. [54] suggested a corrective smoothed particle method (CSPM). In one-dimensional space, the process of CSPM can be briefed as follows.

Performing Taylor series expansion at a nearby point x_i, a sufficiently smooth function $f(x)$ can be expressed as

$$f(\boldsymbol{x}) = f_i + (x - x_i)f_{i,x} + \frac{(x-x_i)^2}{2!}f_{i,xx} + \cdots. \tag{65}$$

Multiplying both sides of (65) by the smoothing function W and integrating over the entire computational domain yield

$$\begin{aligned}\int f(x)W_i(x)dx &= f_i\int W_i(x)dx + f_{i,x}\int (x-x_i)W_i(x)dx \\ &\quad + \frac{f_{i,xx}}{2}\int (x-x_i)^2 W_i(x)dx + \cdots.\end{aligned} \tag{66}$$

If the terms involving *derivatives* in this equation are neglected, a corrective kernel approximation for function $f(x)$ at particle i is obtained as

$$f_i = \frac{\int f(x)W_i(x)dx}{\int W_i(x)dx}. \tag{67}$$

For a conventional smoothing function (non-negative and symmetric), the second term at the RHS of (66) is zero for interior region and not zero for boundary region. Therefore the corrective kernel approximation expressed in (67) is also of 2nd order accuracy for interior region and 1st order accuracy for boundary region. Comparing (67) with (16), it is found that for the interior regions, the kernel approximations in the original SPH and CSPM are actually the same due to the satisfaction of the normalization condition (in continuous form). For the boundary regions, since the integral of the smoothing function is truncated by the boundary, the normalization condition cannot be satisfied. By retaining the non-unity denominator, CSPM restores the C^0 kernel consistency.

The corresponding particle approximation for function $f(x)$ at particle i can be obtained using summation over nearest particles for each term in (66) and again neglecting the terms related to derivatives

$$f_i = \frac{\sum_{j=1}^{N} f_j W_{ij}\Delta v_j}{\sum_{j=1}^{N} W_{ij}\Delta v_j}. \tag{68}$$

It is noted that the particle approximation of the second term at the RHS of (66) is not necessarily zero even for the interior particles due to the irregularity of the particles. Therefore strictly speaking, the particle approximation expressed in (68) is of 1st order accuracy for both the interior and boundary particles. Only if the particles are uniformly distributed can the particle approximation of the second term at the RHS of (66) be zero. In this case, the particle approximation expressed in (68) is of 2nd order accuracy for the uniformly distributed interior particles.

If replacing $W_i(x)$ in (66) with $W_{i,x}$ and neglecting the *second and higher* derivatives, a corrective kernel approximation for the first derivative is generated as

$$f_{i,x} = \frac{\int [f(x) - f(x_i)] W_{i,x}(x) dx}{\int (x - x_i) W_{i,x}(x) dx}. \tag{69}$$

The particle approximations corresponding to (69) is

$$f_{i,x} = \frac{\sum_{j=1}^{N} (f_j - f_i) W_{i,x} \Delta v_j}{\sum_{j=1}^{N} (\boldsymbol{x}_j - \boldsymbol{x}_i) W_{i,x} \Delta v_j}. \tag{70}$$

Similarly, The CSPM kernel approximations for the derivatives are also of second order accuracy (or 1st order consistency) for interior regions, but 1st order accuracy (or 0th order consistency) for boundary regions. Except for cases with uniformly distributed interior particles, the CSPM particle approximations for the derivatives are of 1st order accuracy (or 0th order consistency) for both the interior and boundary particles.

4.4 An SPH Formulation for Discontinuity

It is clear that CSPM can have better accuracy than the conventional SPH method as it improves the boundary deficiency problem. It was reported that the CSPM can also reduce the so-called tensile instability inherent in the traditional SPH method [89, 90].

One notable point in CSPM is that it is based on Taylor series analysis on the kernel approximation of a field function and its derivatives. To perform Taylor series analysis, the function under consideration should be sufficiently smooth. Therefore, CSPM is not applicable to problems with discontinuities such as hydrodynamic problems that generate shock waves.

Liu and his co-workers proposed a further improvement on SPH in resolving discontinuity problems, and they call this as a discontinuous SPH, or DSPH [55]. The idea of DSPH one-dimensional space is briefed here as follows.

Examine the kernel approximation for any function $f(\boldsymbol{x})$ in the support domain of $\boldsymbol{x}_i$. The support domain is bounded by a and b with a dimension of $2\kappa h$, shown in Fig. 6. Assuming that function $f(\boldsymbol{x})$ has an *integrable* discontinuity at d in the support domain and that it is located in the right

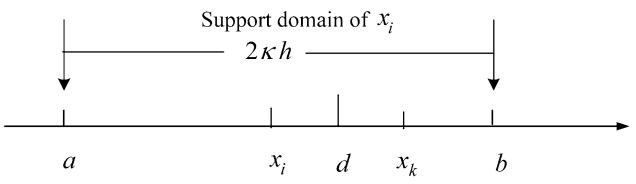

Fig. 6 Kernel approximations for a one-dimensional function with a discontinuity at point d. The support domain of $\boldsymbol{x}_i$ is bounded by a and b with a dimension of $2\kappa h$

half of the support domain, i.e., $\boldsymbol{x}_i < d \le b$, the integration of the multiplication of $f(\boldsymbol{x})$ and the smoothing function W over the entire support domain can be divided into two parts

$$\int_a^b f(\boldsymbol{x}) W_i(\boldsymbol{x}) d\boldsymbol{x} = \int_a^d f(\boldsymbol{x}) W_i(\boldsymbol{x}) d\boldsymbol{x} + \int_d^b f(\boldsymbol{x}) W_i(\boldsymbol{x}) d\boldsymbol{x}. \tag{71}$$

Expanding $f(\boldsymbol{x})$ in the first integral on the right hand side around point $\boldsymbol{x}_i$, and around another arbitrary point $\boldsymbol{x}_k$ in the second integral, where $d \le \boldsymbol{x}_k \le b$ gives

$$\begin{aligned}
&\int_a^b f(\boldsymbol{x}) W_i(\boldsymbol{x}) d\boldsymbol{x} \\
&= f(\boldsymbol{x}_i) \int_a^d W_i(\boldsymbol{x}) d\boldsymbol{x} + f(\boldsymbol{x}_k) \int_d^b W_i(\boldsymbol{x}) d\boldsymbol{x} \\
&\quad + f'(\boldsymbol{x}_i) \int_a^d (\boldsymbol{x} - \boldsymbol{x}_i) W_i(\boldsymbol{x}) d\boldsymbol{x} \\
&\quad + f'(\boldsymbol{x}_k) \int_d^b (\boldsymbol{x} - \boldsymbol{x}_k) W_i(\boldsymbol{x}) d\boldsymbol{x} + r(h^2).
\end{aligned} \tag{72}$$

Rearranging by combining some similar terms with some transformations yields

$$\begin{aligned}
&\int_a^b f(\boldsymbol{x}) W_i(\boldsymbol{x}) d\boldsymbol{x} \\
&= f(\boldsymbol{x}_i) \int_a^b W_i(\boldsymbol{x}) d\boldsymbol{x} + [f(\boldsymbol{x}_k) - f(\boldsymbol{x}_i)] \int_d^b W_i(\boldsymbol{x}) d\boldsymbol{x} \\
&\quad + f'(\boldsymbol{x}_i) \int_a^b (\boldsymbol{x} - \boldsymbol{x}_i) W_i(\boldsymbol{x}) d\boldsymbol{x} \\
&\quad + \int_d^b [(\boldsymbol{x} - \boldsymbol{x}_k) f'(\boldsymbol{x}_k) - (\boldsymbol{x} - \boldsymbol{x}_i) f'(\boldsymbol{x}_i)] W_i(\boldsymbol{x}) d\boldsymbol{x} \\
&\quad + r(h^2).
\end{aligned} \tag{73}$$

Since the kernel W is assumed to be even, normalized, and has a compact support, we have $|\boldsymbol{x} - \boldsymbol{x}_k| \le \kappa h$. In the above equation, we assume that $f'(\boldsymbol{x})$ must exist and be bounded in $[a, d) \cup (d, b]$. In other words, the derivative of $f(\boldsymbol{x})$ exists, and when $\boldsymbol{x}$ approaches d from both sides, it is bounded within a finite limit. Hence, the last two terms (excluding the residual term) on the RHS of the above equation can be bounded by terms of order of h respectively. Therefore, the above equation can be rewritten as:

$$\begin{aligned}
&\int_a^b f(\boldsymbol{x}) W_i(\boldsymbol{x}) d\boldsymbol{x} \\
&= f(\boldsymbol{x}_i) \int_a^b W_i(\boldsymbol{x}) d\boldsymbol{x} + [f(\boldsymbol{x}_k) - f(\boldsymbol{x}_i)] \int_d^b W_i(\boldsymbol{x}) d\boldsymbol{x} \\
&\quad + r(h).
\end{aligned} \tag{74}$$

This equation can be re-written as

$$f(\boldsymbol{x}_i) = \frac{\int_a^b f(\boldsymbol{x}) W_i(\boldsymbol{x}) d\boldsymbol{x}}{\int_a^b W_i(\boldsymbol{x}) d\boldsymbol{x}} - \left\{ \frac{[f(\boldsymbol{x}_k) - f(\boldsymbol{x}_i)] \int_d^b W_i(\boldsymbol{x}) d\boldsymbol{x}}{\int_a^b W_i(\boldsymbol{x}) d\boldsymbol{x}} \right\} + r(h), \quad (75)$$

which is the kernel approximation of the field function with a discontinuity.

Similarly, the kernel approximation of the derivative is obtained as

$$\begin{aligned} f'(\boldsymbol{x}_i) &= \frac{\int_a^b [f(\boldsymbol{x}) - f(\boldsymbol{x}_i)] W_{ix}(\boldsymbol{x}) d\boldsymbol{x}}{\int_a^b (\boldsymbol{x} - \boldsymbol{x}_i) W_{ix}(\boldsymbol{x}) d\boldsymbol{x}} \\ &\quad - \left\{ \frac{[f(\boldsymbol{x}_k) - f(\boldsymbol{x}_i)] \int_d^b W_{ix}(\boldsymbol{x}) d\boldsymbol{x}}{\int_a^b (\boldsymbol{x} - \boldsymbol{x}_i) W_{ix}(\boldsymbol{x}) d\boldsymbol{x}} \right. \\ &\quad \left. + \frac{\int_d^b [(\boldsymbol{x} - \boldsymbol{x}_k) f'(\boldsymbol{x}_k) - (\boldsymbol{x} - \boldsymbol{x}_i) f'(\boldsymbol{x}_i)] W_{ix}(\boldsymbol{x}) d\boldsymbol{x}}{\int_a^b (\boldsymbol{x} - \boldsymbol{x}_i) W_{ix}(\boldsymbol{x}) d\boldsymbol{x}} \right\} \\ &\quad + r(h). \end{aligned} \quad (76)$$

The above two equations are the kernel approximations of a field function (and its derivative) with a discontinuity in the support domain. The kernel approximations at the RHS of (75) and (76) consist of two parts. The first parts are the same as those at the RHS of (67) and (69), which describe the kernel approximations of a field function and its derivatives. It is the second parts in the big brackets that describe the behavior of the discontinuity. Neglecting the second parts of (75) and (76) should result in numerical errors since the resultant kernel approximations in the presence of a discontinuity are inconsistent. If the second terms are retained, the resultant kernel approximations are consistent up to the first order.

The particle approximations for the field function and its derivatives at particle i are a little bit different from the particle approximations in the conventional SPH and CSPM due to the presence of the discontinuity. When the domain is discretized by particles, since two particles cannot be located at the same position, the discontinuity should always be located between two particles. In deriving (75) and (76), since the point $\boldsymbol{x}_k$ is arbitrarily selected, it can be taken as the particle that is nearest to and on the right hand side of the discontinuity (Fig. 7).

The particle approximation of the discontinuous function is

$$f_i = \frac{\sum_{j=1}^N (\frac{m_j}{\rho_j}) f_j W_{ij}}{\sum_{j=1}^N (\frac{m_j}{\rho_j}) W_{ij}}$$

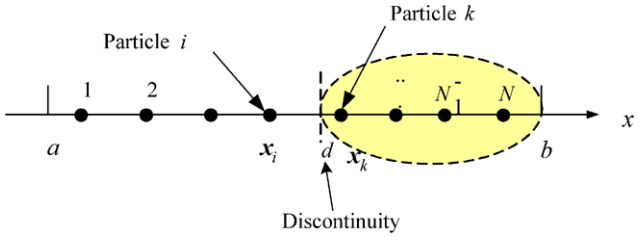

Fig. 7 Particle approximations for a function with a discontinuity at point d. In the process from the kernel approximation to particle approximation, an arbitrary point $\boldsymbol{x}_k$ is associated with a particle k that is the nearest particle on the right hand side of the discontinuity. The total number of particles in the support domain of $[a, b]$ is N

$$- \left\{ \frac{[f(\boldsymbol{x}_k) - f(\boldsymbol{x}_i)] \sum_{j=k}^N (\frac{m_j}{\rho_j}) W_{ij}}{\sum_{j=1}^N (\frac{m_j}{\rho_j}) W_{ij}} \right\}. \quad (77)$$

And similarly, the particle approximation of the derivative of the discontinuous function is

$$\begin{aligned} f_i &= \frac{\sum_{j=1}^N (\frac{m_j}{\rho_j}) (f(\boldsymbol{x}_j) - f(\boldsymbol{x}_i)) \nabla_i W_{ij}}{\sum_{j=1}^N (\frac{m_j}{\rho_j}) (\boldsymbol{x}_j - \boldsymbol{x}_i) \nabla_i W_{ij}} \\ &\quad - \left\{ \frac{[f(\boldsymbol{x}_k) - f(\boldsymbol{x}_i)] \sum_{j=k}^N (\frac{m_j}{\rho_j}) \nabla_i W_{ij}}{\sum_{j=1}^N (\frac{m_j}{\rho_j}) (\boldsymbol{x}_j - \boldsymbol{x}_i) \nabla_i W_{ij}} \right. \\ &\quad \left. + \frac{\sum_{j=k}^N (\frac{m_j}{\rho_j}) [(\boldsymbol{x}_j - \boldsymbol{x}_k) f'(\boldsymbol{x}_k) - (\boldsymbol{x}_j - \boldsymbol{x}_i) f'(\boldsymbol{x}_i)] \nabla_i W_{ij}}{\sum_{j=1}^N (\frac{m_j}{\rho_j}) (\boldsymbol{x}_j - \boldsymbol{x}_i) \nabla_i W_{ij}} \right\}. \end{aligned} \quad (78)$$

Also, the particle approximations consist of two parts, the first primary parts similar to those in the CSPM approximation and the second additional parts in the big brackets developed for the discontinuity treatment. It should be noted that the summations of the numerators of the additional parts are only carried out for particles in the right portion of the support domain $[d, b]$ shaded in Fig. 7. The coordinates of these particles are $\boldsymbol{x}_j$ ($j = k, k+1, \ldots, N$) that satisfy $(\boldsymbol{x}_k - \boldsymbol{x}_j)(\boldsymbol{x}_k - \boldsymbol{x}_i) \leq 0$. Particles at the same side as i do not contribute to the summation in the additional parts. Otherwise, the additional part would become zero, and the modification term would disappear.

Equations (75) and (76), (77) and (78) are the essential DSPH formulations for approximating a discontinuous function and its first derivative. It is possible to extend the DSPH to higher order derivatives, and multi-dimensional space.

The different performances of the SPH, CSPM and DSPH in resolving discontinuity have been demonstrated by a number of numerical tests. One of them is the sod tube problem, which has been studied by many researchers for validation purposes [47, 91]. The shock-tube is a long straight tube filled with gas, which is separated by a membrane into two parts of different pressures and densities. The

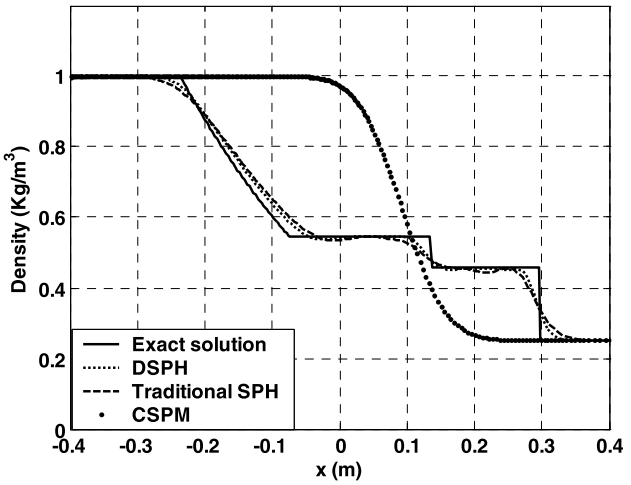

Fig. 8 Density profiles for the shock tube problem obtained using different versions of SPH formulation. DSPH gives the best result. CSPM failed to capture the major shock physics ($t = 0.2$ s)

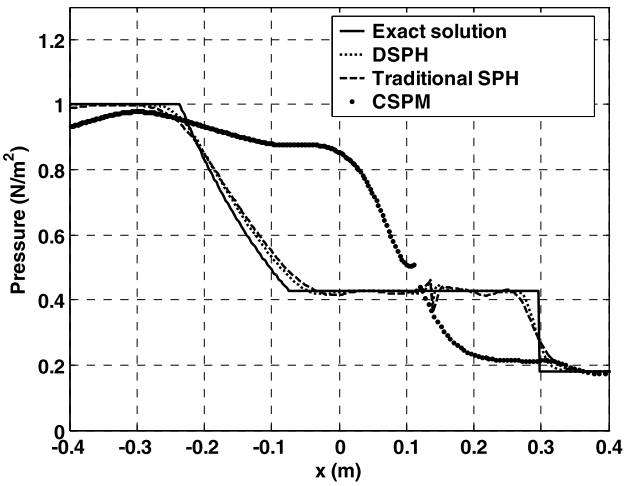

Fig. 9 Pressure profiles for the shock tube problem obtained using different versions of SPH formulation

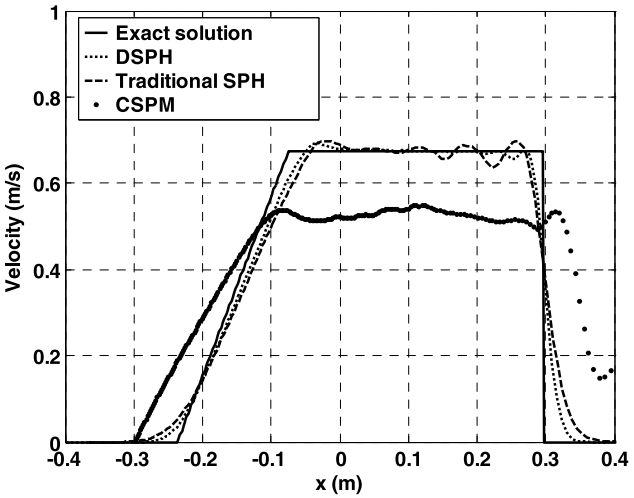

Fig. 10 Velocity profiles for the shock tube problem obtained using different versions of SPH formulation

gas in each part is initially in an equilibrium state of constant pressure, density and temperature. When the membrane is taken away suddenly, a shock wave, a rarefaction wave and a contact discontinuity will be produced. The shock wave moves into the region with lower density gas; the rarefaction wave travels into the region with higher density gas; while the contact discontinuity forms near the center and travels into the low-density region behind the shock. Exact solution is available for comparison for this one-dimensional problem.

In this example, the cubic spline function is used as the smoothing function to simulate this shock tube problem. The initial conditions are same as those introduced by Sod [92]

$$x \le 0, \qquad \rho = 1, \qquad \boldsymbol{v} = 0, \qquad e = 2.5,$$
$$p = 1, \qquad \Delta x = 0.001875,$$
$$x > 0, \qquad \rho = 0.25, \qquad \boldsymbol{v} = 0, \qquad e = 1.795,$$
$$p = 0.1795, \qquad \Delta x = 0.0075$$

where ρ, p, e, and $\boldsymbol{v}$ are the density, pressure, internal energy, and velocity of the gas, respectively. Δx is the particle spacing. A total of 400 particles are deployed in the one-dimensional problem domain. All particles have the same mass of $m_i = 0.001875$. 320 particles are evenly distributed in the high-density region $[-0.6, 0.0]$, and 80 particles are evenly distributed in the low-density region $[0, 0.6]$. The initial particle distribution is to obtain the required discontinuous density profile along the tube. The equation of state for the ideal gas $p = (\gamma - 1)\rho e$ is employed in the simulation with $\gamma = 1.4$.

In the simulation, the time step is 0.005 s and the simulation is carried out for 40 steps. In resolving the shock, the Monaghan type artificial viscosity is used, which also serves to prevent unphysical penetration [49]. Figures 8, 9, 10 and 11 show, respectively, the density, pressure, velocity and internal energy profiles.

It can be seen that the obtained results from the DSPH agree well with the exact solution in the region $[-0.4, 0.4]$. The shock is observed at around $x = 0.3$ within several smoothing lengths. The rarefaction wave is located between $x = -0.3$ and $x = 0$. The contact discontinuity is between $x = 0.1$ and $x = 0.2$. Just as reported by Hernquist and Katz [91] and Monaghan [47], the traditional SPH with artificial viscosity yields comparable results in capturing shock physics. The DSPH gives slightly better results than the traditional SPH method though only 40 steps passed. If more dynamic steps are involved, the better performance of the DSPH is more evident [55].

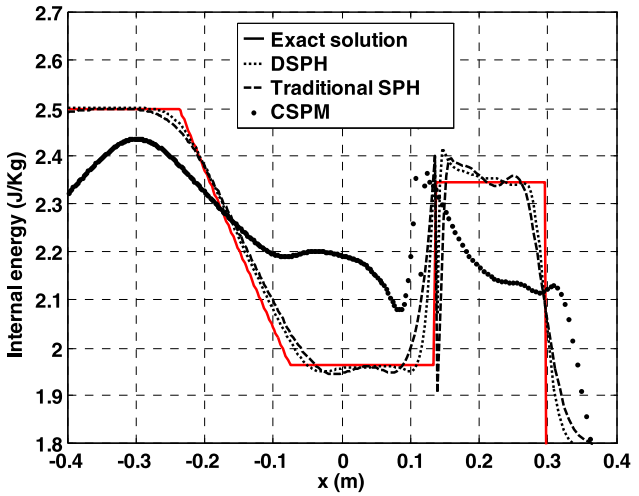

Fig. 11 Energy profiles for the shock tube problem obtained using different versions of SPH formulation

CSPM failed to captures the major shock physics. In this example, CSPM performs poorer even than the traditional SPH method. The poor performance of the CSPM in simulating shock waves should arise from the denominator that in fact acts as a normalization factor. Revisiting (67), it is found that the summation of the smoothing function around the discontinuity region is far from the unity. When it is used to normalize the summation of the density, the local features of shock wave can be smoothed out, and hence the shock physics can be concealed. In contrast, the traditional SPH does not suffer from this smoothing effect, and the DSPH benefits from the addition part in resolving the shock physics. Their performance, therefore, should be better than that of the CSPM. It is clear that the different performances of CSPM and DSPH originate from the additional corrective parts in DSPH that approximate the discontinuity.

4.5 A General Approach to Restore Particle Inconsistency

Liu et al. gave a general approach to restore particle inconsistency through reconstructing the smoothing function [6]. In general, a smoothing function can be written in the following form

$$\begin{aligned} W(\boldsymbol{x}-\boldsymbol{x}_j,h) &= b_0(\boldsymbol{x},h)+b_1(\boldsymbol{x},h)\left(\frac{\boldsymbol{x}-\boldsymbol{x}_j}{h}\right) \\ &\quad + b_2(\boldsymbol{x},h)\left(\frac{\boldsymbol{x}-\boldsymbol{x}_j}{h}\right)^2+\cdots \\ &= \sum_{I=0}^{k} b_I(\boldsymbol{x},h)\left(\frac{\boldsymbol{x}-\boldsymbol{x}_j}{h}\right)^I . \end{aligned} \tag{79}$$

By substituting the above smoothing function into (45), and after some trivial transformation, the discretized form of (45) can be written as

$$\left.\begin{array}{l} \sum_{I=0}^{k} b_I(\boldsymbol{x},h)\sum_{j=1}^{N}(\frac{\boldsymbol{x}-\boldsymbol{x}_j}{h})^I \Delta\boldsymbol{x}_j = 1 \\ \sum_{I=0}^{k} b_I(\boldsymbol{x},h)\sum_{j=1}^{N}(\frac{\boldsymbol{x}-\boldsymbol{x}_j}{h})^{I+1} \Delta\boldsymbol{x}_j = 0 \\ \vdots \\ \sum_{I=0}^{k} b_I(\boldsymbol{x},h)\sum_{j=1}^{N}(\frac{\boldsymbol{x}-\boldsymbol{x}_j}{h})^{I+k} \Delta\boldsymbol{x}_j = 0 \end{array}\right\} . \tag{80}$$

The $k+1$ coefficients $b_I(\boldsymbol{x},h)$ can then be determined by solving the following matrix equation

$$\underbrace{\begin{Bmatrix} m_0(\boldsymbol{x},h) & m_1(\boldsymbol{x},h) & \cdots & m_k(\boldsymbol{x},h) \\ m_1(\boldsymbol{x},h) & m_2(\boldsymbol{x},h) & \cdots & m_{1+k}(\boldsymbol{x},h) \\ \vdots & \vdots & \ddots & \vdots \\ m_k(\boldsymbol{x},h) & m_{k+1}(\boldsymbol{x},h) & \cdots & m_{k+k}(\boldsymbol{x},h) \end{Bmatrix}}_{M} \underbrace{\begin{Bmatrix} b_0(\boldsymbol{x},h) \\ b_1(\boldsymbol{x},h) \\ \vdots \\ b_k(\boldsymbol{x},h) \end{Bmatrix}}_{b} = \underbrace{\begin{Bmatrix} 1 \\ 0 \\ \vdots \\ 0 \end{Bmatrix}}_{I}, \tag{81}$$

or

$$\mathbf{M}\boldsymbol{b} = \boldsymbol{I}, \tag{82}$$

where

$$m_k(\boldsymbol{x},h) = \sum_{j=1}^{N}\left(\frac{\boldsymbol{x}-\boldsymbol{x}_j}{h}\right)^k \Delta\boldsymbol{x}_j, \tag{83}$$

$\mathbf{M}$ is a moment matrix, $\boldsymbol{b}$ is a vector of coefficients, $\boldsymbol{I}$ is a vector of given constants.

After determining the coefficients $b_I(\boldsymbol{x},h)$, the smoothing function expressed in (79) can be calculated. The procedure ensures particle consistency to kth order. Therefore, the particle consistency restoring process actually gives an approach to construct some kind of smoothing function for the SPH methods.

Comparing with the traditional smoothing function, which is only dependent on the particle distance and applicable for all the particles, the consistency restored smoothing function is particle-wise. It therefore depends on both the distance and positions of the interacting particles. The cost-effectiveness for this approach in constructing particle-wise smoothing functions needs to be considered since it will require additional CPU time to solve the particle-wise equation (79) for all the particles. Moreover, since all particles are moving, the particle location is changing as well. Hence, the particle-wise smoothing functions need to be computed for every time step. Another problem is that, to solve (81), the moment matrix $\mathbf{M}$ is required to be non-singular. Therefore, the particle distribution must satisfy certain conditions to avoid singular momentum matrix. This implies that when we enforce on consistency, we will face the stability problem shown as the bad-conditioned moment matrix in the

SPH settings. In contrast, in the original SPH method, particles can be arbitrary distributed, though the obtained results may be less accurate.

As far as the approximation is concerned, restoring particle consistency is an improvement on the accuracy of the particle approximation, provided that the moment matrix $\mathbf{M}$ is not singular. However, it is noted that restoring the consistency in discrete form leads to some problems in simulating hydrodynamic problems. Firstly, the resultant smoothing function is negative in some parts of the region. Negative value of smoothing function can leads to unphysical representation of some field variables, such as negative density, negative energy that can lead to a breakdown of the entire computation. Secondly, the resultant smoothing function may not be monotonically decreasing with the increase of the particle (node) distance. Moreover, the constructed smoothing function may not be symmetric and using this non-symmetric smoothing function violates the equal mutual interaction in physics.

4.6 Finite Particle Method

Considering the disadvantages of the above-mentioned particle inconsistency restoring approach in constructing a point-wise smoothing function, Liu et al. devised another particle consistency restoring approach, which retains the conventional non-negative smoothing function instead of reconstructing a new smoothing function [56, 57]. This approach has been termed as *Finite Particle Method* (FPM), in which a set of basis functions can be used in the numerical approximation.

Performing Taylor series expansion at a nearby point $\boldsymbol{x}_i = \{x_i, y_i, z_i\}$ and retaining the second order derivatives, a sufficiently smooth function $f(\boldsymbol{x})$ at point $\boldsymbol{x} = \{x, y, z\}$ can be expressed as follows

$$f(\boldsymbol{x}) = f_i + (\boldsymbol{x}^\alpha - \boldsymbol{x}_i^\alpha) f_{i,\alpha} + \frac{(\boldsymbol{x}^\alpha - \boldsymbol{x}_i^\alpha)(\boldsymbol{x}^\beta - \boldsymbol{x}_i^\beta)}{2!} f_{i,\alpha\beta} + r((\boldsymbol{x} - \boldsymbol{x}_i)^3), \tag{84}$$

where α, β are the dimension indices repeated from 1 to 3 (or from x to z). $r((\boldsymbol{x} - \boldsymbol{x}_i)^3)$ is the remainder of the expansion. f_i, $f_{i,\alpha}$ and $f_{i,\alpha\beta}$ are defined as

$$f_i = f(\boldsymbol{x}_i), \tag{85}$$

$$f_{i,\alpha} = f_\alpha(\boldsymbol{x}_i) = (\partial f / \partial \boldsymbol{x}^\alpha)_i, \tag{86}$$

$$f_{i,\alpha\beta} = f_{\alpha\beta}(\boldsymbol{x}_i) = (\partial^2 f / \partial \boldsymbol{x}^\alpha \partial \boldsymbol{x}^\beta)_i. \tag{87}$$

Multiplying both sides of (84) with a function $\varphi_1(\boldsymbol{x} - \boldsymbol{x}_i)$ and integrating over the problem space Ω can yield the following equation

$$\begin{aligned}\int_\Omega f(\boldsymbol{x})\varphi_1(\boldsymbol{x} - \boldsymbol{x}_i)d\boldsymbol{x} &= f_i \int_\Omega \varphi_1(\boldsymbol{x} - \boldsymbol{x}_i)d\boldsymbol{x} + f_{i,\alpha}\int_\Omega (\boldsymbol{x}^\alpha - \boldsymbol{x}_i^\alpha)\varphi_1(\boldsymbol{x} - \boldsymbol{x}_i)d\boldsymbol{x} \\ &\quad + \frac{f_{i,\alpha\beta}}{2}\int_\Omega (\boldsymbol{x}^\alpha - \boldsymbol{x}_i^\alpha)(\boldsymbol{x}^\beta - \boldsymbol{x}_i^\beta)\varphi_1(\boldsymbol{x} - \boldsymbol{x}_i)d\boldsymbol{x} \\ &\quad + r((\boldsymbol{x} - \boldsymbol{x}_i)^3).\end{aligned} \tag{88}$$

It is seen that the integration is carried out over the entire problem space, and can be quite time-consuming. One usual assumption is that a field variable at point $\boldsymbol{x}_i$ is only strongly influenced by the field variables at nearby points and that the influence of the field variables at points far away from point $\boldsymbol{x}_i$ is very weak and hence can be neglected. Therefore, the global integration can be converted into a local integration by defining a *support domain* for point $\boldsymbol{x}_i$ in which the field variables at point $\boldsymbol{x}_i$ can be determined. The shape of the support domain can be conveniently taken as a circle (in 2D) or a sphere (in 3D) with a radius of κh, in which κ is a constant scalar factor, and h is a length characterizing the support domain. The function $\varphi_1(\boldsymbol{x} - \boldsymbol{x}_i)$ is also limited to the local support domain, and can be rewritten as $\varphi_1(\boldsymbol{x} - \boldsymbol{x}_i, h)$.

Since the points distributed in the problem space are actually particles, each occupying individual lumped volume, (88) can be numerically approximated by summation over the particles surrounding point x_i as follows

$$\begin{aligned}\sum_{j=1}^{N} f(\boldsymbol{x}_j)\varphi_1(\boldsymbol{x}_j - \boldsymbol{x}_i, h)\Delta V_j &= f_i \sum_{j=1}^{N}\varphi_1(\boldsymbol{x}_j - \boldsymbol{x}_i, h)\Delta V_j \\ &\quad + f_{i,\alpha}\sum_{j=1}^{N}(\boldsymbol{x}_j^\alpha - \boldsymbol{x}_i^\alpha)\varphi_1(\boldsymbol{x}_j - \boldsymbol{x}_i, h)\Delta V_j \\ &\quad + \frac{f_{i,\alpha\beta}}{2}\sum_{j=1}^{N}(\boldsymbol{x}_j^\alpha - \boldsymbol{x}_i^\alpha)(\boldsymbol{x}_j^\beta - \boldsymbol{x}_i^\beta)\varphi_1(\boldsymbol{x}_j - \boldsymbol{x}_i, h)\Delta V_j,\end{aligned} \tag{89}$$

where N is the number of particles within the support domain of particle i. The remainder term $r((\boldsymbol{x} - \boldsymbol{x}_i)^3)$ in (88) is omitted in (89) for the sake of conciseness. The summation over the particles is illustrated in Fig. 3.

Equation (89) can be further simplified as the following equation at point $\boldsymbol{x}_i$

$$B_{1i} = A_{1ki} F_{ki}, \tag{90}$$

where

$$F_{ki} = [\, f_i \;\; f_{i,\alpha} \;\; f_{i,\alpha\beta} \,]^T, \tag{91}$$

$$B_{1i} = \sum_{j=1}^{N} f(\boldsymbol{x}_j)\varphi_1(\boldsymbol{x}_j - \boldsymbol{x}_i, h)\Delta V_j, \tag{92}$$

$$\begin{aligned} A_{1ki} = \Bigg[& \sum_{j=1}^{N} \varphi_1(\boldsymbol{x}_j - \boldsymbol{x}_i, h)\Delta V_j \\ & \times \sum_{j=1}^{N} (\boldsymbol{x}_j^{\alpha} - \boldsymbol{x}_i^{\alpha})\varphi_1(\boldsymbol{x}_j - \boldsymbol{x}_i, h)\Delta V_j \\ & \times \frac{1}{2}\sum_{j=1}^{N} (\boldsymbol{x}_j^{\alpha} - \boldsymbol{x}_i^{\alpha})(\boldsymbol{x}_j^{\beta} - \boldsymbol{x}_i^{\beta})\varphi_1(\boldsymbol{x}_j - \boldsymbol{x}_i, h)\Delta V_j \Bigg]. \end{aligned} \tag{93}$$

Corresponding to 1, 2, and 3 dimensional cases, there are one function value, 1, 2 and 3 first derivatives, and 1, 3 and 6 second derivatives that will be approximated. It is clear that k in (91), (93) and (90) is 3, 6, and 10 respectively corresponding to 1, 2, and 3 dimensional cases. To calculate the function value, the first and the second derivatives at $\boldsymbol{x}_i$, 2, 5, and 9 other equations similar to (90) are required. Therefore in 1, 2, and 3 dimensional cases, totally 3, 6, and 10 functions ($\varphi_M(\boldsymbol{x} - \boldsymbol{x}_i, h)$, $M = 3$, 6, or 10) are required in order to approximate the function value, the first and second derivative. These functions form a set of basis functions used for approximating the function value, its first and second derivatives. A conventional SPH smoothing function and its first and second derivatives can form a set of basis function in the FPM. For example, in 2D space, a smoothing function W, its two first order derivatives, W_α and W_β, and its three second order derivatives, $W_{\alpha\alpha}$, $W_{\alpha\beta}$ and $W_{\beta\beta}$ forms a set of 6 basis functions.

In summary, multiplying a set of basis functions on both sides of (84), integrating over the problem domain, summing over the nearest particles within the local support domain of particle i, a set of matrix equation can be produced to approximate the function value as well as the first and second derivatives at particle i. The matrix equations at particle i at can be written as

$$B_{Mi} = A_{Mki} F_{ki} \quad \text{or} \quad \mathbf{B} = \mathbf{A}\boldsymbol{F} \tag{94}$$

where

$$B_{Mi} = \sum_{j=1}^{N} f(\boldsymbol{x}_j)\varphi_M(\boldsymbol{x}_j - \boldsymbol{x}_i, h)\Delta V_j, \tag{95}$$

$$\begin{aligned} A_{Mki} = \Bigg[& \sum_{j=1}^{N} \varphi_M(\boldsymbol{x}_j - \boldsymbol{x}_i, h)\Delta V_j \\ & \times \sum_{j=1}^{N} (\boldsymbol{x}_j^{\alpha} - \boldsymbol{x}_i^{\alpha})\varphi_M(\boldsymbol{x}_j - \boldsymbol{x}_i, h)\Delta V_j \\ & \times \frac{1}{2}\sum_{j=1}^{N} (\boldsymbol{x}_j^{\alpha} - \boldsymbol{x}_i^{\alpha})(\boldsymbol{x}_j^{\beta} - \boldsymbol{x}_i^{\beta})\varphi_M(\boldsymbol{x}_j - \boldsymbol{x}_i, h)\Delta V_j \Bigg]. \end{aligned} \tag{96}$$

Equation (94) is the basis of the finite particle method and can be used to approximate a function value and its derivatives for a field variable. It is seen that only if the coefficient matrix A is not singular, can these M equations determine a unique set of solutions at particle i for the M unknowns in vector F. Solving the above pointwise matrix equations, the function value as well as the first and second derivatives at every particle can be simultaneously approximated. Note that the conditioning of A matrix reflects the stability of the FPM model.

Since the governing equations in CFD only involve the first and second derivatives, only the derivatives up to the second order are retained in (84). For problems in other areas such as computational solid mechanics, high order derivatives may be involved. If third or higher order derivatives are to be approximated, in expanding $f(\boldsymbol{x})$ at $\boldsymbol{x}_i$, the interested derivatives need to be retained in (84). To obtain the increased number of unknowns, more functions like $\varphi_M(\boldsymbol{x} - \boldsymbol{x}_i, h)$ are necessary to complete the matrix equation (94). Therefore, except for the increased number of unknowns, increased number of basis functions, and therefore more computational efforts, the solution procedure for the interested unknowns is the same.

Comparing conventional SPH and FPM, it is clear that both FPM and SPH are meshfree particle methods in which particles with lumped volumes are used to represent the state of a system. The particles form a frame for interpolation, differencing or integration in a certain approximation. Both FPM and SPH can be used as Lagrangian methods if allowing the particles to move in the problem space. However, the difference between FPM and SPH is obvious.

1. FPM uses a set of basis function to approximate the function value and its derivatives, whereas SPH employs a smoothing function and its derivatives to approximate a function value and the corresponding derivatives. The smoothing functions in SPH should have some special properties as described in Sect. 3. However, the basis functions in FPM are more general. Any set of functions which do not lead to a singular coefficient matrix A can be used as basis functions. Therefore the smoothing function and its specific derivatives actually can be one possible choice as a suitable set of basis functions.
2. SPH can be regarded as a special case of FPM, whereas FPM is a generalized version of SPH with modifications.

In (84), if all the terms related to derivatives are neglected, multiplying both sides of (84) with the smoothing function W, and integrating over the problem space can lead to the approximation in SPH. Summation over the nearest particles within the support domain of a particle further produces the particle approximation of the field variable at that particle (see (89)).

3. FPM should have better accuracy than SPH. Since no derivative term is retained in (84), the SPH method actually is of first order accuracy. If a symmetric smoothing function is used, the terms related to the first order derivatives are actually zero for the interior particles in the problem domain. Therefore SPH is of second order accuracy in interior parts. In contrast, since up to second order derivatives are retained in the expansion process, the accuracy of FPM is of third order. Moreover, if higher derivatives are retained, better accuracy can be achieved. FPM should have a better accuracy than SPH both for the interior particles and boundary particles.
4. The accuracy of FPM is not sensitive by the selection of smoothing length, and extremely irregular particle distribution. This has been demonstrated by Liu and his coworkers in testing one- and two-dimensional cases.
5. As the solution is to be obtained from solving the matrix (94), a good matrix inversion algorithm is necessary to prevent the co-efficient matrix to be negative.
6. The matrix (94) is to be solved at every particle, and every time step. It can be more computationally expensive than the conventional SPH method.

One simpler example of FPM is to only consider the first derivative in (84). Using the smoothing function and its first derivatives as the basis functions, the following equations can be obtained

$$\int f(\boldsymbol{x}) W_i(\boldsymbol{x}) d\boldsymbol{x} = f_i \int W_i(\boldsymbol{x}) d\boldsymbol{x} + f_{i,\alpha} \int (\boldsymbol{x}^\alpha - \boldsymbol{x}_i^\alpha) W_i(\boldsymbol{x}) d\boldsymbol{x}, \tag{97}$$

and

$$\int f(\boldsymbol{x}) W_{i,\beta} dx = f_i \int W_{i,\beta} d\boldsymbol{x} + f_{i,\alpha} \int (\boldsymbol{x}^\alpha - \boldsymbol{x}_i^\alpha) W_{i,\beta}(\boldsymbol{x}) d\boldsymbol{x}. \tag{98}$$

Again β is the dimension index repeated from 1 to d. The corresponding discrete forms for (97) and (98) are

$$\sum_{j=1}^{N} f_j W_{ij} \Delta v_j = f_i \cdot \sum_{j=1}^{N} W_{ij} \Delta v_j + f_{i,\alpha} \cdot \sum_{j=1}^{N} (\boldsymbol{x}_j^\alpha - \boldsymbol{x}_i^\alpha) W_{ij} \Delta v_j, \tag{99}$$

Table 1 Kernel consistency of SPH, CSPM, and FPM

	Interior domain	Boundary area
SPH	1st order	less than 0th order
CSPM	1st order	0th order
FPM	1st order	1st order

and

$$\sum_{j=1}^{N} f_j W_{ij,\beta} \Delta v_j = f_i \cdot \sum_{j=1}^{N} W_{ij,\beta} \Delta v_j + f_{i,\alpha} \cdot \sum_{j=1}^{N} (\boldsymbol{x}_j^\alpha - \boldsymbol{x}_i^\alpha) W_{ij,\beta} \Delta v_j. \tag{100}$$

There are $d+1$ equations for $d+1$ unknowns (f_i and $f_{i,\alpha}$). Equations (99) and (100) are therefore complete for solving with respect to f_i and $f_{i,\alpha}$, and the solutions for f_i and $f_{i,\alpha}$ are

$$\begin{bmatrix} f_i \\ f_{i,\alpha} \end{bmatrix} = \begin{bmatrix} \sum_{j=1}^{N} W_{ij} \Delta v_j & \sum_{j=1}^{N} (\boldsymbol{x}_j^\alpha - \boldsymbol{x}_i^\alpha) W_{ij} \Delta v_j \\ \sum_{j=1}^{N} W_{ij,\beta} \Delta v_j & \sum_{j=1}^{N} (\boldsymbol{x}_j^\alpha - \boldsymbol{x}_i^\alpha) W_{ij,\beta} \Delta v_j \end{bmatrix}^{-1} \times \begin{bmatrix} \sum_{j=1}^{N} f_j W_{ij} \Delta v_j \\ \sum_{j=1}^{N} f_j W_{ij,\beta} \Delta v_j \end{bmatrix}. \tag{101}$$

In (99) and (100), the terms related to the function and the first order derivatives are all retained, only the terms related to second or high order derivatives are neglected. Therefore the resultant particle approximations for a function and its derivatives (see (101)) are able to exactly reproduce a constant and a linear function (C^0 and C^1 consistency). Hence the algorithm shown in (101) actually restores the particle consistency that conventional SPH method does not have. Again, this particle consistency restoring approach is independent of the particle distribution (either regular or irregular), and the choices of the smoothing kernel and smoothing length. Another advantage is that this particle consistency restoring approach does not change the conventional smoothing function and should be preferable in simulating hydrodynamics.

In summary, the consistency of the conventional SPH method, CSPM, and FPM (if using (101), rather than (94), which is associated with higher order particle consistency than (101)) are described in Tables 1 and 2.

Figure 12 shows the approximation results for a linear function $f(x, y) = x + y$ using discrete models of SPH and FPM. The particles are uniformly distributed. It is seen

Table 2 Particle consistency of SPH, CSPM, and FPM

	Interior domain		Boundary area
	Regular distribution	Irregular distribution	
SPH	1st order	less than 0th order	less than 0th order
CSPM	1st order	0th order	0th order
FPM	1st order	1st order	1st order

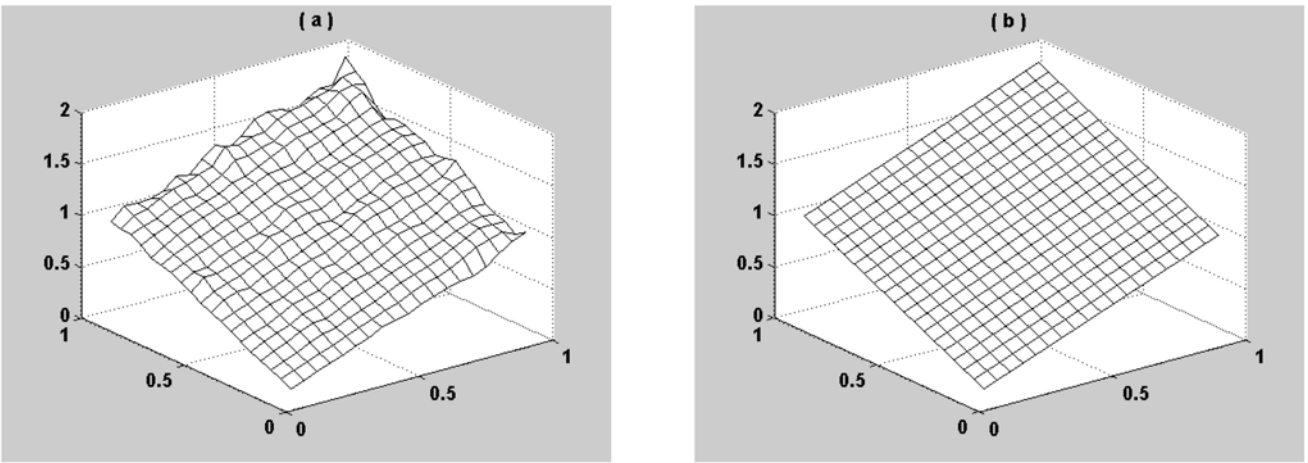

Fig. 12 Approximation results for a linear function $f(x, y) = x + y$ using (**a**) SPH and (**b**) FPM in a domain of [0, 1, 0, 1]

that the SPH results are associated with oscillation especially near the boundary, whereas the particle consistency restoring approach can obtain much better results, which are in very good agreement with the analytical solution. It is worth noting that if the particles are randomly or irregularly distributed, FPM can also obtain accurate results, whereas, SPH results can be far away from the analytical solutions. It is also worth noting that in this simple numerical test, the approximation is carried out by obtaining numerical values at current step from the existing numerical values at the particles at the previous step. There is no physical dynamics involved in these two numerical performance studies. Only the accuracy of the numerical approximations of the given function is studied using different approximation methods. It can be expected that numerical errors existing in the present approximated results can propagate to the next approximation steps and can even be magnified. However, when these methods are used to simulate a well-posed physical problem, the physics is governed by the conservation equations. If the discrete model is stable, the error in the current step is controlled by the consistency. Therefore, the errors should be more or less within some level, and will not be magnified from one step to the next step.

4.7 Consistency vs. Stability

We have seen in the two previous sections that a typical dilemma exists for many numerical methods: consistency or stability. For a given "setting" of a numerical model such as a particle method, we may choose one over another, but probably a "balanced" one can be difficult to choose. The original SPH has clearly chosen the stability (and also flexibility) over the consistency, which gives the SPH a distinct feature of working well for many complicated problems with good efficiency, but less accuracy. It always tries to deliver some reasonably good results for the price paid. This seems to be a very practical choice for many practical engineering problems, as should be regarded as an advantage of the SPH method. Attempts to improve the accuracy of SPH via restoring the consistency can be helpful, provided that the stability and efficiency is not too much compromised.

The consistency restoring approaches, such as the FPM, put more emphases on the consistency (hence hopefully accuracy), but the stability (the conditioning of the **M** or **A** matrix) can be in question for some types of problems. Hence proper measures are needed to establish the stability ensuring the accuracy of the solution.

The question is that can we have both the consistency and the stability at the same time? The answer is yes, provided we are willing to change the "setting" and pay the price. The recently proposed GSM method [32–35] is a typical example that guarantees both excellent stability for arbitrary grids and 2nd order accuracy. It uses also the gradient smoothed technique, but in a very carefully designed fashion. However, the GSM is not a particle method any more;

the simplicity and efficiency features of the particle methods are lost. The GSM requires precise evaluation of the integrals for carefully chosen types of smoothing domains, and it works more like FVM. Therefore, the final question depends on what we want and at what cost: choosing a numerical method should be closely related to the nature of the problem, the requirement for the solutions and the resources we have.

5 Special Topics

5.1 Solid Boundary Treatment

Particle methods such as MD, DPD, and SPH are very different from the grid based numerical methods in treating solid boundary, and care must taken in this regards. For finite element methods, proper boundary conditions can be well defined and properly imposed without affecting the stability of the discrete model. In the finite difference method, because the domain is relatively regular, proper ways to handling the boundary conditions have already been developed. In either FEM or FDM, the implementations of boundary conditions (either Neumann boundary conditions or Dirichlet boundary conditions, or mixed boundary conditions) are generally straightforward [2, 3, 5, 93]. In contrast, in the MD, DPD and SPH, the implementation of the boundary conditions is not as straightforward as in the grid based numerical models. This has been regarded historically as one weak point of the particle methods [12, 15, 77, 79, 94–99]. For molecular dynamics and dissipative particle dynamics, it is common to fill the solid obstacle areas with frozen particles. These fixed particles can prevent the mobile particles from penetrating the solid walls, and interact with the mobile particles with proper interaction models. Different complex solid matrix and solid-fluid interface physics can thus be modeled by appropriately deploying fixed particles plus a suitable interaction model with mobile particles. Preventing fluid particles from penetrating solid walls by exerting a repulsive force simulates the boundary condition with zero normal velocity. Different models of reflection or mirror of fluid particles or interaction models of solid particles with fluid particles can also be applied to exert slip or non-slip boundary condition [11, 40, 97, 100–103]. In principal, the boundary treatment techniques in MD and DPD can also be used for SPH. However, SPH is a continuum scale particle method, and the field variables on boundaries such as pressure need to be directly calculated. Therefore solid boundary treatment in SPH is more difficult and numerical techniques for implementing solid wall boundary conditions are also more diversified. Since the invention of the SPH method, a lot of works have been published addressing the treatments of solid wall boundary conditions [94, 97, 104–111].

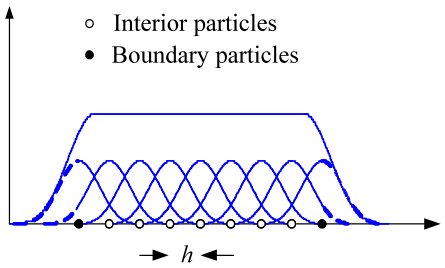

Fig. 13 SPH kernel and particle approximations for interior and boundary particles. The boundary particles suffer from particle insufficiency, and no contribution comes from outside since there are no particles beyond the boundary

As discussed in Sect. 4, the conventional SPH model suffers from particle inconsistency that is closely related to the selection of smoothing function, smoothing length, and most importantly the distribution of particles. An extreme case is the particle distribution near the boundary area. Only particles inside the boundary contribute to the summation of the particle interaction, and no contribution comes from the outside since there are no particles beyond the boundary. This one-sided contribution does not give correct solutions, because on the solid surface, although the velocity is zero, other field variables such as the density are not necessarily zero.

Some improvements have been proposed to treat the boundary condition. Monaghan used a line of ghost or virtual particles located right on the solid boundary to produce a highly repulsive force to the particles near the boundary, and thus to prevent these particles from unphysically penetrating through the boundary [112]. Campbell treated the boundary conditions by including the residue boundary terms in the integration by parts when estimating the original kernel integral involving gradients [113], as discussed in Sect. 3 in deriving the constructing conditions for the smoothing kernel function. Libersky and his co-workers introduced ghost or image (or imaginary) particles to reflect a symmetrical surface boundary condition with opposite velocity on the reflecting image particles [114]. Later, Randles and Libersky proposed a more general treatment of the boundary condition by assigning the same boundary value of a field variable to all the ghost particles, and then interpolating smoothly the specified boundary ghost particle value and the calculated values of the interior particles [52].

In general, it is feasible to use virtual particles to implement the solid boundary conditions. These virtual particles can be allocated on and outside the boundary. These virtual particles can be classified into two categories, virtual particles that are located right on the solid boundary (Type I) and virtual particles that are outside the boundary (Type II) (see Fig. 14). Type I virtual particles are similar to what Monaghan used [112], and they are used to exert a repulsive boundary force on approaching fluid (real) particles

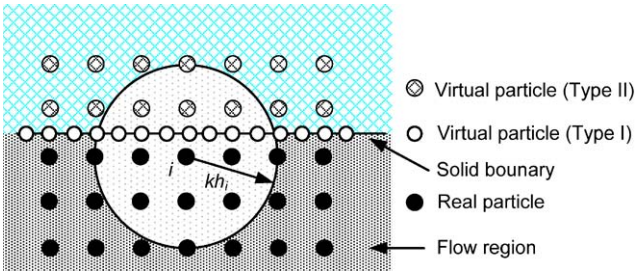

Fig. 14 Schematic illustration of flow region, solid boundary, real fluid particles and virtual particles

to prevent the interior particles from penetrating the boundary. The penalty force is calculated using a similar approach for calculating the molecular force of Lennard-Jones form [115]. If a Type I virtual particle is the neighboring particle of a real particle that is approaching the boundary, a force is applied pairwisely along the centerline of these two particles as follows

$$PB_{ij} = \begin{cases} D[(\frac{r_0}{r_{ij}})^{n_1} - (\frac{r_0}{r_{ij}})^{n_2}]\frac{\boldsymbol{x}_{ij}}{r_{ij}^2}, & (\frac{r_0}{r_{ij}}) \le 1, \\ 0, & (\frac{r_0}{r_{ij}}) > 1. \end{cases} \tag{102}$$

where the parameters n_1 and n_2 are empirical parameters, and are usually taken as 12 and 4 respectively. D is a problem dependent parameter, and should be chosen to be in the same scale as the square of the largest velocity. The cutoff distance r_0 is important in the simulation. If it is too large, some particles may feel the repulsive force from the virtual particles in the initial distribution, thus leads to initial disturbance and even blowup of particle positions. If it is too small, the real particles may have already penetrated the boundary before feeling the influence of the repulsive force. In most practices, r_0 is usually selected approximately close to the initial particle spacing. To more effectively prevent fluid particles from penetrating the solid wall, Type I virtual particles are usually more densely distributed at the solid boundary than the fluid particles (Fig. 14).

Type II virtual particles are usually obtained through reflecting the real fluid particles along the solid boundary. Scalar properties of the virtual particles can be taken as the same as the reflected real particles, while velocity of the virtual particles are usually taken as opposite of the reflected counterparts. As such the non-slip boundary condition is implemented. Due to the compactness of the smoothing kernel function, only the real particles that are within κh to the solid boundary are necessary to be reflected to form Type II virtual particles. Hence there are only several layers of Type II virtual particles outside the solid boundary. For example, if the cubic spline smoothing function is used, there are two layers of Type II virtual particles (if the real particles are regularly distributed). Therefore, for a fluid particle i close to the solid boundary, all the neighboring particles $NN(i)$ that are within its influencing area of κh_i can be categorized into three subsets (see Fig. 14)

(a) $I(i)$: all the *interior particles* that are the neighbors of i (real particles);
(b) $B(i)$: all the *boundary particles* that are the neighbors of i (virtual particles of type I);
(c) $E(i)$: all the *exterior particles* that are the neighbors of i (virtual particles of type II).

These two types of virtual particles are specially marked for contribution in the later summation on the real particles. Type I virtual particles exert repulsive force on an approaching particle, but they usually do not contribute in the particle approximation. Type II virtual particles take part in the kernel and the particle approximations of the real particles. It is clear that by using type II virtual particles, the one-sided particle distribution problem in the conventional SPH method can be somewhat remedied. In different implementations, the position and physical variables for type II virtual particles can be fixed (determined once a set of virtual particles are obtained), or can adapt in the simulation process with the evolution of the corresponding counterpart real particles. In general, adapting type II virtual particles can result in better results. However, the adapting process may be time-consuming, and may be complicated especially when the solid wall is not able to be defined in a simple curve.

In many circumstances, the computational domain can be complicated, and can contain solid obstacles of arbitrary shapes. Generating type II virtual particles may not be an easy task. For such cases, a feasible way is to deploy particles into the computational domain either by placing all the particles in some kind of lattice, or injecting particles into the computational domain and then running SPH simulation for the entire system to reach equilibrium, just as in MD and DPD simulation. The particles outside of the boundary (or within the solid obstacles) can be used as type II virtual particles. This approach has some advantages since the system starts from a quiet or equilibrium state of the same number density without unwanted noise. For implementing the non-slip boundary condition, these virtual particles can move with the velocity as the obstacles to which they are attached. For better accuracy, the velocity of the virtual particles can be obtained from extrapolating the velocity of a neighboring fluid particle, as illustrated in Fig. 15. Assuming the normal distance of a virtual particle to the solid boundary is d_v, and the normal distance of a fluid particle to the solid boundary is d_f, with non-slip boundary condition (velocity on the boundary is zero), the velocity of the virtual particle under consideration should be $\boldsymbol{v}_v = -(d_v/d_f)\boldsymbol{v}_f$. Hence the velocity difference between the fluid and virtual particles is $\boldsymbol{v}_{fv} = (1 + \frac{d_v}{d_f})\boldsymbol{v}_f$, which can be used in calculating viscous forces as addressed in Sect. 5. Note that the positions of the virtual particles do not need to evolve. Also if the

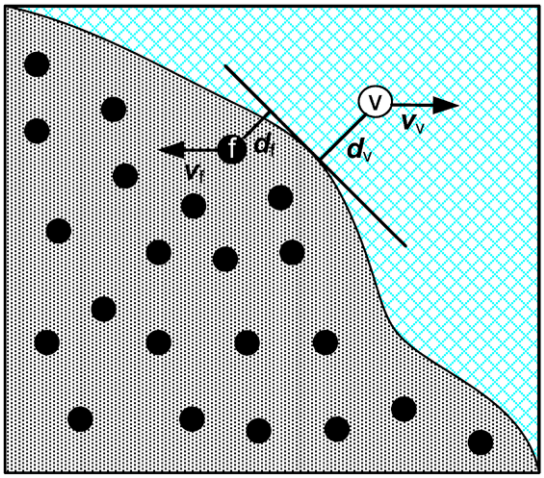

Fig. 15 A general approach to construct type II virtual particles and assign velocities. Only one virtual particle is plotted in the obstacle region for illustration

obstacle is a moving object, the velocity of the fluid particle should be taken as the relative velocity to the obstacle. To prevent numerical singularities caused by a fluid particle closely approaching the solid boundary ($d_f \to 0$), a safety parameter ϖ can be used in calculating the velocity difference between the fluid and virtual particles as $\boldsymbol{v}_{fv} = \varpi \boldsymbol{v}_f$, where $\varpi = \min(\varpi_{\max}, 1 + \frac{d_v}{d_f})$. $\varpi_{\max}$ is an empirical parameter, it is reported that taking 1.5 can result in good results [111].

5.2 Representation of Solid Grains

To model the geometries of a complicated solid matrix, the entire computational domain can be discretized using a 'shadow' grid. The grid cells are labeled "0" for regions occupied by pore spaces and "1" for solid-filled regions (Fig. 16a). This simple identification of fluid and solid cells can be used to represent any arbitrary complex geometry. The unit vectors normal to the solid-fluid interfaces define the local orientation of the fluid-solid interface and can be obtained by simply calculating the surface gradient from the indicator numbers ("0" for liquid regions and "1" for solid regions). As discussed in Sect. 6.1 in constructing type II virtual particles, we can place particles in the entire computational domain regularly in some kind of lattice according to a designated number density. It is also applicable to inject particles into the computational domain, and run SPH simulation until the system arrives at an equilibrium. At the beginning of each simulation, the particles are initialized and positioned randomly within the entire computational domain until a pre-defined particle number density is reached, and the system is then run to equilibrium. The particles within the solid cells (marked as "1") are then 'frozen' (their positions are fixed) to represent the solid grains (Fig. 16b). The solid grains in obstacles can occupy a considerable fraction of the entire computational domain, and hence the number of frozen particles representing the solids can be very large. Most of the frozen particles inside the solid grains are more than 1 cut-off distance away from the adjacent fluid cells. These particles do not contribute to the solid-fluid interactions and consequently they have no influence on the movement of the flow particles within the fluid cells. Therefore, only the frozen particles that are within 1 cut-off distance from the solid-fluid interface are retained as boundary particles (Fig. 16c), and the rest of the particles further inside the solid grains are removed from the model domain.

Figures 17 and 18 show two example of solid obstacle representation. In Fig. 17, the flow region is a porous media system, in which the circular obstacles occupy a great amount of the computational domain. Figure 17a shows the original porous media system where the circular obstacles are filled with (solid) particles. Figure 17b shows the porous media system for later simulation where only the (solid) particles within 1 cut-off distance away from the adjacent fluid cells are retained. In Fig. 18, the flow region is a fractured network system and the obstacles also occupy most of the computational domain (Fig. 18a). After treatment, only the fracture particles within 1 cut-off distance away from the adjacent fluid cells are retained. For both cases, it is convenient and flexible to treat the complex geometries by identifying the flow and obstacle regions separately with the indicator

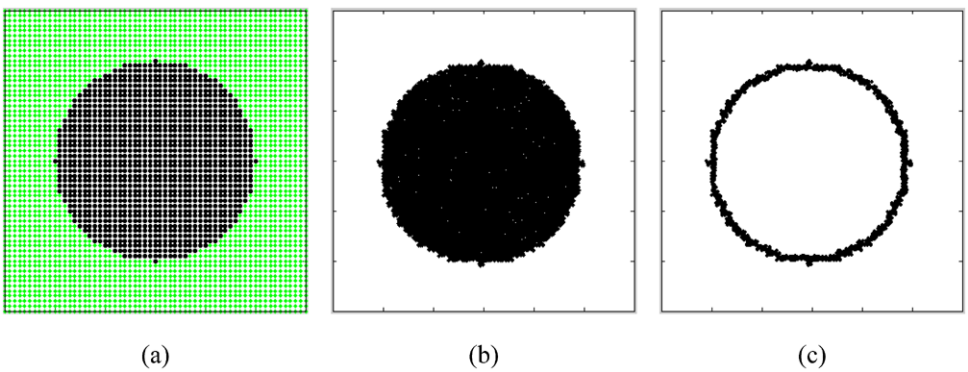

Fig. 16 Schematic illustration of the treatment of solid obstacles. (**a**) The cells in the entire computational domain are first labeled, "0" for fluid (void) cells and "1" for solid (obstacle) cells. (**b**) The SPH particles in the obstacle cells are frozen. (**c**) Only the frozen particles that are close to the fluid cells (within 1 cut-off distance) are retained as boundary particles

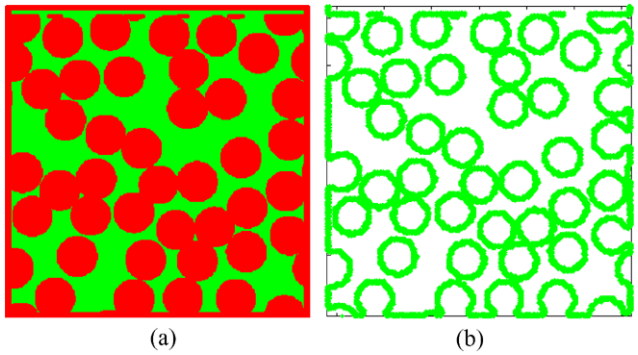

Fig. 17 An example of solid obstacle representation in a porous media flow region with circular obstacles. (**a**) Original porous media system. (**b**) Solid particle distribution for later simulation

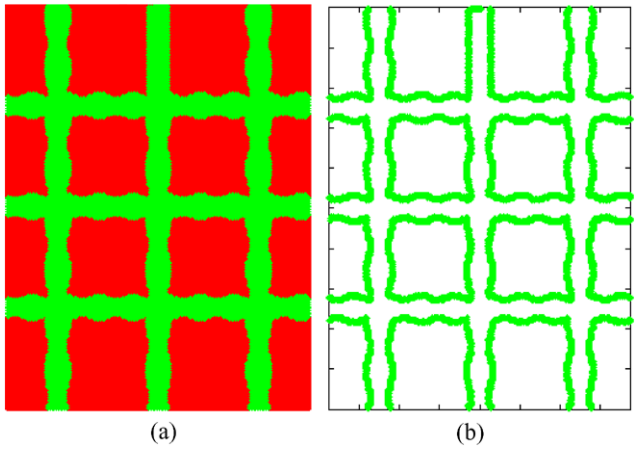

Fig. 18 An example of solid obstacle representation in a fracture network in which most of computational domain is full of obstacles. (**a**) Original fractured network system. (**b**) Solid particle distribution for later simulation

numbers. Also since only the solid particles that are within 1 cut-off distance away from the adjacent fluid cells are retained for later simulation, the number of particles can be greatly reduced, and therefore the computational efficiency can be significantly improved.

The above approach of deploying frozen particles to represent solid grains and interact with flow particles is applicable to particle methods such as MD, DPD, and SPH, and it is especially effective for complex boundaries [99, 116–118]. For problems with comparatively simpler geometries, some other approaches are commonly used. These approaches may also involve particles fixed on the solid boundaries with or without equilibrium process, and may involve non-fixed boundary particles updated with the neighboring flow particles. Although fixed boundary particles are more frequently used in SPH literature, non-fixed boundary particles updated with the neighboring flow particles may produce better results [6, 110, 111, 119].

5.3 Material Interface Treatment

For modeling systems with multiple materials, an effective algorithm is required for efficiently describing the material interface dynamics. It is somewhat different from the grid based numerical methods in correctly detecting contact and effectively treating it in particle methods like SPH. Traditionally SPH uses particles to represent the state of a system under consideration. One point is that the SPH particles are interpolation points on which mass of each particle has been lumped. An SPH particle has a finite mass and density, and hence can have a finite volume. However, in contrast to FEM, FDM and FVM, in which a cell or an element has a definite shape, an SPH particle has never assumed as a definite shape. On the other hand, the shape of a particle can also be associated with the influencing area (or support domain, that is kh) of the particle. Generally an SPH particle is assumed to be circular (or spherical) when using a smoothing kernel function with a scalar smoothing length (Fig. 19a). In some cases, an SPH particle can be elliptical (or ellipsoidal) when a tensor smoothing length is used [120–124] (Fig. 19b). In few simulations, it even can be taken as a square or a cube [125] (Fig. 19c). In the SPH simulation, the mass of a particle is usually assumed to be constant, and updating the density means change of the volume. If the particle takes a definite shape such as a circular, then the size of the particle also changes. Therefore different shapes and sizes of the SPH particles increase the difficulty in implementing the contact algorithm. During the course of SPH development, different contact algorithms have emerged [126–142]. For simplicity, only SPH models with circular or spherical shaped particles are discussed here. The SPH particles are assumed to be hard-spheres rather than soft balls, as models with soft balls also increase the difficulty in implementing the contact algorithm.

In the SPH particle models, if particles from different materials are not bonded together, particles from one material can influence, and also be influenced by the particles from the other material, according to conventional SPH algorithm. Figure 20 shows an example of the material interface at the initial stage, and at a later stage in the evolution. Initially the SPH particles are distributed regularly, and there is no intersection and deformation of particles. With the SPH evolution, particles from different materials influence each other, and the conventional SPH algorithm can introduce errors since particles from material A influence the particles from material B in calculating the strain and strain rate, and vice versa. This interaction between particles from different materials can introduce shear and tensile stress, which prevent sliding and separation of different materials. Special algorithms are required if an SPH model is used for simulation of problems with sliding and separation.

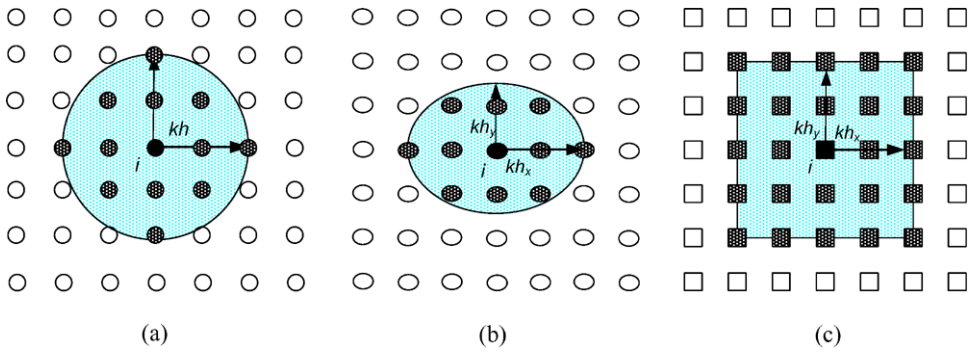

Fig. 19 Possible shapes of an SPH particle. (**a**) Circular shape corresponding to a scalar smoothing length, (**b**) elliptical shape corresponding to a tensor smoothing length at different directions, (**c**) square shape whereas the smoothing length can also be a tensor

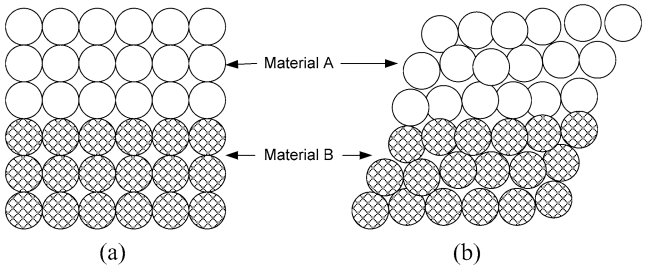

Fig. 20 Illustration of material interface with SPH particle model. (**a**) Initial SPH particle distribution, and (**b**) SPH particle evolution. Interaction between particles from different materials can introduce shear and tensile stress and can prohibit sliding and separation of different materials

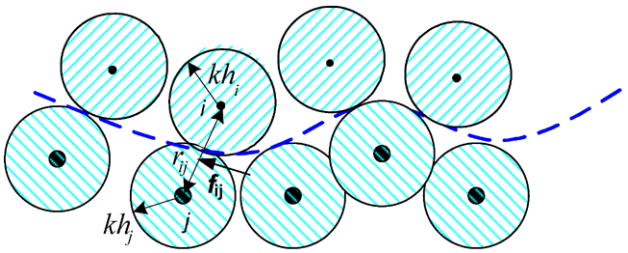

Fig. 21 An illustration of particle and particle contact

Major steps to be considered in a contact algorithm in the SPH simulation include (1) identifying the boundary, (2) detecting the contact and (3) applying repulsive contact forces. Boundary (or interface) has usually been considered to be a surface one half of the local smoothing length away from the boundary SPH particles [52, 127]. A convenient way to detect particle-particle contact is to check the proximity of two approaching particles from different materials, and compare with the summation of the smoothing lengths of the particles. As shown in Fig. 21, the contact and penetration between two particles can be identified by

$$pe = \frac{kh_i + kh_j}{r_{ij}} \geq 1, \tag{103}$$

where r_{ij} is the distance between particle i and particle j. After detection of the contact and penetration, a restoring contact force needs to be applied along the centerline of the two particles (position vector of particle i and particle j).

There are different choices for the restoring contact force, which is usually a function of penetration. One possible choice is the penalty force in Lennard-Jones form. Liu et al. had used this penalty force for simulating underwater explosion when dealing with different material interface [143]. In their work, the Lennard-Jones form penalty force is applied pairwisely on the two approaching particles along the centerline of the two particles

$$\boldsymbol{f}_{ij} = \begin{cases} \bar{p}(pe^{n_1} - pe^{n_2})\frac{\boldsymbol{x}_{ij}}{r_{ij}^2}, & pe \geq 1, \\ 0, & pe < 1, \end{cases} \tag{104}$$

where the parameters $\bar{p}$, n_1, n_2 are usually taken as 10^5, 6 and 4 respectively. In fact, these parameters can be adjusted to suit the needs of different problems, and the involved driven force in underwater explosions can vary in a very big range [144]. The application of the penalty force in combination with the summation between the interface particles has been shown to well prevent the unphysical penetration in the simulation of underwater explosion, though numerical oscillations near the vicinity of the interface can still exist.

It is reasonable that when the penetration of two contacting particle increases (or particle distance decreases), the magnitude of the restoring force should also increase. Monaghan [145] used the following form of repulsive force, which is controlled by the kernel and the global distribution of the particles

$$f_{ij} = \frac{W_{ij}}{W(\Delta p)}, \tag{105}$$

where Δp denotes the average particle spacing in the neighborhood of particle i (proportional to smoothing length h).

Vignjevic et al. [146] used the following repulsive force for treating possible contact and penetration between solid particles

$$\boldsymbol{f}_i = K_f \sum_{j=1}^{N} \frac{m_j}{\rho_i \rho_j} \frac{\partial W_{ij}}{\partial \boldsymbol{x}_i^{\beta}}, \tag{106}$$

where K_f is a user defined empirical parameter. In their work, the force was applied to boundary particles that are within the influencing area kh of each other. This repulsive force introduces the derivatives of the smoothing kernel, which in general reaches the maximum at a certain location between the origin and the boundary of the influencing area, and vanishes at the origin and the boundary point (see Fig. 4). Considering that decreasing the inter-particle distance means bigger repulsive force, using the kernel itself rather than its derivative physically would be more reasonable. For example, one possible choice can be

$$\boldsymbol{f}_i = K_f \sum_{j=1}^{N} \frac{m_j}{\rho_i \rho_j} W_{ij} \frac{x_{ij}}{r_{ij}^2}. \tag{107}$$

5.4 Tensile Instability

When using the SPH method for hydrodynamics with material strength, one numerical problem called tensile instability [45, 62, 63, 74, 145, 147–152] may arise. The tensile instability is the situation that when particles are under tensile stress state, the motion of the particle becomes unstable. It could result in particle clumping or even complete blowup in the computation. Swegle et al. demonstrated the tensile instability effects in a two-dimensional space as illustrated in Fig. 22 [45]. It is a simple test in which the particles representing the object initially are distributed regularly and under uniform initial stress. The boundary particles are fixed (two layers) and the interior particles are free to move due to some kind of external perturbation. If applying a very small velocity perturbation on a center particle, theoretically, it will take a long time for a particle under consideration to move over single particle spacing. However, in an SPH simulation with a common cubic spline smoothing kernel function, if the stress is tensile, after a number of time steps (while the number of steps is not sufficiently to move the particles even a single particle spacing), the interior particles can clumped together unphysically, and form a void. It shows that the particle system exhibits a numerical instability from tensile stress.

According to Swegle, the tensile instability depends neither on the artificial viscosity, no on the time integration scheme. It is closely related to the selection of smoothing kernel function. In a one-dimensional von Neumann stability analysis, Swegle et al. gave a criterion for being stable or instable in terms of the stress state and the second derivative

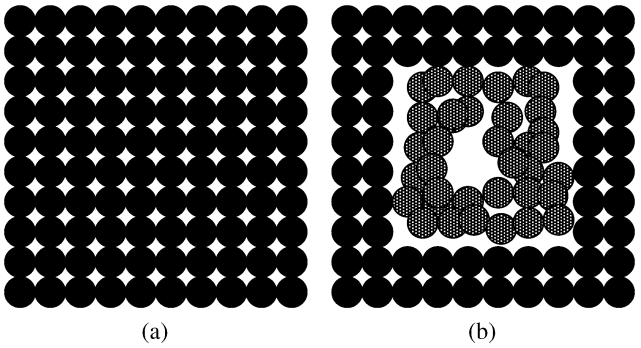

Fig. 22 Schematic illustration of the tensile instability in a two-dimensional space. (**a**) Initial particle distribution; (**b**) Particle distribution in a certain stage under the effect of tensile instability

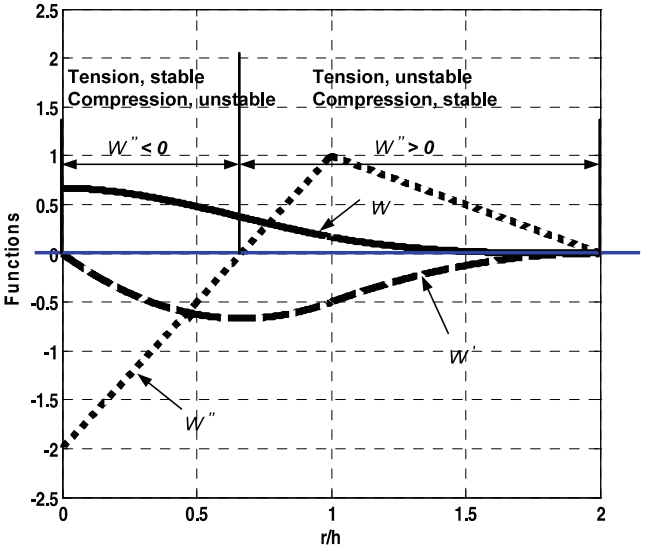

Fig. 23 Schematic illustration of tensile instability with the cubic spline function and its first and second derivatives

of the smoothing function, i.e., a sufficient condition for the unstable growth is

$$W_{\alpha\alpha}\sigma^{\alpha\alpha} > 0, \tag{108}$$

where $W_{\alpha\alpha}$ is the second derivative of the smoothing function.

In the SPH method, the cubic spline smoothing function (illustrated in Fig. 4) is mostly commonly used. The initial smoothing length is usually set to be equal to the particle spacing. Under such circumstances, the first nearest neighbor particles are located at $r/h = 1$; and the next nearest neighbor particles are at $r/h = 2$. As can be seen from Fig. 23, the second derivatives of the cubic spline function from $r/h = 1$ to $r/h = 2$ are always positive. Therefore it is expected that, according to (108), the SPH method with the cubic spline function would be stable in a compressed state but could be unstable in a tensile state in this region.

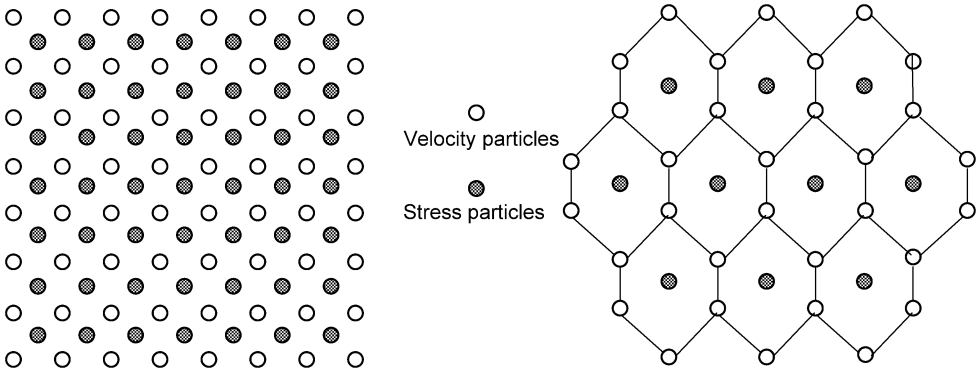

Fig. 24 Two possible setups of velocity and stress particles

Several remedies have been proposed to improve or avoid such tensile instability. Morris suggested using special smoothing functions since the tensile instability is closely related to the second order derivative of the smoothing function [46]. Though successful in some cases, they do not always yield satisfactory results generally. Chen and his coworkers proposed the corrective smoothed particle method (CSPM), which was reported to improve the tensile instability [89]. Recently Monaghan and his colleagues proposed an artificial force to stabilize the computation [145, 153].

The basic reason of tensile instability is that the SPH method is essentially a collocation method, in which the particle approximations are conducted ONLY over the particles that represent the entire system. This leads to insufficient "sampling" points for establishing equations, and can result in numerical instability problem [4]. The situation is very much similar to the so-called "node integration" in the implementation of the element free Galerkin method (EFG) [154]. In the EFG method, the instability is restored by adding stabilization terms in the Galerkin weak form. Based on this analysis, we need somehow bring in more information from other points, in addition to these particles.

One of such a method is to make use of the information at additional points in the support domain, rather than use only these collocation particles. Dyka et al. first introduced additional stress points other than the normal particles in a one-dimensional algorithm aimed at removing the tensile instability in SPH [62, 63]. The stress points were also shown to be stable in tension and contributed considerably to the accuracy in wave propagation problems. Later, this approach has been further extended to multi-dimensional space by staggering the SPH particles using stress points so that there are essentially an equal number in each set of points [64, 108, 151]. Basically in this approach, two sets of particles are used. One set of SPH particles carry velocity, and are referred to as "velocity particles". The other companion set of particles carry all required field variables except for the velocity, and are referred to as "stress particles". Figure 24 shows two possible setups of velocity and stress particles.

Randles and Libersky pointed out that, the tensile instability for problems involving material strength generally is latent. The growth rate of damages in solid continuum models is often much faster than the grow rate of the tensile instability [64].

Except for problems with material strength which can experience tensile instability, fluid mechanics problems sometimes can also meet tensile instability. Melean et al. had showed the tensile instability in a formation of viscous drop [155], and the instability can be removed by using the artificial stress proposed by Monaghan [145, 153].

6 Applications

The original applications of the SPH method is in astrophysical phenomena, such as the simulations of binary stars and stellar collisions [49, 156, 157], supernova [158, 159], collapse as well as the formation of galaxies [160, 161], coalescence of black holes with neutron stars [162, 163], single and multiple detonation of white dwarfs [164], and even the evolution of the universe [165]. It also has been extended to a vast range of problems in both fluid and solid mechanics because of the strong ability to incorporate complex physics into the SPH formulations [6]. The applications of SPH to many other engineering applications include

- multi-phase flows [119, 166–174],
- coastal hydrodynamics including water wave impact, dam break, sloshing and overtopping [112, 175–200],
- environmental and geophysical flows including flood and river dynamics, landslide, flow in fractures and porous media, seepage, soil mechanics and mudflow [117, 201–221],
- heat and/or mass conduction [53, 222–227],
- ice and cohesive grains [228–234],
- microfluidics and/or micro drop dynamics [123, 152, 169, 235–246],
- high explosive detonation and explosion [55, 125, 143, 247–256],

- underwater explosions and water mitigation [125, 143, 247–249, 255],
- elastic and/or plastic flow [52, 114, 257–259],
- fracture of brittle solids [260],
- metal forming and high pressure die casting [68, 261–270],
- magneto-hydrodynamics and magnetic field simulation [271–282],
- problems with fluid-solid interactions [176, 196, 210, 283–288], and
- many other problems like blood flow [289–292], traffic flow [293].

In this review, we will discuss applications of SPH to the following areas:

- high strain hydrodynamics with material strength,
- high explosive detonation and explosions, and underwater explosion,
- microfluidics and micro drop dynamics,
- coast hydrodynamics and offshore engineering, and
- environmental and geophysical flows.

6.1 High Strain Hydrodynamics with Material Strength

High strain hydrodynamics is generally characterized by the presence of shock waves, intense localized materials response and impulsive loadings. Numerical simulation of high strain hydrodynamics with material strength such as high velocity impact (HVI) and penetrations is one of the formidable but attractive tasks in computational solid mechanics. Most of the wave propagation hydro-codes use traditional grid based methods such as finite difference methods and finite element methods to simulate high strain hydrodynamics. Some of them are associated with advanced features which attempt to combine the best advantages of FDM and FEM. Examples include arbitrary Lagrange-Eulerian (ALE) coupling and coupling Eulerian-Lagrangian (CEL). Though many successful achievements have been made using these methods, some numerical difficulties still exist. These numerical difficulties generally arise from large deformations, large inhomogeneities, and moving interfaces, free or movable boundaries [256, 294–297].

SPH method has been intensively used for simulating such phenomena of high strain hydrodynamics with material strength, due to its special features of meshfree, Lagrangian and particle nature. Many researchers have investigated impact (either high velocity or not) and penetration using SPH method [50, 51, 86, 129, 132, 134, 139, 140, 298–335]. The applications are mainly in defense industry, and typical numerical examples range from Taylor bar impacting on a solid wall and spherical projectile/bumper collision/penetration [114, 330], projectile impact and penetration and an aircraft fuselage nose impacting a rigid target [300], to bird strike impacting on an aircraft Wing [335], and even to a high-quality high-fidelity visualization of the September 11 attack on the world trade center [328].

Libersky and his co-workers have carried out the pioneering work of applying the SPH method to high strain hydrodynamic problems including hyper velocity impact (HVI), fracture and fragmentation [52, 114, 258]. The group from the Applied Physics Division of Los Alamos National Laboratory (LANL) has modeled high velocity impacts ranging from the very small size (femtogram-scale projectiles that have been accelerated by a Van de Graaf machine to create craters in various types of targets) to the very large size (Shoemaker-Levy comet impact with the planet Jupiter). Johnson et al. [51, 314] proposed a normalized smoothing function (NSF) for axisymmetric problems based on the condition of uniform strain rate, and have made outstanding contributions in the application of SPH to impact problems. Attaway, Pampliton and Swegle et al. have worked in coupling the SPH processor with a transient-dynamics FEM code, PRONTO, in which high-strain areas that typically tangle or break conventional finite element meshes are resolved using the SPH method [126, 336].

Zhou and Liu have revisited the Taylor-Bar-Impact with the focus on the variation of results corresponding to the different model parameters which represent varied SPH implementation in a series of three-dimensional computational simulations, and have provided informative data on appropriate SPH implementation options [259]. They also have investigated normal and oblique hypervelocity impacts of a sphere on the thin plate, producing large deformation of structures. Figure 25 shows the snapshots of three-dimensional simulation of normal hypervelocity impact of a sphere on the thin plate at $t = 0$, 10, 15, and 20 μs. Figure 26 shows the top view (a) and three dimensional view (b) of oblique hypervelocity impact of a sphere on the thin plate at $t = 20$ μs with a striking angle of 30°. They observed that for oblique hypervelocity impacts of a sphere on the thin plate, the shape of the crater is no longer in circle, and the shape of the debris cloud changes with different striking angles while the ratio of the debris cloud (length over width) remains approximately 1.3.

The standard SPH method uses an isotropic smoothing kernel which is characterized by a scalar smoothing length. One of the problems associated with the standard SPH is that the isotropic kernel of SPH can be seriously mismatched to the anisotropic volume change that generally occur in many problems. To closely match the anisotropic volume changes, an anisotropic smoothing kernel which can be characterized by a matrix (in two-dimensional space) or tensor (in three-dimensional space) smoothing length can be efficacious. This leads to the development of the adaptive smoothed particle hydrodynamics (adaptive SPH or ASPH) in which the smoothing length can be adapted with the volume changes or other dimension-dependent features. The

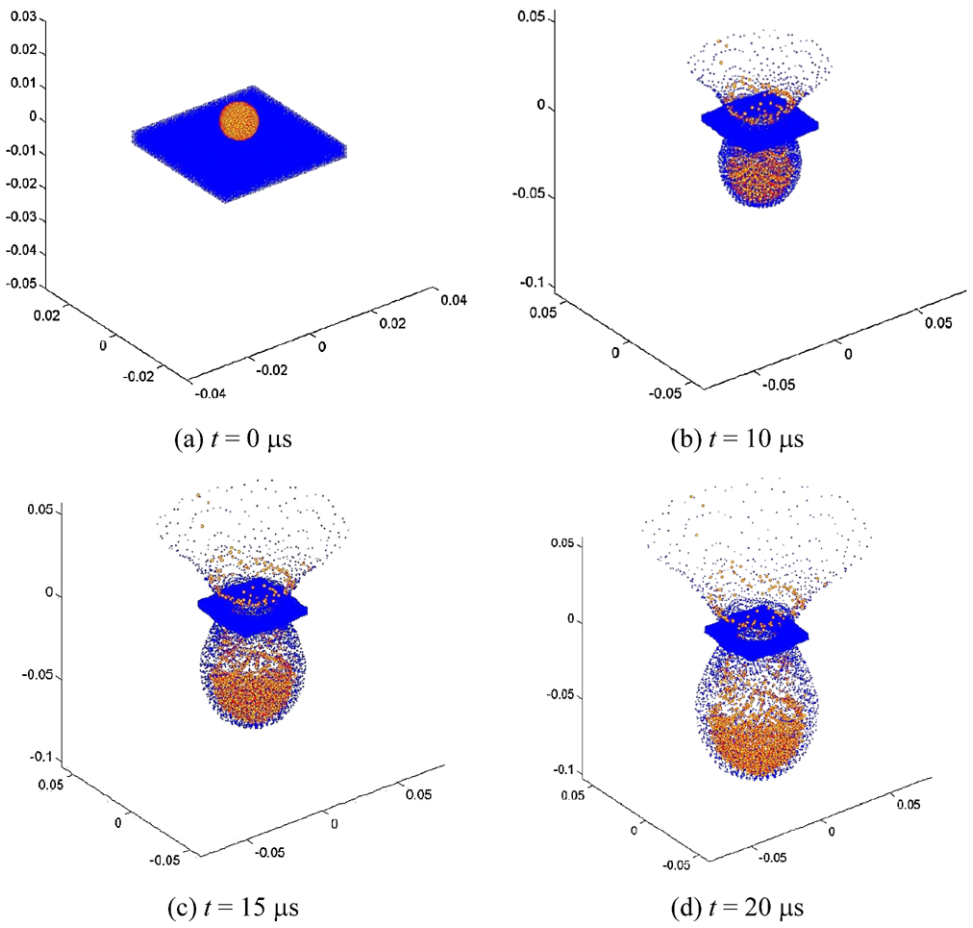

Fig. 25 Snapshots of three-dimensional simulation of normal hypervelocity impact of a sphere on the thin plate at $t = 0$, 10, 15, and 20 μs (from [259])

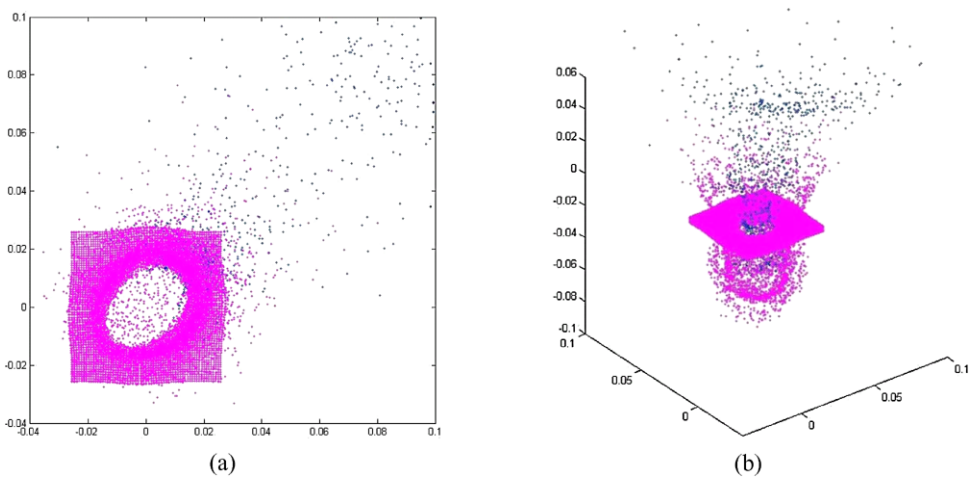

Fig. 26 Top view (**a**) and three dimensional view (**b**) of oblique hypervelocity impact of a sphere on the thin plate at $t = 20$ μs with a striking angle of 30° (from [259])

idea of using anisotropic kernel with SPH dates back to Bicknell and Gingold [337]. Fulbright et al. also presented three-dimensional SPH designed to model systems dominated by deformation along a preferential axis using spheroidal kernels [338]. Later on Shapiro et al. systematically introduced anisotropic kernels, tensor smoothing and shock-tracking to SPH to create ASPH [121]. Owen et al. presented an alternative formulation of the ASPH algorithm for evolving anisotropic smoothing kernels [120]. Except for problems with anisotropic deformations, the concept of elliptical kernel has also been applied to channel flows with very large length width ratio for saving computational efforts [123]. The numerical results presented in the references further demonstrated that ASPH has significantly better performance than the standard SPH in terms of resolving ability for a wide range of problems.

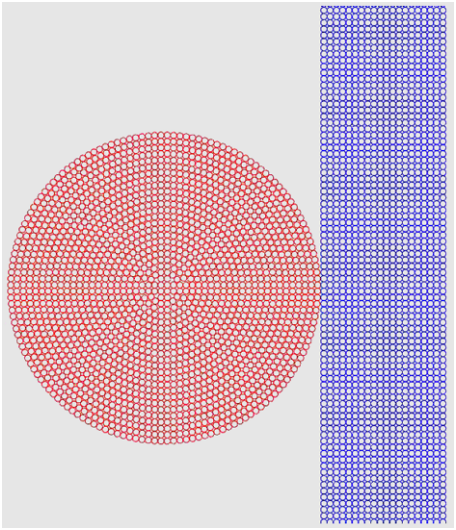

Fig. 27 Initial particle distribution in the vicinity of the contact area for both the SPH and ASPH simulation of a cylinder impacting on a plate (from [124])

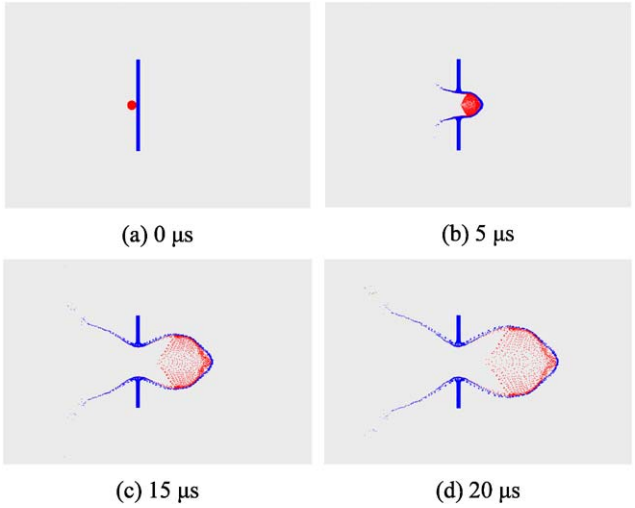

Fig. 28 Particle distributions obtained using the SPH method for simulating an Al cylinder penetrating an Al plate at 0, 5, 15, and 20 μs respectively (from [124])

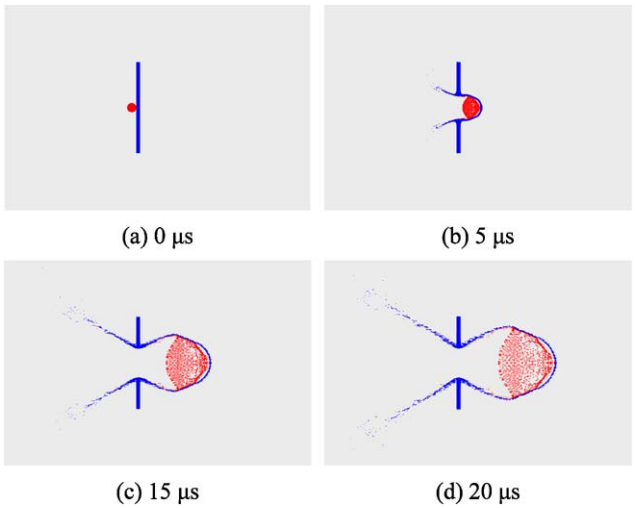

Fig. 29 Particle distributions obtained using ASPH for simulating an Al cylinder penetrating an Al plate at 0, 5, 15, and 20 μs respectively (from [124])

Liu and his co-workers have developed an adaptive smoothed particle hydrodynamics method (ASPH) for high strain Lagrangian hydrodynamics with material strength [124, 339]. In ASPH, the isotropic kernel in the standard SPH is replaced with an anisotropic kernel whose axes evolve automatically to follow the mean particle spacing as it varies in time, space, and direction around each particle. Except for the features inherited from the standard SPH, ASPH can capture dimension-dependent features such as anisotropic deformations with a more generalized elliptical or ellipsoidal influence domain. A series of comparative studies show that ASPH has better accuracy than the standard SPH when being used for high strain hydrodynamic problems with inherent anisotropic deformations.

A typical example is the simulation of an aluminum (Al) cylinder on an Al thin plate, as shown in Fig. 27. In the simulation, the cylinder is of 1.0 cm diameter. The plate is 0.4 cm thick. The plate length is of 10 cm. The particles are all initialized as squares of 0.02 cm in side dimensions. The particles in the cylinder, which is an infinite cylinder in plane symmetry, are arranged in circumferential rings as this gives a most realistic representation of the geometry. The particles in the plate are arranged in a rectangular Cartesian array. There are 500 particles along the length and 20 particles along the thickness of the plate. There are 1956 particles in the cylinder and 10000 particles in the plate, for a total of 11956 particles. The cylinder is initially in contact with the center of the plate. The problems are run with the plate free of constraints. The impact speed of the cylinder is 6180 m/s. The problems are run to 20 μs after the impact. The environmental and initial temperature of the cylinder and plate are set to 0°C. Figure 28 shows the particle distributions obtained by using SPH at 0, 5, 15, and 20 μs respectively. Figure 29 shows the particle distributions obtained using ASPH at the same stages. In general, both SPH and ASPH can get agreeable results with the experimental observations [340]. The symmetry of the problem is well preserved. Figure 30 shows the close-up view of the particle distributions near the penetrated edge of the plate obtained using SPH (a) and ASPH (b) at 20 μs. In comparison with the SPH simulation, the orientation and anisotropy of the deformation of the particles can be clearly seen in the ASPH simulation.

6.2 Detonation, Explosion and Underwater Explosion

The explosion of a high explosive (HE) charge can rapidly convert the original explosive charge into gaseous products

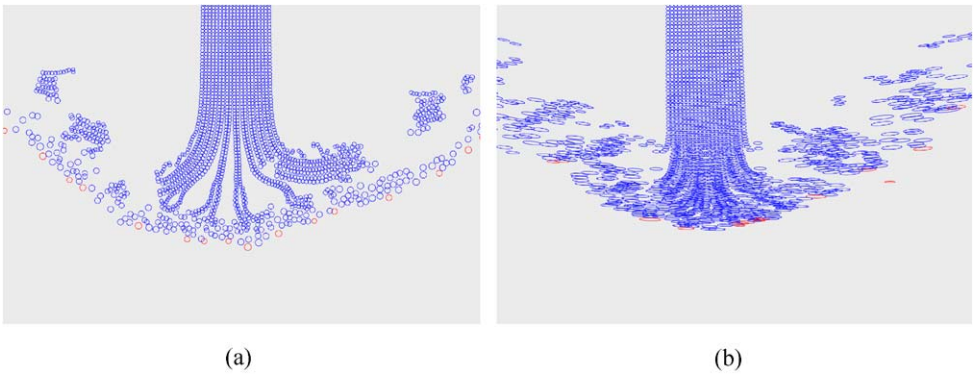

Fig. 30 Close-up view of the particle distributions near the penetrated edge of the plate obtained using SPH (**a**) and ASPH (**b**) at 20 μs (from [124])

with extremely high pressure through a chemical reaction process. The high pressure can lead to damages to nearby personnel and structures. A typical HE explosion consists of the *detonation* process through the HE at a constant detonation velocity and the later *expansion* process of the gaseous products to the surrounding medium (Fig. 31). The detonation process is accompanied by the propagation of the reactive wave that advances through the explosive with a constant velocity related to the particular type of explosive concerned. In a steady state detonation process, the reaction rate is essentially infinite and the chemical equilibrium is attained. After the completion of the detonation, the detonation-produced explosive gas expands outwards. This gas expansion generally involves moving material interfaces if the explosive is surrounded by outside medium or free surfaces if the explosion occurs in the vacuum.

When the detonation and explosion happen underwater, the explosion physics can be more complicated. The underwater explosion (UNDEX) [341, 342] produced by the detonation of a submerged high explosive poses a serious threat to the integrity of nearby structures. Issues related to the underwater explosion include (1) the detonation process of the high explosive (HE) charge, (2) the expansion process of the detonation-produced explosive gas into the surrounding water, and (3) the interaction of underwater shocks with the nearby structures. In the detonation process, the high explosive is converted into gaseous products at very high temperature and pressure through a violent chemical reaction, occurring with extreme rapidity and releasing a great deal of heat. The propagation of the detonation wave through an explosive is so rapid that the gaseous products directly behind the wave front are not in pressure equilibrium with the gas further behind the wave front. As the detonation wave reaches the interface between the explosive and the surrounding water, a high pressure shock wave of step exponential type is transmitted to propagate through the water, followed by a series of bubble pulsation associated with the repeating expansion and contraction of the bubble of the explosive gas. In the entire process of the underwater explosions, some special features such as large deformations, large inhomogeneities, moving material interfaces, deformable boundaries, and free surfaces usually exist.

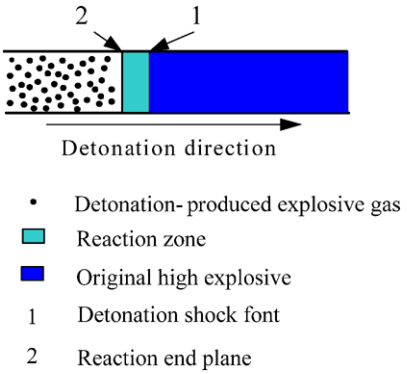

Fig. 31 Detonation of a 1D high explosive. The reaction end plane is an interface of the pressurized high explosive charge and the explosive gas produced in the detonation process

Theoretical solutions to the detonation and explosion of high explosive, and underwater explosion are only limited to some simple cases. Experimental studies need to resort to dangerous and expensive firing trials, and sometimes certain physical phenomena related to the explosions cannot be scaled in a practical experimental setup. Recently, more and more analyses of detonation, explosion and underwater explosions are based on numerical simulations with the advancement of the computer hardware and computational techniques [8, 343, 344]. However, numerical simulations of the high energy phenomena are generally very difficult for the conventional grid based numerical methods. First, during the detonation process in the explosion, a very thin reaction zone divides the domain into two inhomogeneous parts and produces large deformations. Second, in the expansion process, there are free surfaces and moving interfaces involved. It is even more difficult to simulate underwater explosion, as underwater explosion phenomena are subject to a number of physical laws and properties, including the physical conditions at the interface of the explosive gas and the surrounding water. The surrounding water has such properties as large density that is approximately 1000 times of the air density, low compressibility, and large sound speed.

Owing to the dynamic properties of the water (especially in the regions surrounding the explosive gas), the pressures are generally very high and the wave velocities are dependent on the magnitude of the pressure and the displacement of the water as it progresses. These complications for waves of finite amplitude are expressed in much more difficult mathematical statements than those which suffice to explain the propagation of small amplitude waves whose velocities are practically independent on the magnitude of the pressure.

Traditional Lagrangian techniques such as the finite element methods are capable of capturing the history of the detonation and explosion events associated with each material. It is, however, difficult to apply practically, since the severely distorted mesh may result in very inefficient small time step, and may even lead to the breakdown of the computation. Traditional Eulerian techniques, such as the finite difference methods or finite volume methods, can well resolve the problem due to the large deformations in the global motions, but it is very difficult to analyze the details of the flow because of the lack of history and the smearing of information as the mass moves through the fixed-in-space Eulerian mesh [256]. Considering the difficulties of grid based numerical models, the meshfree particle methods can be a good alternate for simulating detonation, explosion and underwater explosions [125, 136, 143, 247, 248, 252, 255, 256, 345–350].

Liu and his co-workers have conducted a series of original work in extending the SPH method for simulating explosion phenomena including high explosive detonation, explosion [248, 351], shaped charge [247], and underwater explosions [143, 255]. Since the detonation and expansion speed are extremely high, the gaseous products can be assumed to be inviscid and the explosion process is adiabatic. The Euler equations can be used to model the explosion process together with a suitable equation of state. The SPH equations of motion derived in Sect. 2.5 can thus be used to model high explosive explosion phenomena, with the viscosity terms in the momentum and energy equations ignored. For the explosive gas, the standard Jones-Wilkins-Lee (JWL) [352] equation of state has been employed. These works not only show the feasibility of applying the SPH method to explosion phenomena, but also identify some important and unresolved issues. A Gruneisen form of equation of state for water has been used, which is a polynomial form either in compressed or expanded state [353].

To show the effectiveness of the SPH method in dealing with detonation and explosion, a benchmark one-dimensional TNT slab denotation and explosion is provided here, in which a 0.1 m long TNT slab detonates at one end of the TNT slab.

If the solid wall boundary condition is used to prevent material transport from everywhere, a symmetric setup can be employed to deploy the particles, and thus makes the detonation of the 0.1 m long slab from one end to the other

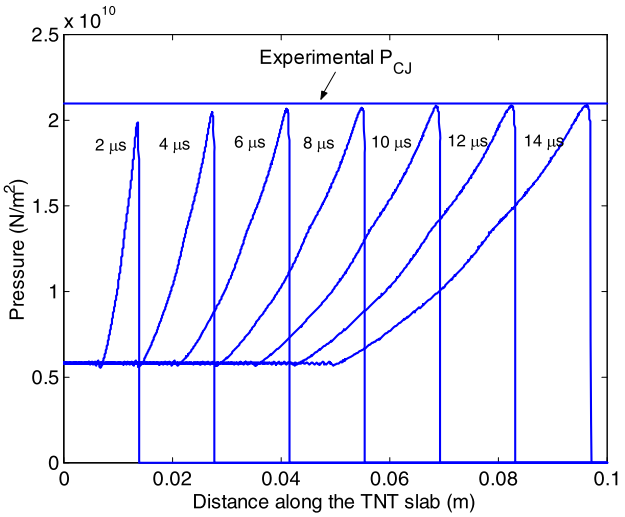

Fig. 32 Pressure profiles along the TNT slab during the detonation process (from [248])

end equivalent to the detonation of a 0.2 m long slab from the middle point to both ends. Before detonation, particles are evenly distributed along the slab. The initial smoothing length is one and a half times the particle separation. After ignition, a plane detonation wave is produced. According to the detonation velocity, it takes around 14.4 μs to complete the detonation to the end of the slab. Figure 32 show the pressure profile along the slab at 2 μs interval from 2 to 14 μs by using 4000 particles. The dashed line in Fig. 32 represents the experimentally determined C-J detonation pressure, which is, according to the Chapman and Jouguet's hypothesis, the pressure at the tangential point of the Hugoniot curve and the Rayleigh line, and represents the pressure at the equilibrium plane at the trailing edge of the very thin chemical reaction zone. For this one-dimensional TNT slab detonation problem, the experimental C-J pressure is 2.1×10^{10} N/m^2. It can be seen from Fig. 32 that, with the process of the detonation, the detonation pressure converges to the C-J pressure.

If the free boundary applies to the end of the detonation, the explosive gas behind the C-J plane disperses outwards with the forward propagating detonation wave. A theoretical solution for this one-dimensional TNT detonation-dispersion problem exists. Figure 33 shows the comparisons of velocity profiles between theoretical values and the presented SPH results at 1 and 2 μs. The presented SPH results are in close agreement with the theoretical values.

Figure 34 shows the pressure evolution in an underwater explosion process in a confined square chamber [143]. The initial outward propagating shock wave, reflection wave from the solid wall, explosive gas expansion and later compression can all be seen from the figure. Right after the detonation, a shock wave is generated in the water and propagates outwards. At the same time, the rarefaction wave is

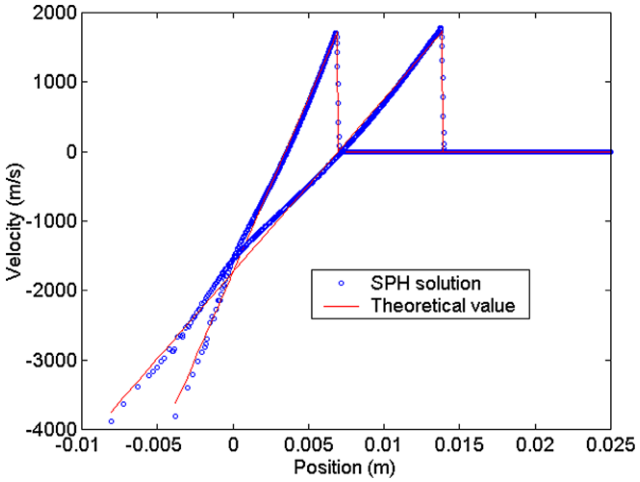

Fig. 33 Velocity transients at 1 and 2 μs for the TNT slab detonation-dispersion process (from [248])

also produced within the explosive gas and advances inward. With the advancement of the shock wave through the water, the gas bubble expands within the surrounding water. The shock wave reaches the solid wall around the instant of 200 μs, and then reflects from the solid wall. This reflection wave propagates inward and tends to compress the expanding gas. At around 400 μs, the gas bubble reaches to the maximum and then reduces. With the continued process of shock reflection and explosive gas contraction, the gas bubble then will reach a minimum size, and then expands afterwards. This repeated process of expansion and contraction maintains for many circles, and will finally reach equilibrium at larger time step.

6.3 Microfluidics and Micro Drop Dynamics

By integrating mechanical elements, sensors, actuators, and electronic components using micro-fabrication technology, micro-electro-mechanical systems (MEMS) are fast in response, capable of achieving high spatial resolution, and cost-effective due to the batch micromachining techniques. Characterization of fluid flows in microfluidic devices has increasingly becoming a very important topic since the fluidic behavior in MEMS is very different from what observed in daily life. Flows in microfluidic devices usually involve small or ignorable inertial force, but dominant viscous, electro-kinetic and surface effects especially when the surface-to-volume ratio increases [354]. Analytical or semi-analytical solutions for microfluidics are generally limited to a very few simple cases, whereas experimental studies are usually expensive. Numerical simulation of flows in microfluidic devices, as an effective alternate, has been attracting more and more researchers. However, simulation of microfluidic devices is not easy due to the involved complex features including movable boundaries (free surfaces and moving interfaces), large surface-to-volume ratio, and phenomena due to micro scale physics. Numerical studies with reliable models are needed to develop a better understanding of the temporal and spatial dynamics of multiphase flows in microfluidic devices.

On the other hand, drop formation and break-up in micro/nano scales are fundamentally important to diverse practical engineering applications such as ink-jet printing, DNA and protein micro-/nano-arraying, and fabrication of particles and capsules for controlled release of medicines. Numerical studies provide an effective tool to improve better understanding of the inherent physical dynamics of drop formation and breakup. Computational models for drop formation and breakup in micro/nano scales must be able to handle movable boundaries such as free surfaces and moving interfaces, large density ratios, and large viscosity ratios. These requirements together with micro scale phenomena and possible complex boundaries (fluid-fluid-solid contact line dynamics and fluid-fluid interface dynamics) in microfluidic devices present severe challenges to conventional Eulerian-grid based numerical methods such as FDM and FVM which require special algorithms to treat and track the interfaces. Algorithms based on Lagrangian-grid based methods such as FEM have been shown to agree quantitatively with experimental measurements, but they are only capable of modeling the dynamics of formation of a single drop or the dynamics until the occurrence of the first singularity.

A number of meso-scale methods have been developed for simulating micro- and nano-fluidics such as the direct simulation Monte Carlo (DSMC) for rarefied gas flows [355–359], and dissipative particle dynamics for complex fluid flows [41, 42, 118, 360]. Hoover and his co-workers have first noted the similarity between the particle methods of molecular dynamics and smoothed particle hydrodynamics, and described the inherent links between them [361–363]. Espanol and his colleagues, when studying the dissipative particle dynamics method for meso-scale applications, proposed a fluid particle dynamics model, which is actually a synthesis of dissipative particle dynamics and smoothed particle dynamics [96, 364]. Later on, they invented a smoothed dissipative particle dynamics for micro- or meso-scale applications, by introducing a fluctuation term into the conventional smoothed particle hydrodynamics [365].

There have been a lot of literatures addressing the applications of SPH method to simulating microfluidics and micro drop dynamics. Nugent and Posch described an approach to modeling liquid drops and surface tension for a van der Waals fluid [236]. The cohesive pressure in the equation of state for the van der Waals fluid actually acts an attractive force between SPH particles. Melean and his co-workers investigated the formation of micro drops using

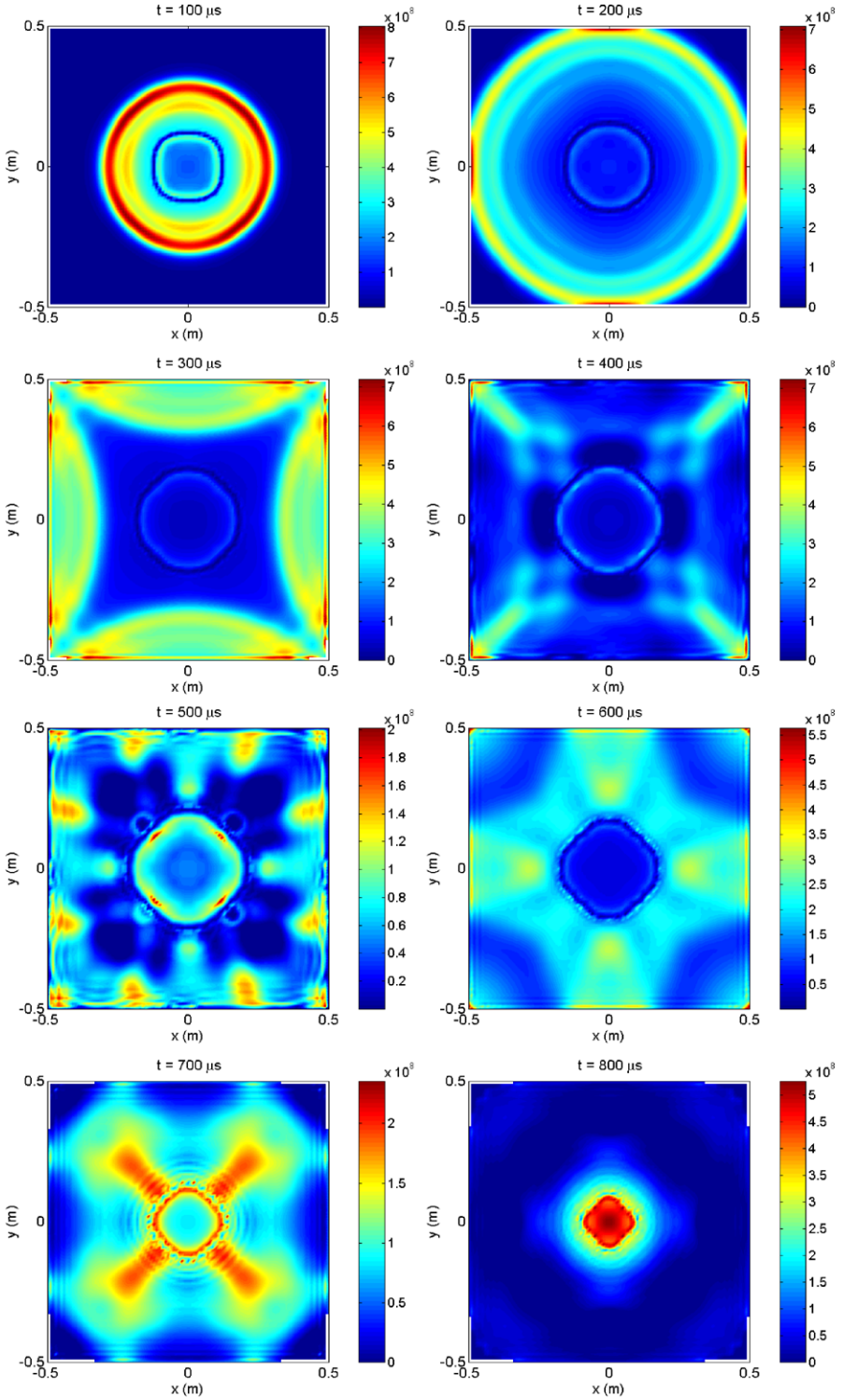

Fig. 34 Pressure distributions in a confined underwater explosion (from [143])

SPH method [155]. It was reported that the tensile instability also exists when using SPH for simulating viscous liquid drops and using an artificial stress proposed by Monaghan et al. [145] can help greatly to remove the tensile instability. Later on the group extended their work to the simulation of coalescence of colliding van der Waals liquid drops [240] and oscillation of viscous drops [239]. Liu et al. applied the SPH method to multiphase fluid flow in micro channels with applications to flip-chip underfill encapsulation process with both isotropic and anisotropic smoothing kernels [123, 366]. Li et al. proposed an SPH model for simulating droplet collision and coalescence [367]. Zhang

et al. developed an SPH model for free surface and solidification problems, which is also applicable to microfluidics and micro drop dynamics such as droplet spreading, splashing and solidification, substrate melting and deformation [243–245]. A revised surface tension model was developed for macro-scale particle methods including SPH by Zhou et al. [246]. Fang et al. also developed an improved SPH model for the simulations of droplet spreading and solidification [238]. Tartakovsky, Meakin and their co-workers have conducted a series of excellent work in applying the SPH method to the modeling of surface tension and contact angle [235], miscible flow in three-dimensional fractures and the two-dimensional Rayleigh Taylor instability [368], unsaturated flow in complex fractures [117], reactive transport and precipitation [369], mixing-induced precipitation [370] and non-aqueous phase liquid flow and dissolution [371].

There are basically two approaches in modeling the multiphase fluid flow in micro fluidic devices, and multiphase drop dynamics. The first approach is to use the continuum surface force (CSF) model proposed by Brackbill et al. [372], and introduced the surface tension force into the momentum equation as presented in Sect. 5. This approach is straightforward, and real physical parameters are used in the simulation. It is important to note that the surface tension parameters in this approach are user-input parameters, and surface curvature needs to be calculated to get the surface tension force. Some researchers have used this approach in SPH method to model multiphase fluid flow [123, 373].

With this CSF model, the surface tension is added to the momentum equation as an external source force. The surface tension force F can be formulated as follows

$$F = 2\gamma k(x) V \nabla V, \tag{109}$$

where γ is the surface tension coefficient, k is the surface curvature. V is the volume of a fluid cell. Let n be the surface normal which can be computed from the gradient of the fluid cell as $n = \nabla V$, the surface curvature k is defined as

$$k = \nabla \cdot \hat{n} = \frac{1}{|n|}\left[\left(\frac{n}{|n|}\cdot\nabla\right)|n| - (\nabla \cdot n)\right], \tag{110}$$

where $\hat{n}$ is the unit surface normal defined as

$$\hat{n} = \frac{n}{|n|}. \tag{111}$$

For fluid cells near a solid wall, a wall adhesion model is applied to adjust the surface normal through using the contact angle θ that a fluid is assumed to make with the wall. The dynamic contact angle can be different for different contacting points. However, in micro channel flows with a small buck velocity, the dynamic contact angle can be assumed to be constant along the flow direction as the starting contact angle. The unit normal $\hat{n}$ is adjusted as follows for fluid cells close to the wall

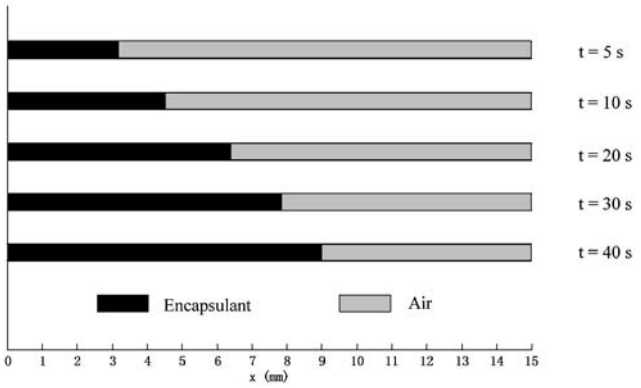

Fig. 35 Snapshots of the moving flow leading edge in an SPH simulation of a multiphase fluid flow in a micro channel using the CSF model (from [123])

$$\hat{n} = \hat{n}_w \cos\theta + \hat{n}_t \sin\theta \tag{112}$$

where $\hat{n}_w$ and $\hat{n}_t$ are the unit vectors of the surface normal ($n = \nabla V$) normal and tangential to the wall, respectively. Thereby the unit surface normal $\hat{n}$ for fluid cells near the wall is adjusted using the contact angle. Whereas the unit surface normal $\hat{n}$ for fluid cells one cell away from the wall is normally calculated. After determination of the unit surface normal, the local surface curvature and therefore the surface tension can be calculated.

Figure 35 gives an example of CSF model in simulating micro channel fluid flow. It is an underfill encapsulation process. The encapsulant is used to fill the space between the solder joints under the chip and the encapsulation process is either driven by a capillary action or by a pressurized injection [123].

Another approach is to introduce an inter-particle interaction force (IIF) implicitly in the SPH equations, and can be termed as IIF model. This attractive force between every pair of SPH particles contribute to the surface tension. Considering the SPH equations presented in Sect. 2.5, an equation of state can be used to close the equation system. An equation of state describes the relationship of the pressure p, density ρ and the internal energy per unit mass, e, respectively. For example, the van der Waals (vdW) equation of state can be used to model the behavior of the fluid under consideration. The van der Waals equation of state was derived from statistical mechanics as the mean-field limit for the free energy density of a system of hard particles with a superimposed long-range, attractive pair potential. It is realistic to display a gas-to-liquid phase transition similar to that of a real fluid. The van der Waals equation of state can written as

$$p = \frac{\rho \bar{k} T}{1 - \rho \bar{b}} - a\bar{\rho}^2, \tag{113}$$

and

$$e = \bar{k}T - \rho\bar{a}. \tag{114}$$

In the above two equations, $\bar{k} = k_B/T$, where k_B is the Boltzmann's constant. T is the system temperature. $\bar{a} = a/m^2$, and $\bar{b} = b/m$, where a and b are the parameter describing a van der Waals fluid. a controls the strength of the attractive force, and b relates to the size of the particle.

The second part in (113) describes the cohesion between particles. Using SPH particle approximation for pressure (see (28)), and considering this cohesive pressure part separately, we can get

$$\frac{D\boldsymbol{v}_i^\alpha}{Dt} = 2a\sum_{j=1}^{N} m_j \frac{\partial W_{ij}}{\partial \boldsymbol{x}_i^\alpha}. \tag{115}$$

Similarly substituting the cohesive pressure into the energy (see (28)), it is possible to get its analogous contribution to energy

$$\frac{De_i}{Dt} = -a\sum_{j=1}^{N} m_j \boldsymbol{v}_{ij}^\beta \frac{\partial W_{ij}}{\partial \boldsymbol{x}_i^\beta}. \tag{116}$$

It is clear that the attractive, long-range, inter-atomic vdW force can be transformed into similarly attractive forces between SPH particles. Equation (115) describes a volume force on continuum scale to account for the formation of co-existing liquid-gas phases. Comparing with the above-mentioned approach in using CSF model in calculating surface force, this approach does not need to locate the surface, and then to calculate the local surface curvature. Also, the surface tension is not user-input parameters, while it is implicitly obtained from inter-particle interactions. If the particles are distributed regularly (please refer to Sect. 4.2 on particle consistency), the force obtained from (115) vanishes for interior particles in both liquid and gas phases. While for boundary particles, e.g., particles near the gas-liquid interface, since the inter-particle interaction force between different phases are generally different, a surface force is produced, which is basically perpendicular to the surface, pointing towards the dense phase. Nugent and Posch identified that to obtain acceptable results, a large influencing area (e.g., two times the smoothing length for approximating other field variables and the first part in (113)) is necessary to conduct the particle approximations in (115) and (116).

Figure 36 shows an example of IIF model for the formation of a liquid drop. The initial square-shaped liquid (Fig. 36a) gradually becomes rounded at the corner due to the inter-particle interaction force, and finally forms a circular liquid drop.

Except for the inter-particle interaction force implicitly calculated from the cohesive pressure in the van der Waals

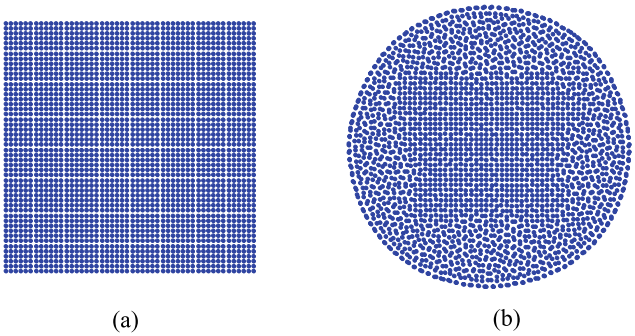

Fig. 36 SPH simulation of the formation of a liquid drop using the IIF model. (**a**) initial stage, (**b**) final stage of liquid drop

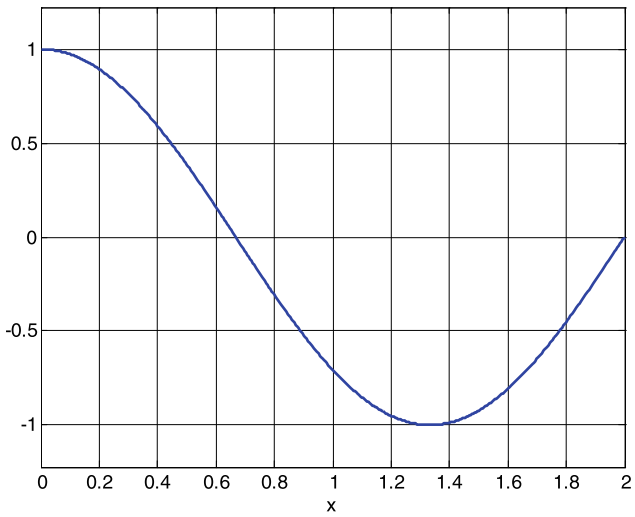

Fig. 37 The shape $(\cos(1.5\pi/kh))$ of the inter-particle interaction force expressed in (117) with $k = 2$

equation of state, Tartakovsky et al. added another inter-particle interaction force, which can be written as

$$\boldsymbol{F}_{ij} = \boldsymbol{s}_{ij}\cos(1.5\pi/kh)\boldsymbol{r}_{ij}, \tag{117}$$

where $\boldsymbol{s}_{ij}$ is an interaction coefficient. Figure 37 shows the shape of the inter-particle interaction force expressed in the above equation $(\cos(1.5\pi/kh)$ only, where $k = 2)$. It is clear that this inter-particle force is repulsive at short range, and attractive at long-distance. Similar to inter-particle force calculated from the cohesive pressure in the van der Waals equation of state, this inter-particle also describes a volume force on continuum scale and can account for the formation of co-existing liquid-gas phases. The force obtained from (117) also vanishes for interior particles in both liquid and gas phases, with small fluctuation around the overall direction of the macroscopic density gradient. For boundary particles, e.g., particles near the gas-liquid interface, a surface force is produced, pointing towards the denser phase. The IIF approach is comparatively simple and straightforward since it does not need to calculate the surface curvature,

which is not an easy task for particle methods like SPH. One problem is that as the IIF model implicitly calculates the surface tension force with parameters from atomistic level, it needs parameter calibration, which relates the physical parameters from atomistic level to continuum level.

6.4 Ocean and Coastal Hydrodynamics and Offshore Engineering

Flow phenomena in ocean and coastal hydrodynamics and offshore engineering are significantly important as they can greatly influence the nearly personnel and structures. The flow phenomena include

- wave dynamics (waver generation, wave breaking, and wave interaction with other structures),
- dam breaking,
- water filling and water discharge (to and from a water tank or reservoir),
- shallow water flows,
- entry of water, sloshing phenomena with fluid-solid interaction, and
- different other problems.

These phenomena involve special features, which make it difficult for numerical simulation. For example, water waves can propagate shoreward where they undergo changes induced by the near-shore topography and increase in height. Upon reaching the shoreline, they can break into pieces, and travel inland for large distances with potential damage of property and loss of life. Experimental setups for fluid flow in coast hydrodynamics and offshore engineering are expensive and only limited to laboratory applications. Numerical simulation has thus become a great tool to predicting fluid flow in ocean and coast hydrodynamics and offshore engineering.

However, numerical simulation of fluid flow in these related areas is a formidable task as it involves not only complex geometries and free surfaces, but also fluid-solid interaction as well as other complex physics in a comparably very large scale. In many circumstances, violent fluid–structure interactions lead to air entrapment and multi-phase flows, where the dynamics of the entrapped air at the impact may play a dominant role during the process and contribute to the high pressure maxima and pressure oscillations. Though conventional grid based methods like FDM, FVM and FEM have achieved greatly in simulating fluid flow in coast hydrodynamics and offshore engineering, there is still a long way to go for practical engineering applications.

Smoothed particle hydrodynamics, due to its meshfree, Lagrangian and particle nature, has been attracting more and more researchers in coast hydrodynamics and offshore engineering. From the very early simulation of a simple dam break problem [112], there have been a lot of literatures addressing the applications of SPH method in related areas.

Shao and his colleagues simulated near-shore solitary wave mechanics by an incompressible SPH method [374]. They later extended the work to simulation of wave breaking and overtopping with turbulence modeling [375], plunging waves using a 2-D sub-particle scale (SPS) turbulence model [376], solitary wave interaction with a curtain-type breakwater [377], and water entry of a free-falling object [190].

Frank and Reich addressed the conservation properties of SPH applied to shallow water equation [378]. Ata and Soulaimani proposed a stabilized SPH method for inviscid shallow water flows [379]. Rodriguez-Paz and Bonet also developed a corrected smooth particle hydrodynamics formulation of the shallow-water equations [380].

Investigation of water wave including water wave generation, water-structure interaction, and water wave breaking has been a very attractive application of the SPH method. Gomez-Gesteira and Dalrymple had investigated wave impact on a tall structure using a three-dimensional SPH method [180]. The research group also investigated water waves and waves breaking using the SPH method [175, 189]. Idelsohn and his co-workers applied the particle finite element method to solve incompressible flows with free-surfaces and breaking waves [381]. Gotoh et al. developed an SPH-LES model for numerical investigation of wave interaction with partially immersed breakwater [178]. They also simulated the coupled motion of progressive wave and floating curtain wall by using the developed SPH-LES model [177]. Gotoh and Sakai also addressed some key issues in the particle method for computation of wave breaking [183]. Recently, the research team developed a corrected incompressible SPH method for accurate water-surface tracking in breaking waves [185]. Crespo et al. presented an example of 3D SPH simulation of large waves mitigation with a dike [176]. Qiu studied the water waves generated by landslide [188]. Yim investigated the water wave generation by a vertical plunger using RANS and SPH models [193]. Cleary and Prakash discussed the feasibility of using SPH method for modeling tsunami effects [205, 266].

There are some references addressing the entry of water, e.g., air cushion effects in a wedge water entry [382], waves produced by a falling mass into a reservoir [383], water entry of a free-falling object [190], and wedge water entries [384].

Simulation of sloshing problems using SPH is a promising research direction. Iglesias et al. simulated the anti-roll tanks and sloshing type problems [196]. Rhee and Engineer studied liquid tank sloshing with Reynolds-averaged Navier-Stokes [199]. Souto-Iglesias et al. assessed the liquid moment amplitude in sloshing type problems with smooth particle hydrodynamics [200]. Anghileri investigated the fluid-structure interaction of water filled tanks during the impact

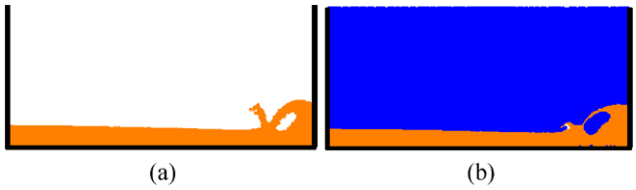

Fig. 38 SPH simulation of the dam-break flow and impact against a vertical wall at (**a**) single phase (water only) with free surface, and (**b**) two phases (water and air) with moving interface (from [387])

with the ground [285]. Delorme et al. simulated the sloshing loads in LNG tankers with SPH [385].

Figure 38 gives an example of the SPH simulation of the dam-break flow and impact again a vertical wall at (a) single phase (water only) with free surface, and (b) two phases (water and air) with moving interface. The flow pattern of flow along the surge front, the impact of fluid against the right hand side vertical wall and the entrapment of air bubble in water are in good agreement with the results from other sources [386].

6.5 Environmental and Geophysical Flows

Environmental and geophysical flows are fundamentally important for human life and economic development. In large scale, there are many typical environmental flow problems including

- flood due to dam break, or overflow of river and reservoir,
- landslide, mudslide, mud-rock flow triggered by heavy rain infiltration or even earth quake,
- sand/dust or dust storm,
- polluted liquid (e.g. oil) and air transport, and
- many others.

Unwanted environmental flows can be hazardous to nearby people and structures. In general, these large scale environmental flows are difficult to be accurately simulated and precisely predicted. On one hand, these large scale environmental flows involve complex geometries and arbitrarily moving interfaces. It is a formidable task to identify the origin of the flows. Therefore, it is hard to determine the initial and boundary condition for numerical simulations. On the other hand, large scale environmental flows are associated with complicated multiple fluid phases and multiple physics with solid-liquid-air phase at different scales. Theses also add difficulties to the numerical simulations for grid based numerical models.

It is very appealing to use SPH to model such large-scale environmental flow problems due to its meshfree, Lagrangian and particle nature. Actually in Sect. 6.4, some large-scale environmental flow problems such as dam breaking and tsunami effects have been discussed. They are also other references addressing the SPH applications in large-scale environmental flow problems. Ghazali and Kamsin presented a real time simulation and modeling of flood hazard [206]. Shen et al. conducted SPH simulation of river ice dynamics [233]. Kipfer and Westermann also investigated the realistic and interactive flows in river hydrodynamics [207]. Xu and Shen studied the fluid-structure interaction of hydrodynamic damper during the rush into the water channel [388].

Landslide and mudslide as well as mud-rock flows can be simulated using the SPH method. Cleary and his co-workers discussed the feasibility of using SPH method for modeling dam break, tsunami, landslide and volcano flows [205, 266]. The SPH method is coupled with discrete element method (DEM) for modeling solid-fluid interaction. Ataie-Ashtiani and Shobeyri simulated landslide impulsive waves by using incompressible smoothed particle hydrodynamics [389]. Qiu presented a two-dimensional SPH simulations of landslide-generated water waves [188]. McDougall and Hungr developed a numerical model for the analysis of rapid landslide motion across three-dimensional terrain [216]. Pastor et al. proposed a depth-integrated, coupled SPH model for flow-like landslides and related phenomena [220].

There are more references with applications to other large-scale environmental flow problems. Bui et al. developed an SPH model for large deformation and failure flows of geo-material using elastic-plastic soil constitutive model [209]. They also presented a numerical simulation of soil-water interaction using the SPH method [210]. Laigle and his colleagues developed an SPH-based numerical investigation of mudflow and other complex fluid flow interactions with structures [214].

Small scale environmental and geophysical flows are also very important, but are usually difficult to simulate because of the associated multiple fluid phases and multiple physics, as well as the existence of complex geometries and arbitrarily moving interfaces. For example, fluid motion in the vadose zone is very important for groundwater recharge, fluid motion and contaminant transport. Flow through fractures and fractured porous media can lead to exceptionally rapid movement of liquids and associated contaminants [99, 390, 391]. The physics of fluid flows in unsaturated fractures and porous media is still poorly understood due to the complexity of multiple phase flow dynamics. Experimental studies of fluid flow in fractures and fractured porous media are limited, and in computer simulations it is usually difficult to take into account the fracture surface properties and microscopic roughness. Predictive numerical models can be divided into two general classes: volume-averaged continuum models (such as those based on Richard's equation) and discrete mechanistic models. Knowledge of the physical properties of the fluids and the geometry of the fracture apertures is required in both classes. Volume-averaged continuum models are more suitable for large-scale systems,

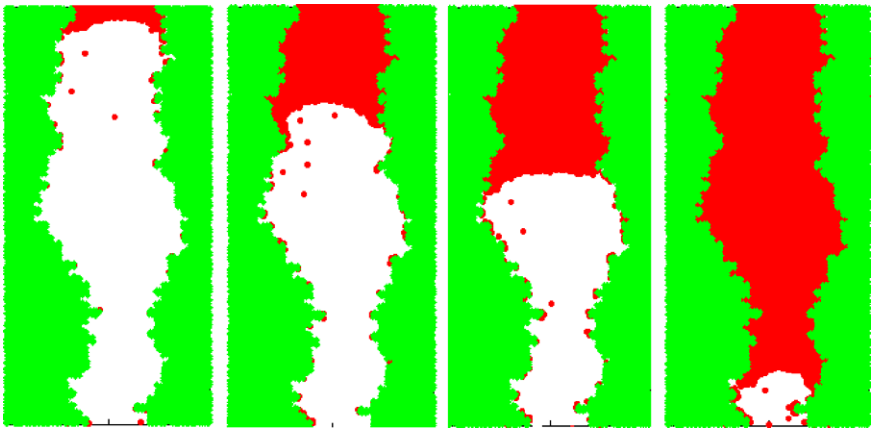

Fig. 39 Snapshots of SPH simulation of multiphase fluid motion in a fracture at 4 representative stages

and they usually involve the representation of fractures as porous media with porosity and permeability parameters adjusted to mimic flow within fractures. However, volume-averaged continuum models are unable to describe the details of flow dynamics in fractures, they do not reproduce the spatio-temporal complexity of multiphase fluid flow in fractures, and they often fail to predict the rapid fluid motion and contaminant transport observed in the fractured vadose zone. Small-scale studies with discrete mechanistic models are needed to develop a better understanding of the temporal and spatial dynamics of fracture flows. However, the complexity of fracture flow dynamics makes it difficult to develop successful numerical models for fluid flows in fracture networks. A broadly applicable model must be able to simulate a variety of phenomena including film flow with free surfaces, stable rivulets, snapping rivulets, fluid fragmentation and coalescence (including coalescence/fragmentation cascades), droplet migration and the formation of isolated single-phase islands trapped due to aperture variability.

Realistic mechanistic models for multiphase fluid flows in fracture and fractured porous media must be able to handle moving interfaces, large density ratios (e.g., $\approx 1000:1$ for water and air), and large viscosity ratios (e.g., $\approx 100:1$ for water and air). These requirements combined with the complex geometries of natural fractures present severe challenges to mechanistic models. Grid based numerical methods such as finite difference methods, finite volume methods and Eulerian finite element methods require special algorithms to treat and track the interface between different phases. However, continuum grid based numerical models usually do not take account of the detailed void and obstacle geometries, fluid-fluid interface dynamics within pores and complex fluid-fluid-solid contact line dynamics. They rely on constitutive equations that describe the coarse-grained behavior and can, at least in principle, be derived from the results of pore scale simulations or experiments. Therefore, small-scale simulations with mechanistic models are needed to develop a better understanding of the temporal and spatial dynamics of multiphase flow through porous media. Pore-scale flows have been studied extensively using grid based methods including finite difference method [392], finite volume method [393, 394], and finite element method [395]. However, due to the difficulties associated with geometrically complex boundaries, fluid-fluid-solid contact line dynamics, and fluid-fluid interface dynamics, it is difficult to apply conventional grid based multiphase simulation methods based on computational fluid dynamics (CFD) coupled with interface tracking algorithms [372, 396–398] to pore-scale multiphase flow modeling.

The SPH method has been recently modified for much smaller scale, typically low Reynolds number, applications The performance of the SPH method was demonstrated for two-dimensional single-phase flows through idealized, pore-scale porous media composed of spatially periodic square and hexagonal arrays of cylinders [202, 399], and two-phase (miscible and immiscible) flows through pore-scale fractures and fracture junctions [117, 368]. One obvious advantage of SPH over conventional grid based methods is that SPH does not require explicit and complicated interface tracking algorithms, and thus there is no need to explicitly track the material interfaces, and processes such as fluid fragmentation and coalescence can be handled without difficulty. SPH also does not require contact angle models since contact angles can be naturally calculated from the shape of the moving particle distributions, and can vary spatially and temporally, depending on the dynamic balance of viscous, capillary and gravitational forces. Figure 39 illustrates the snapshots of SPH simulation of multiphase fluid motion in a fracture at 4 representative stages. Water was injected into the top entrance of the fracture using a syringe pump and drained out through the bottom of the fracture.

7 Summary

Smoothed particle hydrodynamics (SPH) is a meshfree particle method, which not only uses particles as the computa-

tional frame for interpolation or differencing, but also uses the particles to carry the material properties. In this survey, the smoothed particle hydrodynamics method, and its recent development in numerical algorithms and applications have been reviewed. In methodology and numerical approximation, the basic concepts of kernel and particle approximations as well as different techniques for developing SPH formulations have been addressed. Different smoothing kernel functions have been reviewed with constructing conditions provided. The emphasis is on the consistency problem, which traditionally limits the accuracy of the SPH method. A number of consistency restoring approaches have been surveyed. An SPH formulation for discontinuity, a general approach for restoring particle consistency, and a finite particle method are described. Several important numerical topics have been investigated, including (1) solid boundary treatment, (2) representation of solid obstacles, (3) material interface treatment and (4) tensile instability. In applications, different applications of the SPH mEthod have been reviewed, with emphasis on (1) high strain hydrodynamics with material strength, (2) high explosive detonation and explosions, and underwater explosion, (3) microfluidics and micro drop dynamics, (4) coast hydrodynamics and offshore engineering, and (5) environmental and geophysical flows.

The last decades have witnessed the great success of SPH developments in methodology and applications, and there are still many tasks and challenges remaining. To achieve a reliable solution, the computational accuracy, consistency, efficiency, stability and convergence need to be incorporated into good SPH algorithms.

In general, SPH has great potential in many problems in engineering and science. It has salient advantages over traditional grid based numerical models in treating large deformation, tracking free surfaces, moving interfaces, and deformable boundaries, resolving moving discontinuities such as cracks and shock waves. The attraction of the SPH method has been showcased in diversified applications, as reviewed in Sect. 7.

One obvious advantage is that the SPH method provides a feasible physical model for non-continuum, as it has some same features as the classic molecular dynamics method and the dissipative particle dynamics method. Therefore it would be very attractive to apply the SPH method to simulating problems where the main concern of the object is a set of discrete physical particles rather than a continuum, e.g., the interaction of stars in astrophysics, movement of millions of atoms in an equilibrium or non-equilibrium state, dynamic behavior of protein molecules, and environmental flows with solid and fluid particles such as landslide and mudslide. There is no need for discretization to begin with for such situations. Also since SPH shares many similarities with other particle methods such as MD and DPD, it is natural to couple these three methods, from molecular dynamics (at nano- and micro-scales), to dissipative particle dynamics (at meso-scales), and then to smoothed particle hydrodynamics (at macro-scales) for simulations with multiple scale physics. It is attractive to develop reliable models of length scale coupling for problems with multiple physics and multiple scales, such as ink-jet printing, DNA and protein micro-/nano-arraying, and fabrication of particles and capsules for controlled release of medicines.

Acknowledgements The first author, M.B. Liu, has been supported by the National Natural Science Foundation of China (NSFC Grant No. 10942004).

References

1. Chung TJ (2002) Computational fluid dynamics. Cambridge University Press, Cambridge
2. Anderson JD (2002) Computational fluid dynamics: the basics with applications. McGraw Hill, New York
3. Zienkiewicz OC, Taylor RL (2000) The finite element method. Butterworth-Heinemann, Stonham
4. Liu GR (2002) Meshfree methods: moving beyond the finite element method. CRC Press, Boca Raton
5. Hirsch C (1988) Numerical computation of internal & external flows: fundamentals of numerical discretization. Wiley, New York
6. Liu GR, Liu MB (2003) Smoothed particle hydrodynamics: a meshfree particle method. World Scientific, Singapore
7. Liu GR, Gu YT (2005) An Introduction to meshfree methods and their programming. Springer, Dordrecht, p 479
8. Zhang SZ (1976) Detonation and its applications. Press of National Defense Industry, Beijing
9. Zukas JA (1990) High velocity impact dynamics. Wiley, New York
10. Hockney RW, Eastwood JW (1988) Computer simulation using particles. Institute of Physics Publishing, Bristol
11. Allen MP, Tildesley DJ (1987) Computer simulation of liquids. Oxford University Press, Oxford
12. Li S, Liu WK (2002) Meshfree and particle methods and their applications. Appl Mech Rev 55(1):1–34
13. Belytschko T, Krongauz Y, Organ D, Fleming M, Krysl P (1996) Meshless methods: an overview and recent developments. Comput Methods Appl Mech Eng 139(1–4):3–47
14. Idelsohn SR, Onate E (2006) To mesh or not to mesh? That is the question. Comput Methods Appl Mech Eng 195(37–40):4681–4696
15. Nguyen VP, Rabczuk T, Bordas S, Duflot M (2008) Meshless methods: a review and computer implementation aspects. Math Comput Simul 79(3):763–813
16. Liu GR (2008) A generalized Gradient smoothing technique and the smoothed bilinear form for Galerkin formulation of a wide class of computational methods. Int J Comput Methods 5(2):199–236
17. Liu GR (2009) A G space theory and weakened weak (W2) form for a unified formulation of compatible and incompatible methods, part I: theory. Int J Numer Methods Eng. doi:10.1002/nme.2719
18. Liu GR (2009) A G space theory and weakened weak (W2) form for a unified formulation of compatible and incompatible methods, part II: applications to solid mechanics problems. Int J Numer Methods Eng. doi:10.1002/nme.2720
19. Liu GR (2009) On the G space theory. Int J Comput Methods 6(2):257–289

20. Liu GR, Nguyen-Thoi T, H. N-X, Lam KY (2008) A node-based smoothed finite element method (NS-FEM) for upper bound solutions to solid mechanics problems. Comput Struct 87:14–26
21. Liu GR, Zhang GY (2008) Upper bound solution to elasticity problems: a unique property of the linearly conforming point interpolation method (LC-PIM). Int J Numer Methods Eng 74:1128–1161
22. Liu GR, Nguyen-Thoi T, Lam KY (2009) An edge-based smoothed finite element method (ES-FEM) for static, free and forced vibration analyses in solids. J Sound Vib 320:1100–1130
23. Zhang GY, Liu GR, Nguyen TT, Song CX, Han X, Zhong ZH, Li GY (2007) The upper bound property for solid mechanics of the linearly conforming radial point interpolation method (LC-RPIM). Int J Comput Methods 4(3):521–541
24. Liu GR, Zhang GY (2009) A normed G space and weakened weak (W2) formulation of a cell-based smoothed point interpolation method. Int J Comput Methods 6(1):147–179
25. Liu GR, Zhang GY (2008) Edge-based Smoothed Point Interpolation Methods. Int J Comput Methods 5(4):621–646
26. Liu GY, Zhang GY (2009) A novel scheme of strain-constructed point interpolation method for static and dynamic mechanics problems. Int J Appl Mech 1(1):233–258
27. Liu GR, Xu X, Zhang GY, Nguyen-Thoi T (2009) A superconvergent point interpolation method (SC-PIM) with piecewise linear strain field using triangular mesh. Int J Numer Methods Eng 77:1439–1467
28. Liu GR, Xu X, Zhang GY, Gu YT (2009) An extended Galerkin weak form and a point interpolation method with continuous strain field and superconvergence using triangular mesh. Comput Mech 43:651–673
29. Nguyen-Thoi T, Liu GR, Lam KY, Zhang GY (2009) A face-based smoothed finite element method (FS-FEM) for 3D linear and nonlinear solid mechanics problems using 4-node tetrahedral elements. Int J Numer Methods Eng 78:324–353
30. Liu GR, Nguyen-Thoi T, Lam KY (2008) A novel Alpha finite element method (FEM) for exact solution to mechanics problems using triangular and tetrahedral elements. Comput Methods Appl Mech Eng 197:3883–3897
31. Liu GR, Nguyen-Xuan H, Nguyen TT, Xu X (2009) A novel weak form and a superconvergent alpha finite element method for mechanics problems using triangular meshes. J Comput Phys 228(11):3911–4302
32. Liu GR, Zhang J, Lam KY (2008) A gradient smoothing method (GSM) with directional correction for solid mechanics problems. Comput Mech 41:457–472
33. Liu GR, Xu XG (2008) A gradient smoothing method (GSM) for fluid dynamics problems. Int J Numer Methods Fluids 58:1101–1133
34. Xu XG, Liu GR (2008) An adaptive gradient smoothing method (GSM) for fluid dynamics problems. Int J Numer Methods Fluids doi:10.1002/fld.2032
35. Xu XG, Liu GR, Lee KH (2009) Application of gradient smoothing method (GSM) for steady and unsteady incompressible flow problems using irregular triangles. Int J Numer Methods Fluids (submitted)
36. Lucy LB (1977) A numerical approach to the testing of the fission hypothesis. Astron J 82(12):1013–1024
37. Gingold RA, Monaghan JJ (1977) Smoothed particle hydrodynamics—theory and application to non-spherical stars. Mon Not R Astron Soc 181:375–389
38. Liu MB, Liu GR, Lam KY (2003) Constructing smoothing functions in smoothed particle hydrodynamics with applications. J Comput Appl Math 155(2):263–284
39. Fulk DA, Quinn DW (1996) An analysis of 1-D smoothed particle hydrodynamics kernels. J Comput Phys 126(1):165–180
40. Frenkel D, Smit B (2002) Understanding molecular simulation: from algorithms to applications. Academic Press, New York
41. Hoogerbrugge PJ, Koelman J (1992) Simulating microscopic hydrodynamic phenomena with dissipative particle dynamics. Europhys Lett 19:155
42. Groot RD (1997) Dissipative particle dynamics: Bridging the gap between atomistic and mesoscopic simulation. J Chem Phys 107(11):4423
43. Gingold RA, Monaghan JJ (1982) Kernel estimates as a basis for general particle method in hydrodynamics. J Comput Phys 46:429–453
44. Hu XY, Adams NA (2006) Angular-momentum conservative smoothed particle dynamics for incompressible viscous flows. Phys Fluids 18:101702
45. Swegle JW, Hicks DL, Attaway SW (1995) Smoothed particle hydrodynamics stability analysis. J Comput Phys 116(1):123–134
46. Morris JP (1996) Analysis of Smoothed Particle Hydrodynamics with Applications. Monash University
47. Monaghan JJ (1982) Why particle methods work. SIAM J Sci Stat Comput 3(4):422–433
48. Monaghan JJ (1985) Particle methods for hydrodynamics. Comput Phys Rep 3:71–124
49. Monaghan JJ (1992) Smooth particle hydrodynamics. Annu Rev Astron Astrophys 30:543–574
50. Johnson GR (1996) Artificial viscosity effects for SPH impact computations. Int J Impact Eng 18(5):477–488
51. Johnson GR, Beissel SR (1996) Normalized smoothing functions for SPH impact computations. Int J Numer Methods Eng 39(16):2725–2741
52. Randles PW, Libersky LD (1996) Smoothed particle hydrodynamics: some recent improvements and applications. Comput Methods Appl Mech Eng 139(1):375–408
53. Chen JK, Beraun JE, Carney TC (1999) A corrective smoothed particle method for boundary value problems in heat conduction. Int J Numer Methods Eng 46:231–252
54. Chen JK, Beraun JE (2000) A generalized smoothed particle hydrodynamics method for nonlinear dynamic problems. Comput Methods Appl Mech Eng 190:225–239
55. Liu MB, Liu GR, Lam KY (2003) A one-dimensional meshfree particle formulation for simulating shock waves. Shock Waves 13(3):201–211
56. Liu MB, Liu GR (2006) Restoring particle consistency in smoothed particle hydrodynamics. Appl Numer Math 56(1):19–36
57. Liu MB, Xie WP, Liu GR (2005) Modeling incompressible flows using a finite particle method. Appl Math Model 29(12):1252–1270
58. Batra RC, Zhang GM (2004) Analysis of adiabatic shear bands in elasto-thermo-viscoplastic materials by modified smoothed-particle hydrodynamics (MSPH) method. J Comput Phys 201(1):172–190
59. Fang JN, Owens RG, Tacher L, Parriaux A (2006) A numerical study of the SPH method for simulating transient viscoelastic free surface flows. J Non-Newton Fluid 139(1–2):68–84
60. Fang JN, Parriaux A (2008) A regularized Lagrangian finite point method for the simulation of incompressible viscous flows. J Comput Phys 227(20):8894–8908
61. Fang JN, Parriaux A, Rentschler M, Ancey C (2009) Improved SPH methods for simulating free surface flows of viscous fluids. Appl Numer Math 59(2):251–271
62. Dyka CT, Ingel RP (1995) An approach for tension instability in smoothed particle hydrodynamics (SPH). Comput Struct 57(4):573–580
63. Dyka CT, Randles PW, Ingel RP (1997) Stress points for tension instability in SPH. Int J Numer Methods Eng 40(13):2325–2341
64. Randles PW, Libersky LD, (2000) Normalized SPH with stress points. Int J Numer Methods Eng 48(10):1445–1462

65. Vignjevic R, Campbell J, Libersky L (2000) A treatment of zero-energy modes in the smoothed particle hydrodynamics method. Comput Methods Appl Mech Eng 184(1):67–85
66. Dilts GA (1999) Moving-Least-Squares-particle hydrodynamics. I: Consistency and stability. Int J Numer Methods Eng 44:1115–1155
67. Dilts GA (2000) Moving least square particle hydrodynamics ii: conservation and boundaries. Int J Numer Methods Eng 48:1503–1524
68. Bonet J, Kulasegaram S (2000) Correction and stabilization of smooth particle hydrodynamics methods with applications in metal forming simulations. Int J Numer Methods Eng 47(6):1189–1214
69. Chen JS, Pan C, Wu CT, Liu WK (1996) Reproducing kernel particle methods for large deformation analysis of nonlinear structures. Comput Methods Appl Mech Eng 139:195–227
70. Liu WK, Chen Y, Jun S, Chen JS, Belytschko T, Pan C, Uras RA, Chang CT (1996) Overview and applications of the reproducing kernel particle methods. Arch Comput Methods Eng 3(1):3–80
71. Rabczuk T, Belytschko T, Xiao SP (2004) Stable particle methods based on Lagrangian kernels. Comput Methods Appl Mech Eng 193(12):1035–1063
72. Belytschko T, Krongauz Y, Dolbow J, Gerlach C (1998) On the completeness of the meshfree particle methods. Int J Numer Methods Eng 43(5):785–819
73. Zhang GM, Batra RC (2004) Modified smoothed particle hydrodynamics method and its application to transient problems. Comput Mech 34(2):137–146
74. Belytschko T, Guo Y, Liu WK, Xiao SP (2000) A unified stability analysis of meshless particle methods. Int J Numer Methods Eng 48:1359–1400
75. Fulk DA (1994) A numerical analysis of smoothed particle hydrodynamics. Air Force Institute of Technology
76. Monaghan JJ (2005) Smoothed particle hydrodynamics. Rep Prog Phys 68(8):1703–1759
77. Hernquist L (1993) Some cautionary remarks about smoothed particle hydrodynamics. Astrophys J 404(2):717–722
78. Century Dynamics Incorporated (1997) AUTODYN release notes version 3.1. AUTODYN™ interactive non-linear dynamic analysis software
79. Benz W (1990) Smooth particle hydrodynamics: a review. The numerical modelling of nonlinear stellar pulsations, problems and prospects. Kluwer Academic, Boston
80. Morris JP (1996) A study of the stability properties of smooth particle hydrodynamics. Publ Astron Soc Aust 13(1):97–102
81. Omang M, Borve S, Trulsen J (2005) Alternative kernel functions for smoothed particle hydrodynamics in cylindrical symmetry. Shock Waves 14(4):293–298
82. Jin HB, Ding X (2005) On criterions for smoothed particle hydrodynamics kernels in stable field. J Comput Phys 202(2):699–709
83. Capuzzo-Dolcetta R, Di Lisio R (2000) A criterion for the choice of the interpolation kernel in smoothed particle hydrodynamics. Appl Numer Math 34(4):363–371
84. Cabezon RM, Garcia-Senz D, Relano A (2008) A one-parameter family of interpolating kernels for smoothed particle hydrodynamics studies. J Comput Phys 227(19):8523–8540
85. Monaghan JJ, Lattanzio JC (1985) A refined particle method for astrophysical problems. Astron Astrophys 149(1):135–143
86. Johnson GR, Stryk RA, Beissel SR (1996) SPH for high velocity impact computations. Comput Methods Appl Mech Eng 139(1–4):347–373
87. Swegle JW, Attaway SW, Heinstein MW, Mello FJ Hicks DL (1994) An analysis of smoothed particle hydrodynamics. Sandia National Labs., Albuquerque
88. Liu GR, Quek SS (2003) The finite element method: a practical course. Butterworth-Heinemann, Bristol
89. Chen JK, Beraun JE, Jih CJ (1999) An improvement for tensile instability in smoothed particle hydrodynamics. Comput Mech 23(4):279–287
90. Chen JK, Beraun JE, Jih CJ (1999) Completeness of corrective smoothed particle method for linear elastodynamics. Comput Mech 24(4):273–285
91. Hernquist L, Katz N (1989) TREESPH—a unification of SPH with the hierarchical tree method. Astrophys J Suppl Ser 70(2):419–446
92. Sod GA (1978) A survey of several finite difference methods for systems of nonlinear hyperbolic conservation laws. J Comput Phys 27:1–31
93. Fletcher CAJ (1991) Computational techniques for fluid dynamics, 1: fundamental and general techniques. Springer, Berlin
94. Agertz O, Moore B, Stadel J, Potter D, Miniati F, Read J, Mayer L, Gawryszczak A, Kravtosov A, Nordlund A, Pearce F, Quilis V, Rudd D, Springel V, Stone J, Tasker E, Teyssier R, Wadsley J, Walder R (2007) Fundamental differences between SPH and grid methods. Mon Not R Astron Soc 380:963–978
95. Schussler M, Schmitt D (1981) Comments on smoothed particle hydrodynamics. Astron Astrophys 97(2):373–379
96. Espanol P (1998) Fluid particle model. Phys Rev E 57(3):2930–2948
97. Wang L, Ge W, Li J (2006) A new wall boundary condition in particle methods. Comput Phys Commun 174(5):386–390
98. Revenga M, Zuniga I, Espanol P (1998) Boundary models in DPD. Int J Mod Phys C 9(8):1319–1328
99. Liu MB, Meakin P, Huang H (2007) Dissipative particle dynamics simulation of pore-scale flow. Water Resour Res 43:W04411. doi:10.1029/2006WR004856
100. Revenga M, Zuniga I, Espanol P (1998) Boundary models in DPD. Int J Mod Phys C 9(8):1319–1328
101. Revenga M, Zuniga I, Espanol P (1999) Boundary conditions in dissipative particle dynamics. Comput Phys Commun 121(122):309–311
102. Willemsen SM, Hoefsloot HCJ, Iedema PD (2000) No-slip boundary condition in dissipative particle dynamics. Int J Mod Phys C 11(5):881–890
103. Duong-Hong D, Phan-Thien N, Fan X (2004) An implementation of no-slip boundary conditions in DPD. Comput Mech 35(1):24–29
104. Crespo AJC, Gomez-Gesteira M, Dalrymple RA (2007) Boundary conditions generated by dynamic particles in SPH methods. Comput Mater Continua 5(3):173–184
105. Gong K, Liu H (2007). A new boundary treatment for smoothed particle hydrodynamics. In: Asian and Pacific coasts 2007, Nanjing, China
106. Hieber SE, Koumoutsakos P (2008) An immersed boundary method for smoothed particle hydrodynamics of self-propelled swimmers. J Comput Phys 227(19):8636–8654
107. Klessen R (1997) GRAPESPH with fully periodic boundary conditions: fragmentation of molecular clouds. Mon Not R Astron Soc 292(1):11–18
108. Randles PW, Libersky LD (2005) Boundary conditions for a dual particle method. Comput Struct 83(17–18):1476–1486
109. Yildiz M, Rook RA, Suleman A (2009) SPH with the multiple boundary tangent method. Int J Numer Methods Eng 77(10):1416–1438
110. Takeda H, Miyama SM, Sekiya M (1994) Numerical simulation of viscous flow by smoothed particle hydrodynamics. Prog Theor Phys 92(5):939–960
111. Morris JP, Fox PJ, Zhu Y (1997) Modeling low Reynolds number incompressible flows using SPH. J Comput Phys 136(1):214–226
112. Monaghan JJ (1994) Simulating free surface flows with SPH. J Comput Phys 110(2):399–406

113. Campbell PM (1989) Some new algorithms for boundary value problems in smooth particle hydrodynamics. Technical Report, Mission Research Corp, Albuquerque, NM
114. Libersky LD, Petschek AG, Carney TC, Hipp JR, Allahdadi FA (1993) High strain Lagrangian hydrodynamics: a three-dimensional SPH code for dynamic material response. J Comput Phys 109(1):67–75
115. Rapaport DC (2004) The art of molecular dynamics simulation. Cambridge University Press, Cambridge
116. Liu MB, Meakin P, Huang H (2007) Dissipative particle dynamics simulation of fluid motion through an unsaturated fracture and fracture junction. J Comput Phys 222(1):110–130
117. Tartakovsky AM, Meakin P (2005) Simulation of unsaturated flow in complex fractures using smoothed particle hydrodynamics. Vadose Zone J 4(3):848–855
118. Liu MB, Meakin P, Huang H (2007) Dissipative particle dynamics simulation of multiphase fluid flow in microchannels and microchannel networks. Phys Fluids 19(3):033302
119. Colagrossi A, Landrini M (2003) Numerical simulation of interfacial flows by smoothed particle hydrodynamics. J Comput Phys 191(2):448–475
120. Owen JM, Villumsen JV, Shapiro PR, Martel H (1998) Adaptive smoothed particle hydrodynamics: methodology, II. Astrophys J Suppl Ser 116(2):155–209
121. Shapiro PR, Martel H, Villumsen JV, Owen JM (1996) Adaptive smoothed particle hydrodynamics, with application to cosmology: methodology. Astrophys J Suppl Ser 103(2):269–330
122. Fulbright MS, Benz W, Davies MB (1995) A method of smoothed particle hydrodynamics using spheroidal kernels. Astrophys J 440(1):254–262
123. Liu MB, Liu GR (2005) Meshfree particle simulation of micro channel flows with surface tension. Comput Mech 35(5):332–341
124. Liu MB, Liu GR, Lam KY (2006) Adaptive smoothed particle hydrodynamics for high strain hydrodynamics with material strength. Shock Waves 15(1):21–29
125. Swegle JW, Attaway SW (1995) On the feasibility of using smoothed particle hydrodynamics for underwater explosion calculations. Comput Mech 17(3):151–168
126. Attaway SW, Hendrickson BA, Plimpton SJ, Gardner DR, Vaughan CT, Brown KH, Heinstein MW (1998) A parallel contact detection algorithm for transient solid dynamics simulations using PRONTO3D. Comput Mech 22(2):143–159
127. Campbell J, Vignjevic R, Libersky L (2000) A contact algorithm for smoothed particle hydrodynamics. Comput Methods Appl Mech Eng 184(1):49–65
128. Drumm C, Tiwari S, Kuhnert J, Bart HJ (2008) Finite pointset method for simulation of the liquid-liquid flow field in an extractor. Comput Chem Eng 32(12):2946–2957
129. Huang H, Dyka CT, Saigal S (2004) Hybrid particle methods in frictionless impact-contact problems. Int J Numer Methods Eng 61:2250–2272
130. Li Y, Liu GR, Luan MT, Ky Dai, Zhong ZH, Li GY, Han X (2007) Contact analysis for solids based on linearly conforming radial point interpolation method. Comput Mech 39(4):537–554
131. Limido J, Espinosa C, Salauen M, Lacome JL (2007) SPH method applied to high speed cutting modelling. Int J Mech Sci 49(7):898–908
132. Mehra V, Chaturvedi S (2006) High velocity impact of metal sphere on thin metallic plates: a comparative smooth particle hydrodynamics study. J Comput Phys 212(1):318–337
133. Parshikov AN, Medin SA (2002) Smoothed particle hydrodynamics using interparticle contact algorithms. J Comput Phys 180(1):358–382
134. Parshikov AN, Medin SA, Loukashenko II, Milekhin VA (2000) Improvements in SPH method by means of interparticle contact algorithm and analysis of perforation tests at moderate projectile velocities. Int J Impact Eng 24(8):779–796
135. Plimpton S, Attaway S, Hendrickson B, Swegle J, Vaughan C, Gardner D (1998) Parallel transient dynamics simulations: algorithms for contact detection and smoothed particle hydrodynamics. J Parallel Distrib Comput 50(1–2):104–122
136. Prochazka PP, Kravtsov AN, Peskova S (2008) Blast impact on structures of underground parking. Undergr Spaces Des Eng Environ Asp 102:11–19
137. Sauer RA, Li SF (2008) An atomistically enriched continuum model for nanoscale contact mechanics and Its application to contact scaling. J Nanosci Nanotechnol 8(7):3757–3773
138. Schieback C, Burzle F, Franzrahe K, Neder J, Henseler P, Mutter D, Schwierz N, Nielaba P (2009) Computer simulations of complex many-body systems. In: High performance computing in science and engineering '08, Stuttgart, Germany
139. Seo S, Min O, Lee J (2008) Application of an improved contact algorithm for penetration analysis in SPH. Int J Impact Eng 35(6):578–588
140. Vignjevic R, Campbell J (1999) A penalty approach for contact in smoothed particle hydrodynamics. Int J Impact Eng 23(1):945–956
141. Vignjevic R, De Vuyst T, Campbell JC, Source C (2006) A frictionless contact algorithm for meshless methods. Comput Model Eng 13(1):35
142. Belytschko T, Neal MO (1991) Contact-impact by the pinball algorithm with penalty and Lagrangian methods. Int J Numer Methods Eng 31(3):547–572
143. Liu MB, Liu GR, Lam KY, Zong Z (2003) Smoothed particle hydrodynamics for numerical simulation of underwater explosion. Comput Mech 30(2):106–118
144. Liu MB, Liu GR, Lam KY, Zong Z (2001) A new technique to treat material interfaces for smoothed particle hydrodynamics. In: Computational mechanics—new frontiers for new millennium. Elsevier Science, Amsterdam
145. Monaghan JJ (2000) SPH without a tensile instability. J Comput Phys 159(2):290–311
146. Vignjevic R, De Vuyst T, Campbell J (2002) The use of a homogeneous repulsive force for contact treatment in sph. In: WCCM V, Vienna, Austria
147. Balsara DS (1995) von Neumann stability analysis of smoothed particle hydrodynamics suggestions for optimal algorithms. J Comput Phys 121(2):357–372
148. Belytschko T, Xiao S (2002) Stability analysis of particle methods with corrected derivatives. Comput Math Appl 43(3–5):329–350
149. Bonet J, Kulasegaram S (2001) Remarks on tension instability of Eulerian and Lagrangian corrected smooth particle hydrodynamics (CSPH) methods. Int J Numer Methods Eng 52:1203–1220
150. Lanson N, Vila JP (2007) Renormalized meshfree schemes, I: consistency, stability, and hybrid methods for conservation laws. SIAM J Numer Anal 46(4):1912–1934
151. Randles PW, Petschek AG, Libersky LD, Dyka CT (2003) Stability of DPD and SPH. In: Meshfree methods for partial differential equations. Springer, Berlin
152. Sigalotti LDG, Lopez H (2008) Adaptive kernel estimation and SPH tensile instability. Comput Math Appl 55(1):23–50
153. Gray JP, Monaghan JJ, Swift RP (2001) SPH elastic dynamics. Comput Methods Appl Mech Eng 190(49):6641–6662
154. Beissel S, Belytschko T (1996) Nodal integration of the element-free Galerkin method. Comput Methods Appl Mech Eng 139(1–4):49–74
155. Melean Y, Sigalotti LDG, Hasmy A (2004) On the SPH tensile instability in forming viscous liquid drops. Comput Phys Commun 157(3):191–200

156. Benz W (1988) Applications of smooth particle hydrodynamics (SPH) to astrophysical problems. Comput Phys Commun 48(1):97–105
157. Frederic AR, James CL (1999) Smoothed particle hydrodynamics calculations of stellar interactions. J Comput Appl Math 109:213–230
158. Hultman J, Pharayn A (1999) Hierarchical, dissipative formation of elliptical galaxies: is thermal instability the key mechanism? Hydrodynamic simulations including supernova feedback multiphase gas and metal enrichment in cdm: structure and dynamics of elliptical galaxies. Astron Astrophys 347:769–798
159. Thacker RJ, Couchman HMP (2001) Star formation, supernova feedback, and the angular momentum problem in numerical cold dark matter cosmogony: halfway there. Astrophys J 555(1):L17–L20
160. Monaghan JJ, Lattanzio JC (1991) A simulation of the collapse and fragmentation of cooling molecular clouds. Astrophys J 375(1):177–189
161. Berczik P (2000) Modeling the star formation in galaxies using the chemo-dynamical SPH code. Astrophys Space Sci 271(2):103–126
162. Lee WH, Kluzniak W (1999) Newtonian hydrodynamics of the coalescence of black holes with neutron stars, II: tidally locked binaries with a soft equation of state. Mon Not R Astron Soc 308(3):780–794
163. Lee WH (2000) Newtonian hydrodynamics of the coalescence of black holes with neutron stars, III: irrotational binaries with a stiff equation of state. Mon Not R Astron Soc 318(2):606–624
164. Senz DG, Bravo E, Woosley SE (1999) Single and multiple detonations in white dwarfs. Astron Astrophys 349:177–188
165. Monaghan JJ (1990) Modelling the universe. Astron Soc Aust Proc 8(3):233–237
166. Hong JM, Lee HY, Yoon JC, Kim CH (2008) Bubbles alive. ACM Trans Graph 27(3)
167. Monaghan JJ, Kocharyan A (1995) SPH simulation of multiphase flow. Comput Phys Commun 87:225–235
168. Hu XY, Adams NA (2006) A multi-phase SPH method for macroscopic and mesoscopic flows. J Comput Phys 213(2):844–861
169. Garg R, Narayanan C, Lakehal D, Subramaniam S (2007) Accurate numerical estimation of interphase momentum transfer in Lagrangian-Eulerian simulations of dispersed two-phase flows. Int J Multiph Flow 33(12):1337–1364
170. Liu J, Koshizuka S, Oka Y (2005) A hybrid particle-mesh method for viscous, incompressible, multiphase flows. J Comput Phys 202(1):65–93
171. Password F (2003) Cosmological smoothed particle hydrodynamics simulations: a hybrid multiphase model for star formation. Mon Not R Astron Soc 339(2):289–311
172. Ritchie BW, Pa Thomas (2001) Multiphase smoothed-particle hydrodynamics. Mon Not R Astron Soc 323(3):743–756
173. Hu XY, Adams NA (2009) A constant-density approach for incompressible multi-phase SPH. J Comput Phys 228(6):2082–2091
174. Hu XY, Adams NA (2007) An incompressible multi-phase SPH method. J Comput Phys 227(1):264–278
175. Dalrymple RA, Rogers BD (2006) Numerical modeling of water waves with the SPH method. Coast Eng 53(2–3):141–147
176. Crespo AJC, Gomez-Gesteira M, Dalrymple RA (2007) 3D SPH simulation of large waves mitigation with a dike. J Hydraul Res 45(5):631–642
177. Shao SD, Gotoh H (2004) Simulating coupled motion of progressive wave and floating curtain wall by SPH-LES model. Coast Eng J 46(2):171–202
178. Gotoh H, Shao SD, Memita T (2004) SPH-LES model for numerical investigation of wave interaction with partially immersed breakwater. Coast Eng 46(1):39–63
179. Shao SD (2006) Incompressible SPH simulation of wave breaking and overtopping with turbulence modelling. Int J Numer Methods Fluids 50(5):597–621
180. Gomez-Gesteira M, Dalrymple RA (2004) Using a three-dimensional smoothed particle hydrodynamics method for wave impact on a tall structure. J Waterw Port C 130(2):63–69
181. Crespo AJC, Gomez-Gesteira M, Carracedo P, Dalrymple RA (2008) Hybridation of generation propagation models and SPH model to study severe sea states in Galician Coast. J Mar Syst 72(1–4):135–144
182. Crespo AJC, Gomez-Gesteira M, Dalrymple RA (2008) Modeling dam break behavior over a wet bed by a SPH technique. J Waterw Port C 134(6):313–320
183. Gotoh H, Sakai T (2006) Key issues in the particle method for computation of wave breaking. Coast Eng 53(2–3):171–179
184. Issa R, Violeau D (2008) Modelling a plunging breaking solitary wave with eddy-viscosity turbulent SPH models. Comput Mater Continua 8(3):151–164
185. Khayyer A, Gotoh H, Shao SD (2008) Corrected incompressible SPH method for accurate water-surface tracking in breaking waves. Coast Eng 55(3):236–250
186. Monaghan JJ, Kos A, Issa N (2003) Fluid motion generated by impact. J Waterw Port C 129(6):250–259
187. Panizzo A (2005). SPH modelling of underwater landslide generated waves. In: Proceedings of the 29th international conference on coastal engineering 2004, Lisbon, Portugal
188. Qiu LC (2008) Two-dimensional SPH simulations of landslide-generated water waves. J Hydraul Eng ASCE 134(5):668–671
189. Rogers BD, Dalrymple RA (2005) SPH modeling of breaking waves. In: Proceedings of the 29th international conference on coastal engineering 2004, Lisbon, Portugal
190. Shao SD (2009) Incompressible SPH simulation of water entry of a free-falling object. Int J Numer Methods Fluids 59(1):91–115
191. Shao SD, Ji CM, Graham DI, Reeve DE, James PW, Chadwick AJ (2006) Simulation of wave overtopping by an incompressible SPH model. Coast Eng 53(9):723–735
192. Violeau D, Buvat C, Abed-Meraim K, de Nanteuil E (2007) Numerical modelling of boom and oil spill with SPH. Coast Eng 54(12):895–913
193. Yim SC, Yuk D, Panizzo A, Di Risio M, Liu PLF (2008) Numerical simulations of wave generation by a vertical plunger using RANS and SPH models. J Waterw Port C 134(3):143–159
194. Zou S, Dalrymple RA (2005) Sediment suspension modeling by smoothed particle hydrodynamics. In: Proceedings of the 29th international conference on coastal engineering 2004, Lisbon, Portugal
195. Bulgarelli UP (2005) The application of numerical methods for the solution of some problems in free-surface hydrodynamics. J Ship Res 49(4):288–301
196. Iglesias AS, Rojas LP, Rodriguez RZ (2004) Simulation of anti-roll tanks and sloshing type problems with smoothed particle hydrodynamics. Ocean Eng 31(8–9):1169–1192
197. Kim Y (2007) Experimental and numerical analyses of sloshing flows. J Eng Math 58(1–4):191–210
198. Lohner R, Yang C, Onate E (2006) On the simulation of flows with violent free surface motion. Comput Methods Appl Mech Eng 195(41–43):5597–5620
199. Rhee SH, Engineer L (2005) Unstructured grid based Reynolds-averaged Navier-Stokes method for liquid tank sloshing. J Fluid Eng 127:572
200. Souto-Iglesias A, Delorme L, Perez-Rojas L, Abril-Perez S (2006) Liquid moment amplitude assessment in sloshing type problems with smooth particle hydrodynamics. Ocean Eng 33(11–12):1462–1484

201. Bursik M, Martinez-Hackert B, Delgado H, Gonzalez-Huesca A (2003) A smoothed-particle hydrodynamic automaton of landform degradation by overland flow. Geomorphology 53(1–2):25–44
202. Zhu Y, Fox PJ, Morris JP (1999) A pore-scale numerical model for flow through porous media. Int J Numer Anal Methods 23(9):881–904
203. Zhu Y, Fox PJ (2002) Simulation of pore-scale dispersion in periodic porous media using smoothed particle hydrodynamics. J Comput Phys 182(2):622–645
204. Tartakovsky AM, Meakin P (2006) Pore scale modeling of immiscible and miscible fluid flows using smoothed particle hydrodynamics. Adv Water Resour 29(10):1464–1478
205. Cleary PW, Prakash M (2004) Discrete-element modelling and smoothed particle hydrodynamics: potential in the environmental sciences. Philos Trans R Soc A 362(1822):2003–2030
206. Ghazali JN, Kamsin A (2008) A real time simulation and modeling of flood hazard. In: 12th WSEAS international conference on systems, Heraklion, Greece
207. Kipfer P, Westermann R (2006) Realistic and interactive simulation of rivers. In: Graphics interface 2006, Quebec, Canada
208. Bui HH, Fukagawa R, Sako K (2006) Smoothed particle hydrodynamics for soil mechanics. Taylor & Francis, London
209. Bui HH, Fukagawa R, Sako K, Ohno S (2008) Lagrangian meshfree particles method (SPH) for large deformation and failure flows of geomaterial using elastic-plastic soil constitutive model. Int J Numer Anal Methods 32(12):1537–1570
210. Bui HH, Sako K, Fukagawa R (2007) Numerical simulation of soil-water interaction using smoothed particle hydrodynamics (SPH) method. J Terramech 44(5):339–346
211. Gallati M, Braschi G, Falappi S (2005) SPH simulations of the waves produced by a falling mass into a reservoir. Nuovo Cimento C 28(2):129–140
212. Herrera PA, Massabo M, Beckie RD (2009) A meshless method to simulate solute transport in heterogeneous porous media. Adv Water Resour 32(3):413–429
213. Hui HH, Fukagawa R, Sako K (2006) Smoothed particle hydrodynamics for soil mechanics. Terramechanics 26:49–53
214. Laigle D, Lachamp P, Naaim M (2007) SPH-based numerical investigation of mudflow and other complex fluid flow interactions with structures. Comput Geosci 11(4):297–306
215. Maeda K, Sakai H (2007) Seepage failure analysis with evolution of air bubbles by SPH. In: New frontiers in Chinese and Japanese geotechniques, proceedings of the 3rd Sino-Japan geotechnical symposium, Chongqing, China
216. McDougall S, Hungr O (2004) A model for the analysis of rapid landslide motion across three-dimensional terrain. Can Geotech J 41(6):1084–1097
217. McDougall S, Hungr O (2005) Dynamic modelling of entrainment in rapid landslides. Can Geotech J 42(5):1437–1448
218. Moresi L, Muhlhous H, Dufour F (2001) An overview of numerical methods for Earth simulations
219. Morris JP, Zhu Y, Fox PJ (1999) Parallel simulations of pore-scale flow through porous media. Comput Geotech 25(4):227–246
220. Pastor M, Haddad B, Sorbino G, Cuomo S, Drempetic V (2009) A depth-integrated, coupled SPH model for flow-like landslides and related phenomena. Int J Numer Anal Methods 33(2)
221. Sakai H, Maeda K (2006) Seepage failure of granular ground accounting for soil-water-gas interaction. In: Geomechanics and geotechnics of particulate media, proceedings of the international symposium on geomechanics and geotechnics of particulate media, Ube, Yamaguchi, Japan
222. Cleary PW (1998) Modelling confined multi-material heat and mass flows using SPH. Appl Math Model 22(12):981–993
223. Jeong JH, Jhon MS, Halow JS, Van Osdol J (2003) Smoothed particle hydrodynamics: applications to heat conduction. Comput Phys Commun 153(1):71–84
224. Jiang F, Sousa ACM (2006) SPH numerical modeling for ballistic-diffusive heat conduction. Numer Heat Transfer B, Fundam 50(6):499–515
225. Jiang FM, Sousa ACM (2006) SPH numerical modeling for ballistic-diffusive heat conduction. Numer Heat Transfer B, Fundam 50(6):499–515
226. Rook R, Yildiz M, Dost S (2007) Modeling transient heat transfer using SPH and implicit time integration. Numer Heat Transfer B, Fundam 51(1):1–23
227. Sousa ACM, Jiang FM (2007) SPH as an inverse numerical tool for the prediction of diffusive properties in porous media. Diffus Solids Liq Heat Transfer, Microstruct Prop 553:171–189
228. Gutfraind R, Savage SB (1998) Flow of fractured ice through wedge-shaped channels: smoothed particle hydrodynamics and discrete-element simulations. Mech Mater 29(1):1–17
229. Oger L, Savage SB (1999) Smoothed particle hydrodynamics for cohesive grains. Comput Methods Appl Mech Eng 180(1):169–183
230. Ji SY, Li H, Shen HT, Wang RX, Yue QJ (2007) A hybrid Lagrangian-Eulerian numerical model for sea-ice dynamics. Acta Oceanol Sin 26:12–24
231. Ji SY, Shen HT, Wang ZL, Shen HH, Yue QJ (2005) A viscoelastic-plastic constitutive model with Mohr-Coulomb yielding criterion for sea ice dynamics. Acta Oceanol Sin 24(4):54–65
232. Schafer C, Speith R, Kley W (2007) Collisions between equal-sized ice grain agglomerates. Astron Astrophys 470(2):733–739
233. Shen HT, Su JS, Liu LW (2000) SPH simulation of river ice dynamics. J Comput Phys 165(2):752–770
234. Wang RX, Ji SY, Shen HT, Yue QJ (2005) Modified PIC method for sea ice dynamics. China Ocean Eng 19(3):457–468
235. Tartakovsky A, Meakin P (2005) Modeling of surface tension and contact angles with smoothed particle hydrodynamics. Phys Rev E 72(2):26301
236. Nugent S, Posch HA (2000) Liquid drops and surface tension with smoothed particle applied mechanics. Phys Rev E 62(4):4968–4975
237. Apfel RE, Tian Y, Jankovsky J, Shi T, Chen X, Holt RG, Trinh E, Croonquist A, Thornton KC, Sacco JA (1997) Free oscillations and surfactant studies of superdeformed drops in microgravity. Phys Rev Lett 78(10):1912–1915
238. Fang HS, Bao K, Wei JA, Zhang H, Wu EH, Zheng LL (2009) Simulations of droplet spreading and solidification using an improved SPH model. Numer Heat Transfer A, Appl 55(2):124–143
239. Lopez H, Sigalotti L, Di G (2006) Oscillation of viscous drops with smoothed particle hydrodynamics. Phys Rev E 73(5):51201
240. Melean Y, Sigalotti LD (2005) Coalescence of colliding van der Waals liquid drops. Int J Heat Mass Transfer 48:4041–4061
241. Melean Y, Sigalotti LDG (2005) Coalescence of colliding van der Waals liquid drops. Int J Heat Mass Transfer 48(19–20):4041–4061
242. Wang W, Huang Y, Grujicic M, Chrisey DB (2008) Study of impact-induced mechanical effects in cell direct writing using smooth particle hydrodynamic method. J Manuf Sci E, Trans ASME 130(2)
243. Zhang MY, Zhang H, Zheng LL (2007) Application of smoothed particle hydrodynamics method to free surface and solidification problems. Numer Heat Transfer A, Appl 52(4):299–314
244. Zhang MY, Zhang H, Zheng LL (2008) Simulation of droplet spreading, splashing and solidification using smoothed particle hydrodynamics method. Int J Heat Mass Transfer 51(13–14):3410–3419

245. Zhang MY, Zhang H, Zheng LL (2009) Numerical investigation of substrate melting and deformation during thermal spray coating by SPH method. Plasma Chem Plasma Process 29(1):55–68
246. Zhou GZ, Ge W, Li JH (2008) A revised surface tension model for macro-scale particle methods. Powder Technol 183(1):21–26
247. Liu MB, Liu GR, Lam KY, Zong Z (2003) Meshfree particle simulation of the detonation process for high explosives in shaped charge unlined cavity configurations. Shock Waves 12(6):509–520
248. Liu MB, Liu GR, Zong Z, Lam KY (2003) Computer simulation of high explosive explosion using smoothed particle hydrodynamics methodology. Comput Fluids 32(3):305–322
249. Liu MB, Liu GR, Lam KY (2002) Investigations into water mitigation using a meshless particle method. Shock Waves 12(3):181–195
250. Liu MB, Liu GR (2004) Smoothed particle hydrodynamics: some recent developments in theory and applications. J Beijing Polytech Univ 30:61–71
251. Liu MB, Liu GR, Lam KY, Zong Z (2003) Computer simulation of shaped charge detonation using meshless particle method. Fragblast 7(3):181–202
252. Alia A, Souli M (2006) High explosive simulation using multimaterial formulations. Appl Therm Eng 26(10):1032–1042
253. Bromm V, Yoshida N, Hernquist L (2003) The first supernova explosions in the universe. Astrophys J 596(2):L135–L138
254. Busegnies Y, Francois J, Paulus G (2007) Unidimensional SPH simulations of reactive shock tubes in an astrophysical perspective. Shock Waves 16(4–5):359–389
255. Liu MB, Liu GR, Lam KY (2003) Comparative study of the real and artificial detonation models in underwater explosions. Electron Model 25(2):113–124
256. Mair HU (1999) Review: hydrocodes for structural response to underwater explosions. Shock Vib 6(2):81–96
257. Swegle JW (1992) Report at Sandia National Laboratories
258. Libersky LD, Petschek AG (1991) Smooth particle hydrodynamics with strength of materials. In: Advances in the free-Lagrange method including contributions on adaptive gridding and the smooth particle hydrodynamics method, proceedings of the next free-Lagrange conference, Jackson Lake Lodge, Moran, WY, USA
259. Zhou CE, Liu GR, Ky Lou (2007) Three-dimensional penetration simulation using smoothed particle hydrodynamics. Int J Comput Methods 4(4):671–691
260. Benz W, Asphaug E (1995) Simulations of brittle solids using smooth particle hydrodynamics. Comput Phys Commun 87(1):253–265
261. Cleary P, Ha J, Alguine V, Nguyen T (2002) Flow modelling in casting processes. Appl Math Model 26(2):171–190
262. Cleary PW, Ha J, Ahuja V (2000) High pressure die casting simulation using smoothed particle hydrodynamics. Int J Cast Met Res 12(6):335–355
263. Chen JS, Pan C, Roque C, Wang HP (1998) A Lagrangian reproducing kernel particle method for metal forming analysis. Comput Mech 22(3):289–307
264. Cleary PW, Ha J (2000) Three dimensional modelling of high pressure die casting. Int J Cast Met Res 12(6):357–365
265. Cleary PW, Prakash M, Ha J (2006) Novel applications of smoothed particle hydrodynamics (SPH) in metal forming. J Mater Process Technol 177(1–3):41–48
266. Cleary PW, Prakash M, Ha J, Stokes N, Scott C (2007) Smooth particle hydrodynamics: status and future potential. Prog Comput Fluid Dyn 7(2–4):70–90
267. Ha J, Cleary PW (2000) Comparison of SPH simulations of high pressure die casting with the experiments and VOF simulations of Schmid and Klein. Int J Cast Met Res 12(6):409–418
268. Ha J, Cleary PW (2005) Simulation of high pressure die filling of a moderately complex industrial object using smoothed particle hydrodynamics. Int J Cast Met Res 18(2):81–92
269. Hu W, Yao LG, Hua ZZ (2007) Parallel point interpolation method for three-dimensional metal forming simulations. Eng Anal Bound Elem 31(4):326–342
270. Prakash M, Cleary PW, Grandfield J, Rohan P, Nguyen V (2007) Optimisation of ingot casting wheel design using SPH simulations. Prog Comput Fluid Dyn 7(2–4):101–110
271. Ala G, Francomano E, Tortofici A, Toscano E, Viola F (2007) Corrective meshless particle formulations for time domain Maxwell's equations. J Comput Appl Math 210(1–2):34–46
272. Ala G, Francomano E, Tortorici A, Toscano E, Viola F (2006) Smoothed particle electromagnetics: a mesh-free solver for transients. J Comput Appl Math 191(2):194–205
273. Ala G, Francomano E, Tortorici A, Toscano E, Viola F, di Ingegneria Elettrica D, e delle Telecomunicazioni E (2007) A meshfree particle method for transient full-wave simulation. IEEE Trans Magn 43(4):1333–1336
274. Borve S, Omang M, Trulsen J (2001) Regularized smoothed particle hydrodynamics: a new approach to simulating magnetohydrodynamic shocks. Astrophys J 561(1):82–93
275. Dolag K, Bartelmann M, Lesch H (1999) SPH simulations of magnetic fields in galaxy clusters. Astron Astrophys 348(2):351–363
276. Francomano E, Tortorici A, Toscano E, Ala G, Viola F (2009) On the use of a meshless solver for PDEs governing electromagnetic transients. Appl Math Comput 209(1):42–51
277. Jiang FM, Oliveira MSA, Sousa ACM (2006) SPH simulation of transition to turbulence for planar shear flow subjected to a streamwise magnetic field. J Comput Phys 217(2):485–501
278. Meglicki Z (1994) Verification and accuracy of smoothed particle magnetohydrodynamics. Comput Phys Commun 81(1–2):91–104
279. Pimenta LCA, Mendes ML, Mesquita RC, Pereira GAS (2007) Fluids in electrostatic fields: an analogy for multirobot control. IEEE Trans Magn 43(4):1765–1768
280. Price DJ, Monaghan JJ (2004) Smoothed particle magnetohydrodynamics, I: algorithm and tests in one dimension. Mon Not R Astron Soc 348(1):123–138
281. Price DJ, Monaghan JJ (2004) Smoothed particle magnetohydrodynamics, II: variational principles and variable smoothing-length terms. Mon Not R Astron Soc 348(1):139–152
282. Price DJ, Monaghan JJ (2004) Smoothed particle magnetohydrodynamics: some shocking results. Astrophys Space Sci 292(1):279–283
283. Antoci C, Gallati M, Sibilla S (2007) Numerical simulation of fluid-structure interaction by SPH. Comput Struct 85(11–14):879–890
284. Prakash M, Cleary PW, Ha J, Noui-Mehidi MN, Blackburn H, Brooks G (2007) Simulation of suspension of solids in a liquid in a mixing tank using SPH and comparison with physical modelling experiments. Prog Comput Fluid Dyn 7(2):91–100
285. Anghileri M, Castelletti LML, Tirelli M (2005) Fluid structure interaction of water filled tanks during the impact with the ground. Int J Impact Eng 31(3):235–254
286. Chikazawa Y, Koshizuka S, Oka Y (2001) A particle method for elastic and visco-plastic structures and fluid-structure interactions. Comput Mech 27(2):97–106
287. Guilcher PM, Ducrozet G, Doring M, Alessandrini B, Ferrant P (2006) Numerical simulation of wave-body interactions using a modified SPH solver. In: Proceedings of the sixteenth international offshore and polar engineering conference, San Francisco, CA
288. Hosseini SM, Amanifard N (2007) Presenting a modified SPH algorithm for numerical studies of fluid-structure interaction problems. IJE Trans B, Appl 20:167–178

289. Muller M (2004) Interactive blood simulation for virtual surgery based on smoothed particle hydrodynamics. Technol Health Care 12(1):25–31
290. Hieber SE (2004) Remeshed smoothed particle hydrodynamics simulation of the mechanical behavior of human organs. Technol Health Care 12(4):305–314
291. Tanaka N, Takano T (2005) Microscopic-scale simulation of blood flow using SPH method. Int J Comput Methods 2(4):555–568
292. Tsubota K, Wada S, Yamaguchi T (2006) Simulation study on effects of hematocrit on blood flow properties using particle method. J Biomech Sci Eng 1(1):159–170
293. Rosswog S, Wagner P (2002) Towards a macroscopic modeling of the complexity in traffic flow. Phys Rev E 65(3):36106
294. Benson DJ (1992) Computational methods in Lagrangian and Eulerian hydrocodes. Comput Methods Appl Mech Eng 99(2–3):235–394
295. Walters WP, Zukas JA (1989) Fundamentals of shaped charges. Wiley, New York
296. Anderson CE (1987) An overview of the theory of hydrocodes. Int J Impact Eng 5(1–4):33–59
297. Anghileri M, Castelletti LML, Invernizzi F, Mascheroni M (2005) A survey of numerical models for hail impact analysis using explicit finite element codes. Int J Impact Eng 31(8):929–944
298. Attaway SW, Heinstein MW, Swegle JW (1993) Coupling of smooth particle hydrodynamics with the finite element method. In: IMPACT-4: structural mechanics in reactor technology conference, Berlin, Germany
299. Batra RC, Zhang GM (2008) Modified Smoothed Particle Hydrodynamics (MSPH) basis functions for meshless methods, and their application to axisymmetric Taylor impact test. J Comput Phys 227(3):1962–1981
300. Brown K, Attaway S, Plimpton S, Hendrickson B (2000) Parallel strategies for crash and impact simulations. Comput Methods Appl Mech Eng 184:375–390
301. De Vuyst T, Vignjevic R, Campbell JC (2005) Coupling between meshless and finite element methods. Int J Impact Eng 31(8):1054–1064
302. Fahrenthold EP, Koo JC (1997) Energy based particle hydrodynamics for hypervelocity impact simulation. Int J Impact Eng 20(1–5):253–264
303. Fawaz Z, Zheng W, Behdinan K (2004) Numerical simulation of normal and oblique ballistic impact on ceramic composite armours. Compos Struct 63(3–4):387–395
304. Fountzoulas CG, Gazonas GA, Cheeseman BA (2007) Computational modeling of tungsten carbide sphere impact and penetration into high-strength-low-alloy (HSLA)-100 steel targets. J Mech Mater Struct 2(10):1965–1979
305. Groenenboom PHL (1997) Numerical simulation of 2D and 3D hypervelocity impact using the SPH option in PAM-SHOCK(TM). Int J Impact Eng 20(1–5):309–323
306. Hayhurst CJ, Clegg RA (1997) Cylindrically symmetric SPH simulations of hypervelocity impacts on thin plates. Int J Impact Eng 20(1–5):337–348
307. Hayhurst CJ, Clegg RA Livingstone IA, Francis NJ (1996) The application of SPH techniques in Autodyn-2D to ballistic impact problems. In: 16th international symposium on ballistics, San Francisco, USA
308. Hiermaier S, Schafer F (1999) Hypervelocity impact fragment clouds in high pressure gas numerical and experimental investigations. Int J Impact Eng 23(1):391–400
309. Ioan A, Brizzolara S, Viviani M, Couty N, Donner R, Hermundstad O, Kukkanen T, Malenica S, Temarel P (2007) Comparison of experimental and numerical impact loads on ship-like sections. In: Advancements in marine structures. Taylor & Francis, London
310. Ji XY, Li YC, Huang XC, Chen G (2007) Coupled FE-SPH simulation of truncated-conical projectiles penetrating steel sheets. In: 7th international conference on shock & impact loads on structures, Beijing, China
311. Johnson AF, Holzapfel M (2003) Modelling soft body impact on composite structures. Compos Struct 61(1–2):103–113
312. Johnson GR (1994) Linking of Lagrangian particle methods to standard finite element methods for high velocity impact computations. Nucl Eng Des 150(2–3):265–274
313. Johnson GR, Beissel SR, Stryk RA (2000) A generalized particle algorithm for high velocity impact computations. Comput Mech 25(2):245–256
314. Johnson GR, Peterson EH, Stryrk RA (1993) Incorporation of an sph option into the epic code for a wide range of high velocity impact computations. Int J Impact Eng 14:385–394
315. Johnson GR, Stryk RA, Beissel SR, Holmquist TJ (2002) An algorithm to automatically convert distorted finite elements into meshless particles during dynamic deformation. Int J Impact Eng 27(10):997–1013
316. Kikuchi M, Miyamoto B (2006) Numerical simulation of impact crush/buckling of circular tube using SPH method. Key Eng Mater 306–308:697–702
317. Kitsionas S, Whitworth AP (2007) High-resolution simulations of clump-clump collisions using SPH with particle splitting. Mon Not R Astron Soc 378(2):507–524
318. Lam KY, Shen YG, Gong SW (2001) A study of axial impact of composite rods using SPH approach. Shock Vib 8(5):303–312
319. Lee M, Yoo YH (2001) Analysis of ceramic/metal armour systems. Int J Impact Eng 25(9):819–829
320. Libersky LD, Randles PW, Carney TC, Dickinson DL (1997) Recent improvements in SPH modeling of hypervelocity impact. Int J Impact Eng 20(6):525–532
321. Lukyanov AA, Reveles JR, Vignjevic R, Campbell J (2005) Simulation of hypervelocity debris impact and spacecraft shielding performance. In: Proceedings of the 4th European conference on space debris
322. Ma S, Zhang X, Qiu XM (2009) Comparison study of MPM and SPH in modeling hypervelocity impact problems. Int J Impact Eng 36(2):272–282
323. Michel Y, Chevalier JM, Durin C, Espinosa C, Malaise F, Barrau JJ (2006) Hypervelocity impacts on thin brittle targets: experimental data and SPH simulations. Int J Impact Eng 33(1–12):441–451
324. Nizampatnam LS, Horn WJ (2008) Investigation of multimaterial bird models for predicting impact loads. In: Proceedings of the Asme turbo expo, Berlin, Germany
325. Park YK, Fahrenthold EP (2005) A kernel free particle-finite element method for hypervelocity impact simulation. Int J Numer Methods Eng 63(5):737–759
326. Rabczuk T, Eibl J (2006) Modelling dynamic failure of concrete with meshfree methods. Int J Impact Eng 32(11):1878–1897
327. Randles PW, Carney TC, Libersky LD, Renick JD, Petschek AG (1994) Calculation of oblique impact and fracture of tungsten cubes using smoothed particle hydrodynamics. Int J Impact Eng 17(4):661–672
328. Rosen P, Popescu V, Hoffmann C, Irfanoglu A (2008) A high-quality high-fidelity visualization of the September 11 attack on the World Trade Center. IEEE Trans Vis Comput Graph 14(4):937–947
329. Shintate K, Sekine H (2004) Numerical simulation of hypervelocity impacts of a projectile on laminated composite plate targets by means of improved SPH method. Compos Part A, Appl Sci 35(6):683–692
330. Stellingwerf RF, Wingate CA (1993) Impact modeling with smooth particle hydrodynamics. In: Conference: smooth particle hydrodynamics in astrophysics OAT workshop, Trieste, Italy

331. Taylor EA (2001) Simulation of hollow shaped charge jet impacts onto aluminium whipple bumpers at 11 km/s. Int J Impact Eng 26(1–10):773–784
332. Vignjevic R, Lepage S, De Vuyst T (2005) Simulation of high velocity impacts on thin metallic targets II (discrete elements). WIT Trans Eng Sci 49:575–582
333. Wang P, Shao JL, Qin CS (2009) Effect of loading-wave-front width on micro-jet from aluminum surface. Acta Phys Sin 58(2):1064–1070
334. Zhang QM, Long RR, Liu ZF, Huang FL (2008) SPH simulations of hypervelocity impact of al spheres on multi-plate structures. Int J Mod Phys B 22(9–11):1604–1611
335. McCarthy MA, Xiao JR, Petrinic N, Kamoulakos A, Melito V (2004) Modelling of bird strike on an aircraft wing leading edge eade from fibre metal laminates, part 1: material modelling. Appl Compos Mater 11(5):295–315
336. Brown K, Attaway S, Plimpton S, Hendrickson B (2000) Parallel strategies for crash and impact simulations. Comput Methods Appl Mech Eng 184(2):375–390
337. Bicknell GV, Gingold RA (1983) On tidal detonation of stars by massive black holes. Astrophys J 273:749–760
338. Fulbright MS, Benz W, Davies MB (1995) A method of smoothed particle hydrodynamics using spheroidal kernels. Astrophys J 440:254
339. Chin GL (2001) Smoothed particle hydrodynamics and adaptive smoothed particle hydrodynamics with strength of materials. National University of Singapore, Singapore
340. Hiermaier S, Konke D, Stilp AJ, Thoma K (1997) Computational simulation of the hypervelocity impact of Al-spheres on thin plates of different materials. Int J Impact Eng 20(1–5):363–374
341. Bangash MYH (1993) Impact and explosion. Blackwell Scientific, Oxford
342. Cole RH (1948) Underwater explosions. Princeton University Press, Princeton
343. Fickett WW (1966) Flow calculations for pulsating one-dimensional detonations. Phys Fluids 9:903–916
344. Mader CL (1998) Numerical modeling of explosives and propellants. CRC Press, New York
345. Libersky LD, Randles PW (2006) Shocks and discontinuities in particle methods. Shock Compress Condens Matter 845:1089–1092
346. Ma S, Zhang X, Lian YP, Zhou X (2009) Simulation of high explosive explosion using adaptive material point method. Comput Model Eng 39(2):101–123
347. Miyoshi H (2008) Numerical simulation of shaped charges using the SPH solver: jet formation and target penetration. Explos Shock Wave Hypervelocity Phenom Mater II
348. Tanaka K (2008) Numerical studies of explosive welding by SPH. Explos Shock Wave Hypervelocity Phenom Mater II 566:61–64
349. Wataru K, Akiko M (2006) Explosion simulation by smoothed particle hydrodynamics. Comput Methods 2:1397–1403
350. Xu JX, Liu XL (2008) Analysis of structural response under blast loads using the coupled SPH-FEM approach. J Zhejiang Univ Sci A 9(9):1184–1192
351. Liu MB, Liu GR, Lam KY (2001) Simulation of the explosive detonation process by using SPH methodology. In: Computational fluids and solid mechanics. Elsevier Science, Amsterdam
352. Dobratz BM (1981) LLNL explosive handbook. Lawrence Livermore National Laboratory, Livermore
353. Chiesum JE, Shin YS (1997) Explosion gas bubbles near simple boundaries. Shock Vib 4(11):11–25
354. Karniadakis GE, Beskok A, Aluru A (2005) Microflows and nanoflows: fundamentals and simulation. Springer, Berlin
355. Bird GA (1994) Molecular gas dynamics and the direct simulation of gas flows. Oxford University Press, Oxford
356. Beskok A, Karniadakis GE (2001) Microflows: fundamentals and simulation. Springer, Berlin
357. Pan L, Ng TY, Xu D, Liu GR, Lam KY (2002) Determination of temperature jump coefficient using the direct simulation Monte Carlo method. J Micromech Microeng 12(1):41–52
358. Pan LS, Liu GR, Khoo BC, Song B (2000) A modified direct simulation Monte Carlo method for low-speed microflows. J Micromech Microeng 10:21–27
359. Pan LS, Liu GR, Lam KY (1999) Determination of slip coefficient for rarefied gas flows using direct simulation Monte Carlo. J Micromech Microeng 9(1):89–96
360. Duong-Hong D, Wang JS, Liu GR, Chen YZ, Han J, Hadjiconstantinou NG (2007) Dissipative particle dynamics simulations of electroosmotic flow in nano-fluidic devices. Microfluid Nanofluid 3:1–7
361. Hoover WG, Hoover CG, Kum O, Castillo VM, Posch HA, Hess S (1996) Smooth particle applied mechanics. Comput Methods Sci Eng 2:6572
362. Hoover WG, Pierce TG, Hoover CG, Shugart JO, Stein CM, Edwards AL (1994) Molecular dynamics, smoothed-particle applied mechanics, and irreversibility. Comput Math Appl 28(10–12):155–174
363. Hoover WG, Hoover CG (2003) Links between microscopic and macroscopic fluid mechanics. Mol Phys 101(11):1559–1573
364. Espanol P (1997) Fluid particle dynamics: a synthesis of dissipative particle dynamics and smoothed particle dynamics. Europhys Lett 39(6):605–610
365. Espanol P, Revenga M (2003) Smoothed dissipative particle dynamics. Phys Rev E 67(2):026705
366. Liu MB, Liu GR, Lam KY (2003) Computer simulation of flip-chip underfill encapsulation process using meshfree particle method. Int J Comput Eng Sci 4(2):405–408
367. Li Q, Cai TM, He GQ, Hu CB (2006) Droplet collision and coalescence model. Appl Math Mech 27(1):67–73
368. Tartakovsky AM, Meakin P (2005) A smoothed particle hydrodynamics model for miscible flow in three-dimensional fractures and the two-dimensional Rayleigh Taylor instability. J Comput Phys 207(2):610–624
369. Tartakovsky AM, Meakin P, Scheibe TD, Eichler West RM (2007) Simulations of reactive transport and precipitation with smoothed particle hydrodynamics. J Comput Phys 222(2):654–672
370. Tartakovsky AM, Redden G, Lichtner PC, Scheibe TD, Meakin P (2008) Mixing-induced precipitation: experimental study and multiscale numerical analysis. Water Resour Res 44(6)
371. Tartakovsky AM, Meakin P, Ward AL (2009) Smoothed particle hydrodynamics model of non-Aqueous phase liquid flow and dissolution. Transp Porous Media 76(1):11–34
372. Brackbill JU, Kothe DB, Zemach C (1992) A continuum method for modeling surface tension. J Comput Phys 100(2):335–354
373. Morris JP (2000) Simulating surface tension with smoothed particle hydrodynamics. Int J Numer Methods Fluids 33(3):333–353
374. Lo YME, Shao S (2002) Simulation of near-shore solitary wave mechanics by an incompressible SPH method. Appl Ocean Res 24(5):275–286
375. Shao S (2006) Incompressible SPH simulation of wave breaking and overtopping with turbulence modelling. Int J Numer Methods Fluids 50(5)
376. Shao S, Ji C (2006) SPH computation of plunging waves using a 2-D sub-particle scale (SPS) turbulence model. Int J Numer Methods Fluids 51(8)
377. Shao SD (2005) SPH simulation of solitary wave interaction with a curtain-type breakwater. J Hydraul Res 43(4):366–375
378. Frank J, Reich S (2003) Conservation properties of smoothed particle hydrodynamics applied to the shallow water equation. BIT 43(1):41–55

379. Ata R, Soulaimani A (2005) A stabilized SPH method for inviscid shallow water flows. Int J Numer Methods Fluids 47(2):139–159
380. Rodriguez-Paz M, Bonet J (2005) A corrected smooth particle hydrodynamics formulation of the shallow-water equations. Comput Struct 83(17–18):1396–1410
381. Idelsohn SR, Onate E, Pin FD (2004) The particle finite element method: a powerful tool to solve incompressible flows with free-surfaces and breaking waves. Int J Numer Methods Eng 61(7):964–989
382. Oger G, Alessandrini B, Ferrant P (2005) Capture of air cushion effects in a wedge water entry SPH simulation. In: Proceedings of the fifteenth international offshore and polar engineering conference
383. Callati M, Braschi G, Falappi S (2005) SPH simulations of the waves produced by a falling mass into a reservoir. Nuovo Cimento C 28(2):129–140
384. Oger G, Doring M, Alessandrini B, Ferrant P (2006) Two-dimensional SPH simulations of wedge water entries. J Comput Phys 213(2):803–822
385. Delorme L, Iglesias AS, Perez SA (2005) Sloshing loads simulation in LNG tankers with SPH. In: International conference on computational methods in marine engineering, Barcelona
386. Greco M, Landrini M, Faltinsen OM (2004) Impact flows and loads on ship-deck structures. J Fluids Struct 19(3):251–275
387. Liu MB, Liu GR, Zong Z (2008) An overview on smoothed particle hydrodynamics. Int J Comput Methods 5(1):135–188
388. Xu QX, Shen RY (2008) Fluid-structure interaction of hydrodynamic damper during the rush into the water channel. J Hydrodyn 20(5):583–590
389. Ataie-Ashtiani B, Shobeyri G (2008) Numerical simulation of landslide impulsive waves by incompressible smoothed particle hydrodynamics. Int J Numer Methods Fluids 56(2):209–232
390. Scanlon BR, Tyler SW, Wierenga PJ (1997) Hydrologic issues in arid, unsaturated systems and implications for contaminant transport. Rev Geophys 35(4):461–490
391. Nativ R, Adar E, Dahan O, Geyh M (1995) Water recharge and solute transport through the vadose zone of fractured chalk under desert conditions. Water Resour Res 31(2):253–261
392. Schwartz LM, Martys N, Bentz DP, Garboczi EJ, Torquato S (1993) Cross-property relations and permeability estimation in model porous media. Phys Rev E 48(6):4584–4591
393. Huang H, Meakin P, Liu MB (2005) Computer simulation of two-phase immiscible fluid motion in unsaturated complex fractures using a volume of fluid method. Water Resour Res. doi:10.1029/2005WR004204
394. Huang H, Meakin P, Liu MB, McCreery GE (2005) Modeling of multiphase fluid motion in fracture intersections and fracture networks. Geophys Res Lett 32:L19402. doi:10.1029/2005GL023899
395. Snyder LJ, Stewart WE (1966) Velocity and pressure profiles for Newtonian creeping flow in regular packed beds of spheres. AIChE J 12(1):167–173
396. Sussman M, Smereka P, Osher S (1994) A level set approach for computing solutions to incompressible two-phase flow. J Comput Phys 114(1):146–159
397. Hirt CW, Nichols BD (1981) Volume of fluid (VOF) method for the dynamics of free boundaries. J Comput Phys 39(1):201–225
398. Unverdi SO, Tryggvason G (1992) A front-tracking method for viscous, incompressible, multi-fluid flows. J Comput Phys 100(1):25–37
399. Zhu Y, Fox PJ (2001) Smoothed particle hydrodynamics model for diffusion through porous media. Transp Porous Media 43(3):441–471